3-23-2017

Using Principal Component Analysis to Improve Fallout Characterization

Derek W. Haws

Follow this and additional works at: https://scholar.afit.edu/etd

   Part of the Optics Commons

USING PRINCIPAL COMPONENT ANALYSIS TO IMPROVE FALLOUT CHARACTERIZATION

THESIS

Derek W. Haws, Captain, USAF

AFIT-ENP-MS-17-M-096

DEPARTMENT OF THE AIR FORCE
AIR UNIVERSITY

AIR FORCE INSTITUTE OF TECHNOLOGY

Wright-Patterson Air Force Base, Ohio

The views expressed in this thesis are those of the author and do not reflect the official policy or position of the United States Air Force, Department of Defense, or the United States Government. This material is declared a work of the U.S. Government and is not subject to copyright protection in the United States.

AFIT-ENP-MS-17-M-096

USING PRINCIPAL COMPONENT ANALYSIS TO IMPROVE FALLOUT
CHARACTERIZATION

THESIS

Presented to the Faculty

Department of Engineering Physics

Graduate School of Engineering and Management

Air Force Institute of Technology

Air University

Air Education and Training Command

In Partial Fulfillment of the Requirements for the

Degree of Master of Science

Derek W. Haws, MBA, BS

Captain, USAF

March 2017

DISTRIBUTION STATEMENT A.
APPROVED FOR PUBLIC RELEASE; DISTRIBUTION UNLIMITED.

AFIT-ENP-MS-17-M-096

USING PRINCIPAL COMPONENT ANALYSIS TO IMPROVE FALLOUT CHARACTERIZATION

Derek W. Haws

Captain, USAF

Committee Membership:

Dr. J. W. McClory
Chair

LTC B. E. O'Day, PhD
Member

Dr. J. Matzel
Member

AFIT-ENP-MS-17-M-096

Abstract

Previous research conducted at Lawrence Livermore National Laboratory (LLNL) and the Air Force Institute of Technology (AFIT) has shown a correlation between actinide location and elemental composition in fallout from historic atmospheric nuclear weapons testing. Fifty spherical fallout samples were collected from near ground zero of a surface burst weapons test. The samples were mounted in an aluminum puck then ground and polished to a hemisphere exposing the central plane. Physical morphologies of the samples ranged from clear to opaque with inclusions, voids, and/or uniform characteristics. Spectroscopy data were collected using optical microscopes and scanning electron microscopy (SEM), with radioactivity recorded through autoradiography. Principal component analysis (PCA) was used to quantify the variations within the samples and to determine the correlations between major elemental compositions and the incorporation of unspent nuclear fuel. Principal component analysis identified four statistically significant principal components accounting for 78% of the variations within the spectroscopy data. Principal component analysis was demonstrated as a suitable mathematical approach to solving the complex system of elemental variables while establishing correlations to actinide incorporation within the fallout samples. A model was developed using spot sampling to categorize the samples, identifying three classes of samples. The model correctly identified samples with above average uniform activity, thereby identifying samples with high forensic value for recovery of unspent nuclear fuel. Final analysis of the full elemental composition and the correlation with regions of increased activity for all fifty samples is currently being completed.

iv

Dedicated to my Wife and Children, Always and Forever

v

Acknowledgments

I would like to thank my family who was the most important factor in the success of this research. Their continual encouragement, support and help everyday ensured the success of the research and sanity of the author.

I am grateful to the committee members, personal at AFIT and LLNL for their assistance and help during this research. The insights and guidance provided kept the research on track and ensured a successful program. Sponsor funds provided by The Defense Threat Reduction Agency secured equipment run time and site visits which made this research possible.

Lastly, to my fellow students who supported each other every day and provided a measure of sanity in the frantic pace that was AFIT.

<div align="right">Derek W. Haws</div>

Table of Contents

List of Figures

xii

List of Tables

USING PRINCIPAL COMPONENT ANALYSIS TO IMPROVE FALLOUT CHARACTERIZATION

I.   Introduction

This research focused on the application of tools and techniques applied to a broad sample set of fallout particles to improve the fallout characterization. The research consisted of characterizing the fallout using scanning electron microscopy coupled with energy-dispersive x-ray spectroscopy (SEM/EDX) and micro X-ray Fluorescence (micro-XRF) to create 2-D elemental surface maps of the fallout particles. Autoradiography was used to create 2-D radiation maps of the fallout particles. Principal component analysis (PCA) was then applied to identify spatial correlations between elemental composition and the presence of unburned weapon fuel in the fallout particles. This analysis resulted in an improved the understanding of fallout formation and provides a means of using particle morphology to reduce the effort needed to identify the presence of higher levels of unburned nuclear fuel in fallout particles.

1.1.   Overview

Current high fidelity methods of post-detonation forensic are time consuming. The ability to focus these methods on areas of highest potential value will reduce the time needed to provide important design information and source attribution following a post-detonation recovery event [1]. Forensic recovery efforts are vital to attribution and fall under the umbrella of deterrence. The ability to attribute a weapon to the manufacturer or

1

nation state will enhance global safety and vigilance against the deliberate use of nuclear weapons [2].

The goal of this research was to improve the fallout characterization process through the use of PCA. Samples collected from a historic weapons test were subjected to non-destructive tests to spatially characterize the level of radioactivity and elemental composition. Understanding the spatial distribution of elemental composition and levels of radioactivity can result in an improved understanding of fallout formation. Improved understanding of fallout formation is vital to the improvement of forensic techniques for post detonation evaluation and attribution. This research builds upon previous Master's theses completed at AFIT and work performed by the National Labs during the last decade.

Samples in this research were selected by Lawrence Livermore National Lab (LLNL) scientists from bulk samples of fallout and soil collected from one historic weapon test. These samples were mounted in an aluminum puck using epoxy then polished down to a hemisphere exposing the mid-plane of each particle. This mounting method provides a means of identification for each sample particle. Recent improvements to the autoradiography system at LLNL were also investigated to determine if the improvements yield better results than those collected during the previous efforts [3] [4].

Once the elemental compositions were mapped using SEM/EDX and spatially correlated with the autoradiography results, PCA was applied to the resulting data set. PCA provides a quantitative method to determine the correlation between elemental composition variations and radioactivity [5]. Past application of PCA to fallout samples

2

showed that it can quickly identify elemental composition that has a strong correlation to the presence of elevated levels of radioactivity allowing a more efficient application of time intensive forensic methods [6]. This research will build upon that success by increasing the available data and improving the correlation between elemental compositions of carrier material and radioactivity, and hence the presence of actinides.

1.2.   Problem Statement

Various methods of spectroscopy were used to characterize the fallout samples taken from a historical nuclear weapons test. This characterization focused on identifying the chemical compositions co-located with radioactivity in the samples. By applying PCA to the spectroscopy data, spatial correlation between the major elemental compositions and radioactivity were revealed. Improving the understanding of spatial correlation between elemental compositions and radioactivity will focus forensic recovery efforts to samples of highest forensics value. Identifying samples of higher potential forensics value will reduce the time and materials required to characterize an event, while increasing the quantity of recovered unspent nuclear fuel.

1.3. Scope of Study

This research focused on the completion of the AR and SEM/EDX data collection for the samples prepared by LLNL. The data was then analyzed using principal component analysis. Completion of the data collection and PCA analysis accomplished the year one and two goals of the three-year Midas program as outlined in the June 2016 quarterly performance report [7] [2].

3

1.4. Sponsorship

This work is paid for under the Midas program, Defense Threat Reduction Agency (DTRA), as part of a three-year joint effort by LLNL and AFIT.

4

The analysis and characterization of fallout samples has been conducted since the first nuclear weapon test. Of specific interest to this study is the work performed using non-destructive techniques to determine the formation and the elemental composition of carrier material correlations to unspent nuclear fuel. The location of unspent fuel within fallout particles is important for proper attribution and forensics work to reconstruct the type of device, location of manufacture and sophistication of design [8].

2.1. Early Work

The blast, thermal, and radiation effects of nuclear weapons have been the focus of weapon research since the first atomic tests [9]. These studies documented the fallout as a radiation source and a means of determining weapon characteristics. Nuclear fallout research conducted during the 1950's and 60's sought to characterize the bulk properties of fallout. A consolidated report was compiled in 1965 providing these bulk properties of nuclear fallout [10]. The goal of this consolidated report was to understand how fallout developed, determine different classifications of fallout, and assess how fallout would be dispersed for various detonation and environmental scenarios. This report led to the current understanding of fallout formation from different weapon types and weapon employment scenarios [10]. This understanding was then applied to deliberate fallout management, improved testing safety and effective fallout use in war time scenarios.

Fallout consists of fission fragments, unspent nuclear fuel, and in surface bursts scenarios, local soil and structures vaporized by the fireball. The early radioactivity from an event is dominated by the short-lived fission fragments and bulk carrier material that

5

may contain activated elements. However, long-lived fragments and unspent nuclear fuel still pose a significant health hazard years to decades after an event. Currently to recover nuclear fuel information a large amount of fallout must be analyzed. This large quantity of fallout presents a significant health hazard to the workers and significant clean-up efforts are required after processing. In early research the recovery of nuclear fuel was a byproduct of determining the splitting ratio for each weapon fuel [10].

Each nuclear fuel has a specific splitting ratio when exposed to different energy neutrons, often referred to as the double humped curve [11]. Figure 1 shows the double humped curve for thermal neutron fission of ^{235}U. The energy of the neutrons and the type of fuel produces a unique spectrum which provides insight into the design of the fission device. Through these early studies, many properties of nuclear fission have been explored and documented [9]. However, much remains unclear concerning the incorporation of the unspent fuel in the fallout.
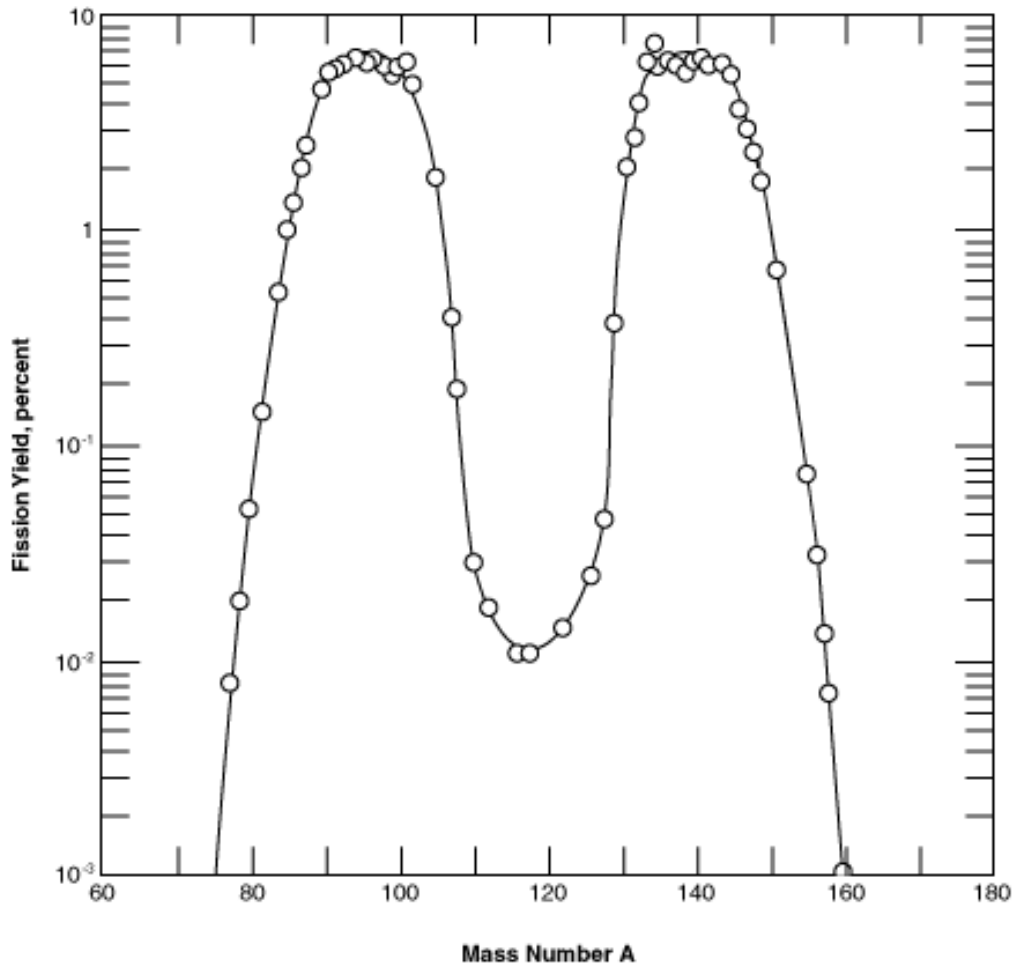
Figure 1. The double hump curve for uranium-235 showing the effective fission yield by mass number for thermal neutrons. Reproduced with permission from [29].

2.2. Recent Work

Research into fallout formation processes has been conducted by LLNL and AFIT with the goal of improving forensic post-detonation recovery efforts. These research efforts focused on the correlation and co-location of elements and unspent fuel via the fallout's radiation signature.

7

Monroe

Completed in 2013, Monroe's research analyzed twelve 1.0 mm diameter fallout samples. These samples were mounted in a one-inch diameter aluminum puck of similar construction to the holder used in this research. Elemental spectroscopy was completed using micro-XRF and SEM/EDS with activity determined using autoradiography. These spectroscopy techniques were used to determine if a positive correlation existed between the unspent fuel and elemental composition. The research focused on developing techniques that could reduce the amount of time spent analyzing fallout particles during a time-critical event. Monroe concluded that micro-XRF could be used for bulk analysis but was not suitable for determining the presence of trace unspent fuel incorporated into the fallout [4]. Figure 2 shows the optical images of the samples while Figure 3 shows the autoradiography images of the samples. Monroe used the optical images to hand align the SEM and autoradiography images for comparison. The aligned autoradiography and elemental concentration images provided an anecdotal correlation between the activity for various regions and the major elements. Monroe concluded that concentrations of calcium and aluminum presented a positive correlation to concentrated actinide regions.
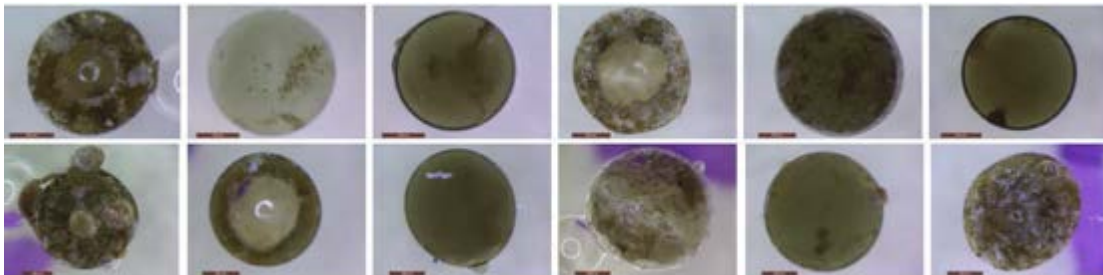
Figure 2. Optical images of the 12 samples used by Monroe [4]. These samples showed a wide range of morphologies capturing bulk characteristics for the fallout sample set.

8
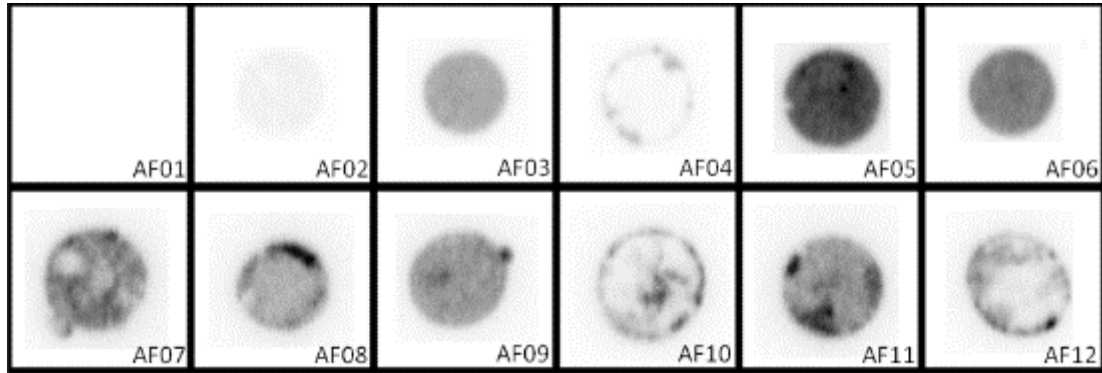
Figure 3. Autoradiography images of the 12 samples areas of high radioactivity appear darker in the image [4].

Dierken

In 2014 Dierken took the results of Monroe and expanded the study to 48 particles < 1 mm in diameter. Using micro-XRF, autoradiography, and SEM, Dierken investigated the fallout particles to determine if previous results held for a larger sample set. Low XRF resolution and degraded equipment performance prevented quantification of results. However, Dierken concluded that regions of high diffusion incorporated more unspent fuel than other regions within the same fallout sample particle. High diffusive regions have a low viscosity allowing elemental mixing to occur to a higher degree than more viscous compositions. The diffusive glass composition that showed higher activity was mafic glass [3]. Mafic glass is characterized by high percentages of calcium (26%) diffused with silicon (45%), aluminum (15%), magnesium (8%) and trace amounts of iron (2%).

Holliday

Holliday recently compiled the results of several studies for publication [11]. His work incorporated Monroe, Dierken, and other LLNL researcher's results. The study investigated historic tests to determine if elemental compositions and actinide

9

correlations were present across a variety of local soil types and weapon emplacements. Based on his findings the fallout could be described by four compositional endmembers. The endmembers represent the idealized elemental composition used to describe the entire sample set. From these studies the resulting endmembers were silicon dioxide, mafic glass, felsic glass, and apparent inclusions. The inclusions are small areas with a dominant high element concentration as an oxide.

All data points from a sample can be described as a linear combination of these endmembers, allowing for statistical variations from point to point. These endmembers were determined through a variety of mathematical methods such as PCA. From the investigations of multiple studies, it was proposed that a simple melt and mix model would accurately describe the incorporation of the unspent nuclear fuel in the fallout samples, instead of the conventional condensation mechanism. Holliday concluded that the endmember composition was more important to the plutonium incorporation than any specific element such as calcium or iron [12]. In Figure 4 a calcium EDS map shows an anecdotal correlation to the areas of activity for this sample.

10
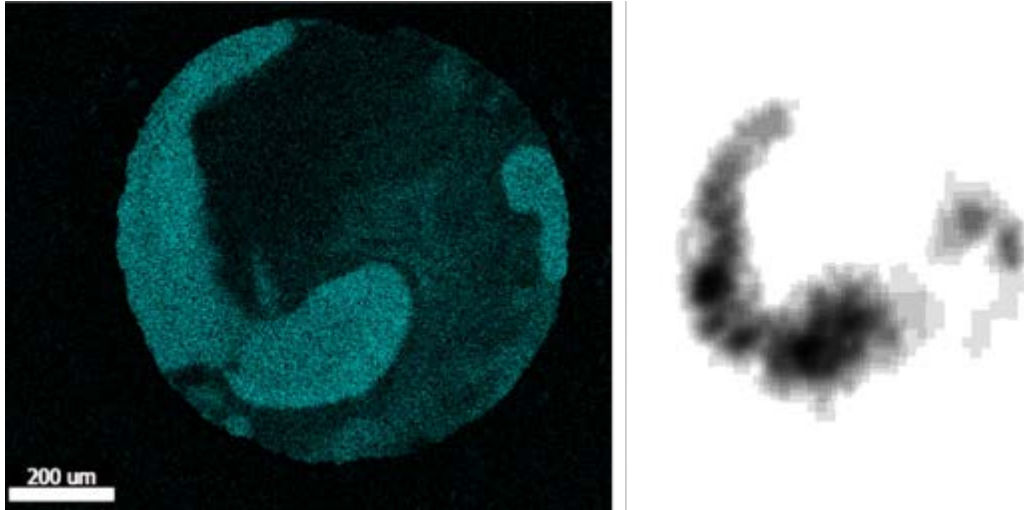
Figure 4. EDS map of calcium concentration and corresponding autoradiography image of sample. The higher activity area is directly correlated to higher concentrations of calcium [12].

However, an abundance of calcium does not indicate the presence of unspent nuclear fuel. Indeed, several samples showed a decrease in activity in regions of calcium or iron rich inclusions [12]. This observation suggests that it is the physical properties of the endmembers not the chemical properties of a single element that is responsible for the incorporation and distribution of unspent nuclear fuel. Based on these endmembers the simple melt and mix model cannot accurately describe the incorporation of nuclear fuel. The melting point of mafic glass (1261^0 C) is much higher than that of felsic glass (720^0 C) which is close to the melting point of the plutonium fuel (640^0 C) but is noted for its decrease in activity.

The physical property identified in Holliday's study most likely responsible for the inclusion of nuclear fuel with this endmember was viscosity. It was proposed that the lower viscosity allowed greater mixing with the plutonium increasing the concentration within this endmember. By looking at the physical properties of the endmembers across a range of temperatures this was one of the only properties that was not bracketed by the

11

other compositions, as shown in Figure 5. Under this assumption, the individual major elements matter only when part of the endmembers and not from other sources.
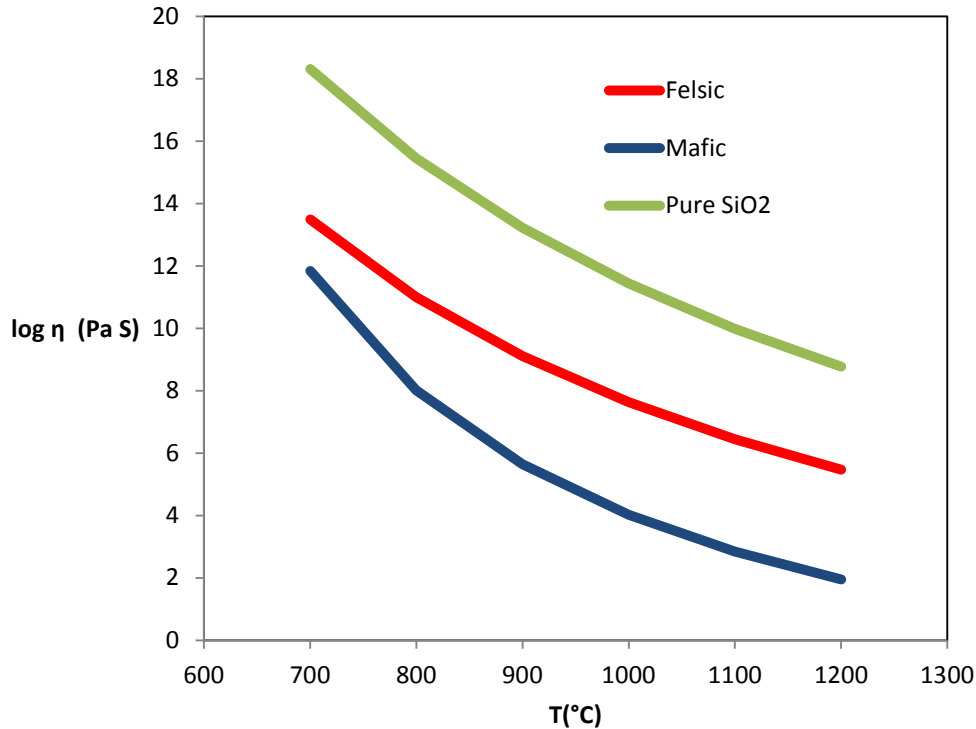
Figure 5. Viscosity as a function of temperature for the major end member compositions of silicon dioxide, felsic and mafic glasses. Figure used with permission [12].

Castro

To provide qualitative results, a mathematical solution was required to provide correlations beyond the anecdotal observations noted earlier. This approach allows the data set to be viewed as a system of equations. By approaching the problem in this way, it is possible to determine qualitatively the correlations between the variables of the system. Castro's research applied principal component analysis (PCA) to three fallout samples sets and a standard reference material provided by the National Institute of Standards (NIST). The goal of this study was to show that PCA was capable of

12

separating data sets based on variations within the data and thus identifying those samples that are compositionally similar and to what degree. Specifically, if it was possible to identify fallout compared to other similar compositions within a data set. Before applying PCA to the data, Castro had to verify that the variables could be described as a linear combination. To be a valid solution, linearity of the system's variables must be established.

PCA is used to analyze complex data sets composed of multiple variables. This method reduces the data to an eigenvector/eigenvalue problem. The solution set of eigenvectors and eigenvalues capture the variations within a data set, and where the largest eigenvalue indicates the eigenvector that captures the greatest variation. The eigenvectors are a mathematical construct that uses the linearity of the variables to represent the system in a new way. One could imagine these eigenvectors as new variables describing each data point in a new basis directly mapped to the original values. Thus, PCA allows determination of which carrier material's elements unspent fuel is most likely to be collocated with.

Using PCA, Castro was able to separate the standard reference material from the fallout samples as shown in Figure 6. The distinct compositional variation between the fallout samples and the reference material is clearly visible in this solution. Using PCA it was possible to separate the reference material (2702 & 2703) and the fallout samples. This was possible due to how well the principal components represented the entire data set and the variations between fallout and the reference material. Castro concluded that PCA was suitable for analysis of spot sampled elemental spectroscopy data [6].

13
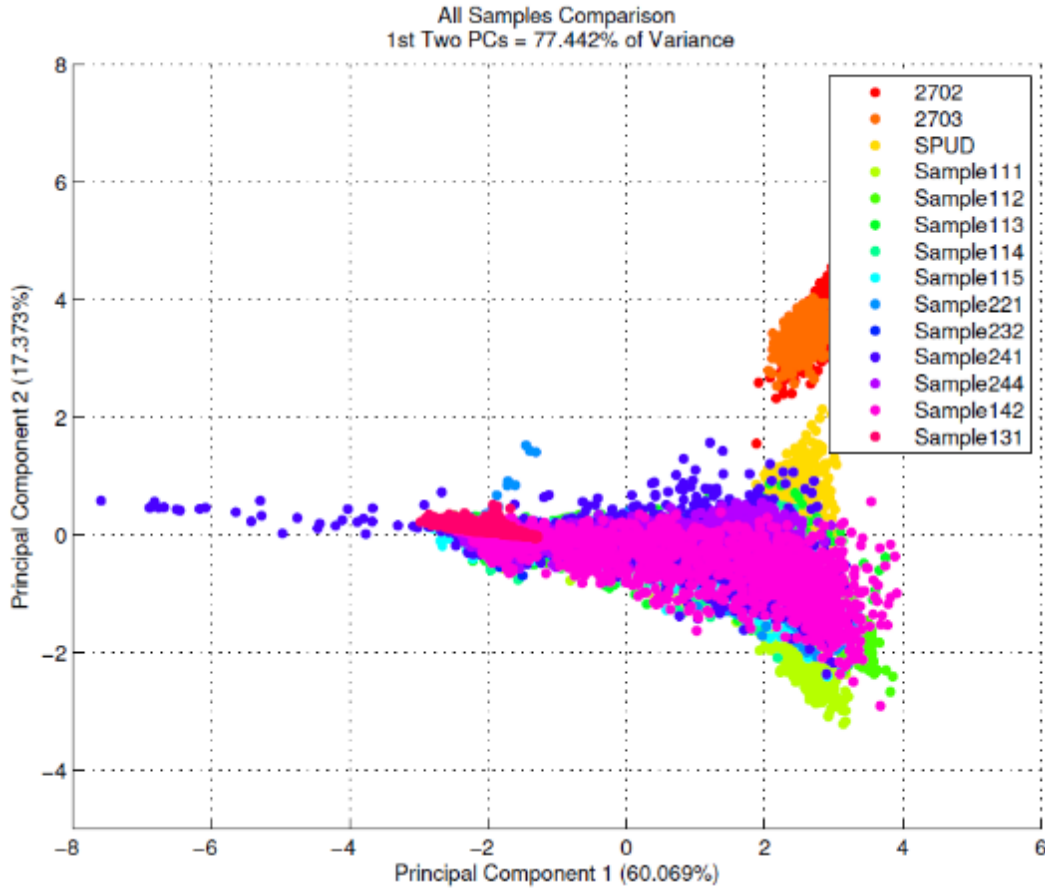
Figure 6. PCA results for the fallout samples and standard reference materials. The standard reference materials were separated from the fallout data by PCA analysis [6]. This shows that PCA is capable of identifying fallout particles with different elemental compositions.

2.3. Fallout Formation

During the first several microseconds of a nuclear event all elements in the

fireball or core are heated to plasma. The rapidly expanding fireball will begin to mix

material from the device and the immediate local environment. As the fireball expands it

begins to cool through radiative heating and spherical divergence. During the expansion

and cooling, local material may not be heated to plasma resulting in various melt phases

or solids being mixed into the weapon debris. During the cooling process elements begin

to condense and form particles with higher melting point elements condensing first [11].

14

Larger particles that experience only local material melting are referred to as fallout and are the focus of this research. With the incorporation of unspent nuclear fuel, these larger fallout particles contain vital forensic information needed to reconstruct the device [13].

In addition to the unspent fuel and melted soil, fallout will also contain fission products. These fission products are the result of the fission of nuclear fuel. Fission products fall within two classes, refractory and volatile. Refractory elements condense around 1620 K while the volatile elements condense in the 1000 K and lower range [11]. Some fission products decay chains transition between the two classes as the isotopes decay to the daughter products. While possible variations mean each fallout particle will be unique, the bulk characteristics will be largely defined by the nuclear fuel, composition of the melted soil, device design and sophistication, temperature ranges, and condensation times.

Fallout produced from a near surface or surface burst will consist of weapon debris and local soil. The expanding fireball will incorporate material from the local environment. Depending on the time of incorporation and the fireball temperature the material can be in several different phases, from a plasma to a solid. The toroidal motion leads to expansion and cooling of the fireball and mixing of the incorporated material. This range of material phases during mixing produces a wide variety in the fallout particles. Some fallout particles will consist of melted soil mixed with condensed elements from the device core. Typically uniform in appearance these particles fall in the homogenous category. The other typical class consists of heterogeneous samples. These samples contain partially melted, solid or liquid phase material mixed with the plasma in the fireball. Because of the range of phases, heterogeneous samples will have obvious

15

regions that are different from other regions of the sample. For a more detailed discussion on fallout formation, decay chains, and daughter products the reader is referred to the bibliography [11] [13] [14].

2.4. Autoradiography

Autoradiography is an imaging technique that uses the source radiation as a means of exposing an image plate or film. This same principal is used in digital and camera films to capture the light from objects and store them on film. This exposure of film by non-visible radiation was first identified by Wilhelm Roentgen in 1895 when he used x-rays to image his wife's hand [15]. All types of ionizing radiation will darken a film when the particles deposit energy in the film. The more energy deposited the darker the film will be. This principal is widely used in medical applications to image organs after absorption of a radioactive solution [16]. Using the exposure on the film, it is possible to determine the activity of the fallout particles. The more activity a particle exhibits the darker the exposure becomes. Imaging all samples simultaneously allows comparisons of the relative sample activities. Additionally, using the correct setup the autoradiography will record the area of the sample that the activity originated in. This is possible by placing the source directly in contact with the film given the specific mean free path of the radiation emitted during film exposure.

Of particular importance to this study is the alpha and beta activity of the fallout which will be recorded in the film. Due to the definitive energy of the alpha particles and their short path lengths, alpha energy will be distinct and sharp when captured on film. The beta energy is a continuous distribution and the beta particles have longer path

16

lengths which causes a blurring or fuzzing of the image. Several assumptions are made concerning the radiation recorded in the autoradiography. First, photons have a relatively large mean free path compared to the film thickness so their interactions will be uniform and minimal. Second, due to the time since the event, no significant exposure from fission fragments will be recorded. Fission fragments are generally unstable with short half-lives when considering the time since the event. With several decades since the event these fission fragments will have decayed to more stable isotopes in their respective chains. The few remaining long lived fission fragment decay schemes are typically gamma radiation which reduces their interaction as already explained. The rapid decay of fission fragments is well documented in various studies making this a reasonable assumption commonly used when studying historical fallout [11] [9] [3] [10] [12]. Under these two assumptions this research will attribute exposure in the autoradiography to alpha and beta activity due to the natural decay of unspent nuclear fuel and not any other source.

2.5. Scanning Electron Microscopy

The scanning electron microscope uses a beam of electrons to excite the surface layer of a sample. The resulting excitation can be used to determine topographical features or the elemental composition. Depending on the configuration the detector will be used to determine the energy of backscattered electrons (BSED) or secondary electrons (SE), or the resulting x-rays can be analyzed using x-ray energy dispersive spectroscopy (EDS). EDS uses characteristic x-rays emitted from the targeted material caused by the interaction of the electron beam with the atoms in the material and

17

determines the energy of the resulting x-rays from the electron interaction. Since characteristic x-rays are element specific, they are commonly used to determine elemental concentrations in a sample. In Figure 7 an incident photon of radiation interacts with an inner shell electron. If the inner shell electron absorbs enough energy from the radiation it is ejected from the atom. When this happens, a higher shell electron decays into the inner shell releasing a specific energy. This energy is dependent on the energy level of the electron that transitions into the inner shell. Each element has specific energies for each shell or line and is well document [17].
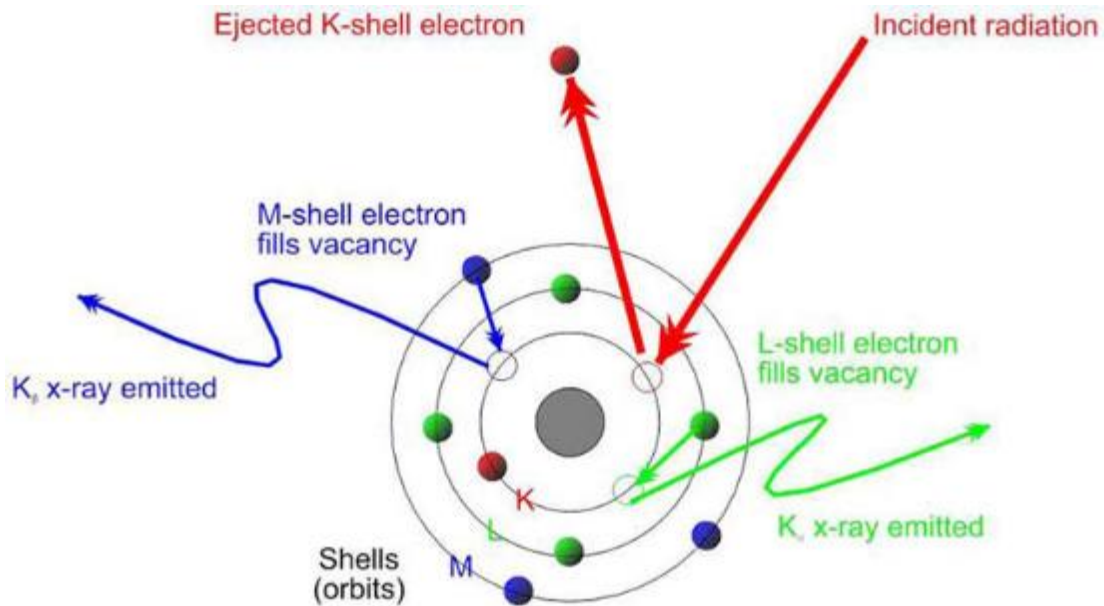
Figure 7. Incident radiation causes an electron to be ejected from the atom. The resulting cascade from a higher electron results in a characteristic x-ray for that element.

This is the same principal used in the x-ray fluorescence which is discussed later. This phenomenon is well characterized and documented in the literature and the reader is referred to the bibliography for a more thorough discussion on the use of EDS and x-ray fluorescence [18].

18

Backscattered electron imaging relies on the principal of elastic scattering. When the electron beam interacts with the surface layer many of the electrons will be scattered off the surface into the detector. As the electrons interact with the surface the elastic collision energies will be proportional to Z^2. Where Z is the atomic number, or the number of protons in each element, and is the defining characteristic for each element. Since each atom has a specific Z the resulting electron energies from interactions are unique to each element. This provides a contrast to the image as the electrons scatter off different elements will have a different energy than the starting beam. This provides a grey scale image of the chemical variability of a sample [16].

Secondary electron imaging uses inelastic scattering to free atomic electrons. The incident electron from the electron beam imparts energy to the bound atomic electron freeing it from the atom. These electrons can be collected or discarded depending on the detector configuration. For the purpose of this study, the secondary electron imaging was used during the x-ray raster mapping and spot sampling. For a more thorough introduction to SEM and its uses the reader is referred to the bibliography [16] [18].

2.6. X-ray Fluorescence

X-ray fluorescence (XRF) uses the principal of characteristic x-rays, just like EDS, to reconstruct the elemental composition of a sample. In this case, the excitation to free an atomic electron is done by either a photon from an isotope such as ^{60}Co with a single energy or through bremsstrahlung radiation which produces photons with a varying band of energy. Typically, a single energy photon source is used when investigating a specific element concentration. The decay source photon energy must be

19

matched to the energy required to eject an inner shell electron of the desired element. As the gamma source decays, the resulting photon has a probability to interact with the atomic electrons. If the gamma ray interacts with an inner shell electron with sufficient energy it will eject the electron. When this happens the resulting cascade of a higher shell electron will release energy in the form of characteristic x-rays which can be measured on a detector [19].

The Horiba XRF uses the alternative method of inner shell electron excitation. A broad spectrum of energies produced through bremsstrahlung radiation as depicted in Figure 8 irradiates the target sample providing the atomic electrons with enough energy to excite the electron to a higher orbital or eject the electron from the atom. The development of the bremsstrahlung radiation relies on the principal of accelerating an electron and impacting it on a high-Z target. The electron is accelerated by a high electric potential across a vacuum. Upon impact with the target, the electron loses energy in the form of x-rays called bremsstrahlung radiation. The resulting energy of the x-ray spectrum is highly dependent on the acceleration energy of the incident electron and the target material [20].
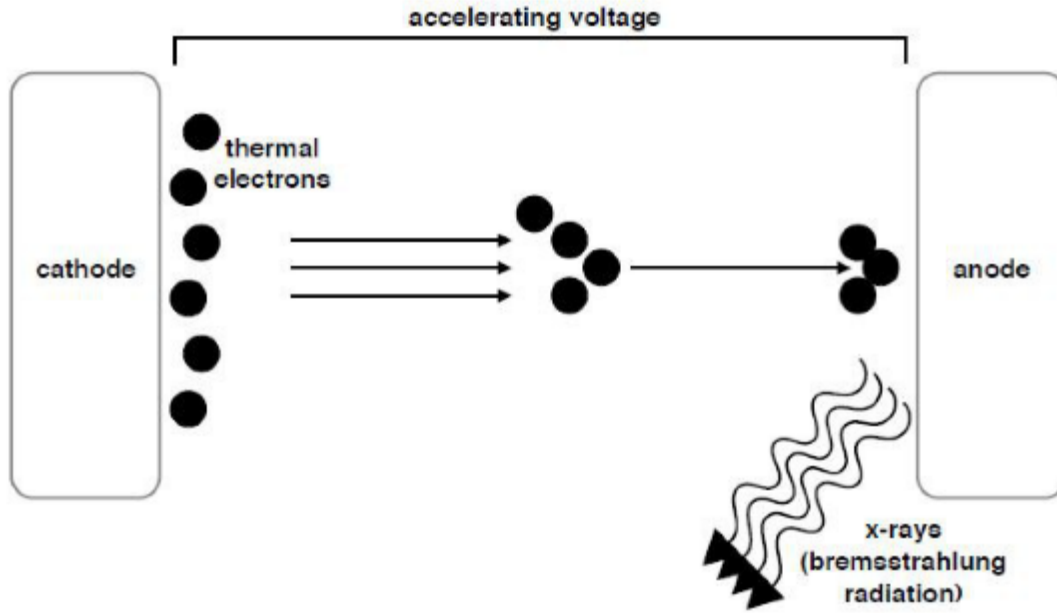
Figure 8. Example generation of bremsstrahlung radiation using acceleration of electrons into a target.

The variables of acceleration voltage and target material provide a method to tailor the resulting bremsstrahlung radiation to specific energy bands for a specific desired result. Using a wide band of energy allows the researcher to excite a wide range of elements in the sample. This produces a data set that records the abundance for many element in the sample and not just a single element. A higher Z anode will provide a higher energy spectrum as will higher acceleration voltage. This is a common method to generate radiation for research and medical techniques. A more though discussion on these devices and applications can be found in the bibliography [19] [17].

2.7. Principal Component Analysis

Principal component analysis is a mathematical technique that takes advantage of linear algebra to reduce the dimensionality of a data set revealing correlations and dependencies that would not otherwise be apparent [21]. Similar to a Fourier transform,

21

a linear combination of the variables can represent the original system with fewer equations. Adding more equations will bring the sum of the linear combinations closer to matching the system with smaller variance captured with each additional principal component. The mathematical construct of sufficient principal components is critical to reducing the dimensionality of a problem. Several methods exist to determine the sufficient number of principal components needed to represent the system, as discussed in Chapter III.3.5

Using PCA to find a mathematical solution removes the dependence on multiple variables and recasting the problem as an eigenvector/eigenvalue problem [22]. This recasting reduces the dimensionality of the system to a smaller number of new variables called principal components. By applying PCA, a problem with hundreds of variables can be expressed in a new frame with only a few variables, in some cases as few as two or three. It is assumed that the eigenvectors of the problem can be written as a linear combination of the variables or observables. If the data cannot be represented by an orthonormal basis, then any PCA solution is suspect. In most cases linearity of the variables is a good starting assumption and can provide insight into the correlations between various variables in a data set [23].

Properly setting up the problem ensures that the data set can be analyzed by PCA. The first step is to recast each data point into a (m x n) matrix configuration. Each row of the matrix represents one data point. The columns of the matrix are assembled from the values of each variable recorded for every data point. With this change the data set is focused on the variables and their values for each point instead of the point itself. The data set is conditioned to remove unit dependence and arbitrary scaling. Without

22

removing unit dependence, it is impossible to compare things like element counts and autoradiography intensity. To remove unit dependence the data is mean centered, which is the process of subtracting the mean from the value of each data point for each variable. The scaling is completed by dividing by the standard deviation of the data point after subtracting off the mean [21].

The first step in solving the eigenvalue problem is taking the m x n matrix and solving for the covariance matrix. The covariance matrix measures the difference between each variable from one point to the next. This step removes influence due to high counts in one variable at one point and recasts the problem solving a simpler, similar problem. Solving a similar matrix is a typical mathematical approach for solving complex systems by reducing the difficulty of the problem. In the new problem, the eigenvectors are the solutions to the covariance matrix, which is n x n, and indicates how quickly each variable changes with respect to the other variables. The larger a covariant matrix value, the greater the correlation between the two original variables with a zero indicating there is no correlation [5], while negative values indicate a negative correlation. Once a solution is found, the covariance matrix is no longer needed and the solution from the covariance matrix is translated to the original problem. The values of the eigenvector components become the weighting factors that are used in the principal components to develop the linear combination. The eigenvalue is the value of this eigenvector with the weighting factors for each of the original variables.

The final limitation of PCA assumes that the largest eigenvalue is the most important in describing the system. Since the eigenvalues are the solutions for a similar matrix developed by looking at how much each variable changes, a sample set that has a

23

wide range of variation within one variable will skew the solution due to the large values this produces in the covariance matrix. One way to verify that the solution represents the true system and not some inflation is to leave out one variable at a time and compare the solutions. Like Fourier transforms, more equations used results in a better representation of the original when using PCA. The more eigenvalues that are used in the analysis the more accurately the PCA will be in describing the data set [21]. However, increasing the number of PCs used also begins to represent the noise and errors inherent in any measurement. For this reason, several methods are developed to ensure that the number of PCs selected is representative of the actual data of the system and not noise and errors.

III. Experiment

3.1. Sample Preparation

In the early 2000's a team from LLNL collected samples from multiple historic US atmospheric nuclear tests. The samples for this study were selected from a plutonium fueled shot collected near ground zero. To reduce bias in the mathematical model only three selection criteria where used to select samples for this study. The first criteria is that the particle exhibited radioactive alpha and beta decays as observed with a detector. Second the particle needed to have a glassy appearance. Combing these two criteria ensured that the particle was likely fallout swept into the nuclear fireball and not ground particles with surface contamination. The final selection criterion was mean radius of the particles. Using a #25 grid the particles where sifted out of the bulk collection cans. A #25 grid has 25 lines per inch which makes the mean radius of the particles approximately 0.5 mm.

After sifting, the particles were monitored individually to determine the alpha and beta counts along with the gamma decay rates. This counting was only performed to ensure that the particle contained radioactivity and will not serve as a data point during this research. A one-inch diameter aluminum puck was drilled with a uniform grid pattern to hold the fallout particles as shown in Figure 9.
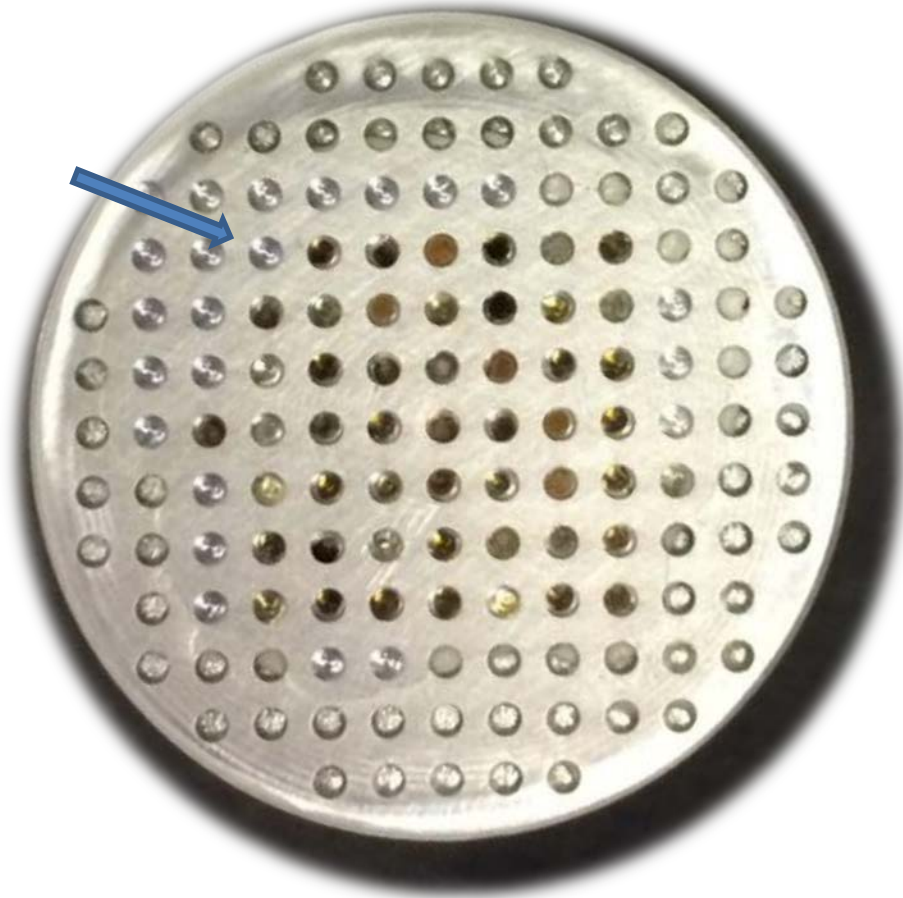
Figure 9. Fallout samples secured in aluminum 1" puck. Samples are numbered from left to right starting at the indent, shown with the blue arrow.

To aid in sample identification the particles are arranged in a grid numbered sequentially from left to right starting at the top left, this corner is identified by the indent and the blue arrow in Figure 9. On rows four and five a particle was off set from the square grid. These three fiducial marks were used to determine the orientation and positon during autoradiography, SEM, and XRF analysis. Each particle was placed such that approximately half of the particle would be below the surface plane of the aluminum puck and secured in their individual holes using an epoxy. Once the epoxy was set, the particles where ground down to a hemisphere using corundum polishing paper of a variety of grit sizes and finished with a 0.25-micron diamond paste. This grinding

26

process ensured a smooth mirror surface while exposing the largest plane of the fallout material. This smooth plane is required by the SEM/EDS for accurate elemental composition data.

Optical imaging was completed for the fifty samples to identify any features, such as voids cracks or surface defects, which could be used to match the autoradiography, SEM, and XRF images. These surface features were removed from the SEM data set to ensure accurate data points. Surface irregularities cause random scattering events lowering the SEM image quality. Increased scattering events reduce the quantity of recovered electrons from the surface which reduces the resolution of the spectroscopy data. These images provide the pixel mapping basis of the different imaging techniques employed to characterize the samples.

3.2. Autoradiography

Autoradiography was used to provide a pixel map of the nuclear fuel radioactivity within the fallout. Recall that the assumption was made in Chapter II paragraph 2.4, that only the nuclear fuel activity is recorded on the film plate. To provide a consistent measurement of activity all the samples were simultaneously imaged. This ensured that the relative intensity of each fallout particle is recorded to compare to the other samples. With all particles coming from the same test and imaged at the same time no adjustment to activity needs to be made to account for the decay of the nuclear fuel.
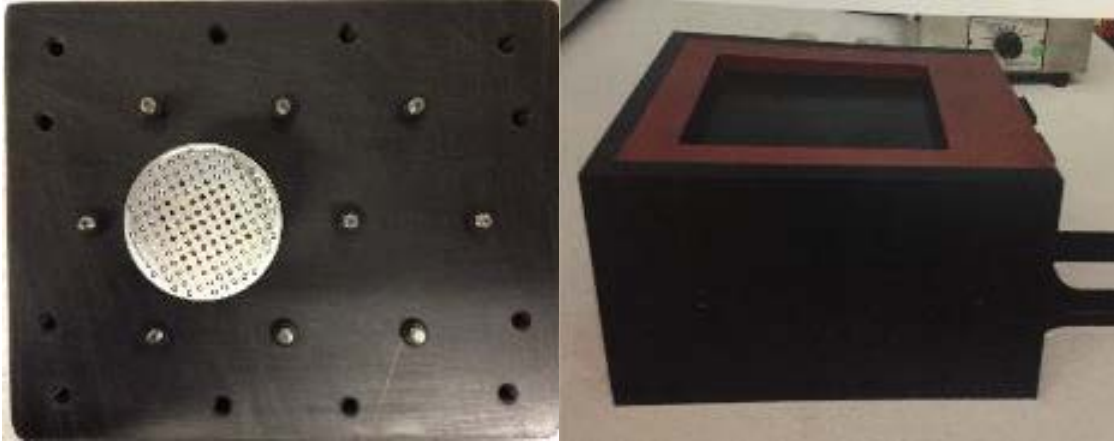
Figure 10. Aluminum puck prepared for autoradiography within the LLNL Stonebox.

The aluminum puck was secured to a height adjustment pin in a custom light tight enclosure provided by LLNL for performing autoradiography measurements on similar samples. Known as the Stonebox this enclosure is shown in Figure 10. The configuration used for this study places the samples in direct contact with the super resolution film with no attenuation medium used. The leveling function of the height adjustment pin ensured that all samples contacted the film uniformly. Direct contact with the film eliminates any attenuation as the alpha and beta particles traveled across an air gap before depositing energy in the film. After leaving the sample in contact with the 5" × 4" film for 18 hours the film was processed using a Typhon FLA 7000 digital scanner shown in Figure 11.
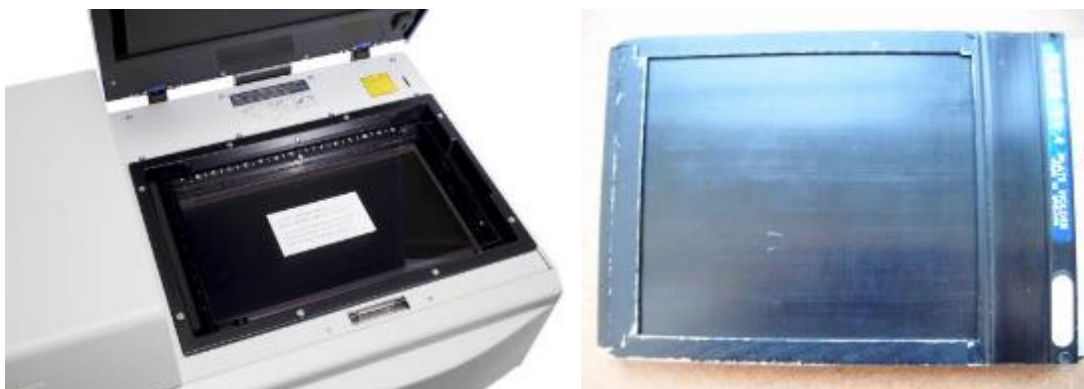
Figure 11. Typhoon scanner and standard film cassette used for the autoradiography.

The Typhoon scanner reads the film peeling off one layer of the image each time allowing multiple processing events and options from one exposure. The settings for the Typhoon imaging software were selected based on previous exposures and calibration curves provided by LLNL and are recorded in Table 1.

Table 1. Typhoon FLA 7000 digital scanner settings used to process the autoradiography image.

Setting options	Value
PMT	626 Volts
Pixel Size	25 microns
Laser Wavelength	650 nm

A darker pixel in the autoradiography image indicates a higher activity in that sample region. The activity recorded per pixel can then be compared to the other pixels as the variation in activity within the sample set. While it is possible to determine the counts from a properly calibrated film exposure it falls outside the scope of this study and only the relative variation between pixels and samples is used. Figure 12 shows the final

29

autoradiograph for the fifty samples numbered as indicated in the Sample Preparation

section presented earlier in this work.
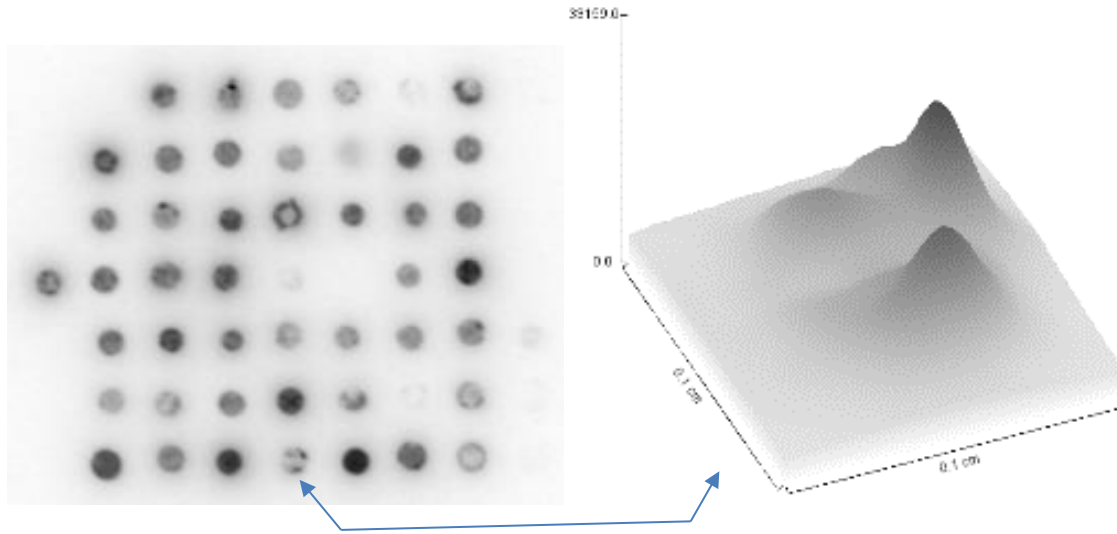
Figure 12. Shown left, autoradiography of the 50 samples used for this study. Shown on the right is a 3-D plot of the intensity of sample 47 taken from the autoradiography data.

3.3. Scanning Electron Microscopy

For this research, LLNL provided the FEI Inspect Model F SEM and detector. To

prevent static charge build up, a nominal 10 nm conductive carbon coating was sputtered

on the surface of the samples. Carbon was chosen to reduce interference with the

elements of interest within the sample. The sputtering was completed using standard

procedures for SEM imaging sample preparation. The settings for the data collection

using the SEM are shown in Table 2.

The BSED images of the samples serve as an additional method for feature

matching during the EDS and XRF compositional analysis. By adjusting the contrast, it

is possible to determine degree of homogeneity of the sample due to the different

30

energies of the backscattered electrons. The apparent homogeneity or heterogeneity is used as a rough classification of the particles into two different categories for analysis.

Table 2. Settings used for the Inspect FEI SEM.

	Acceleration voltage (KeV)	Spot Size setting	Live Time (s)	Resolution (pixels)
BSED	15	5		
EDS	15	5	15	
Raster	15	5		1600×1600

To complete a detailed characteristic x-ray mapping of each sample with the SEM requires months of machine time. To build up the counts of minor elements to detectable levels at a high resolution requires four days per sample [24]. The additional mapping is scheduled to be completed by LLNL over the rest of the fiscal year. As an example, the completed raster scan of sample 47 is shown in Figure 13 where brighter pixels in the image correspond to higher elemental concentrations. This sample was chosen based on its apparent homogeneity in the BSED image and unique radiation signature captured in the autoradiography shown in Figure 12.

31
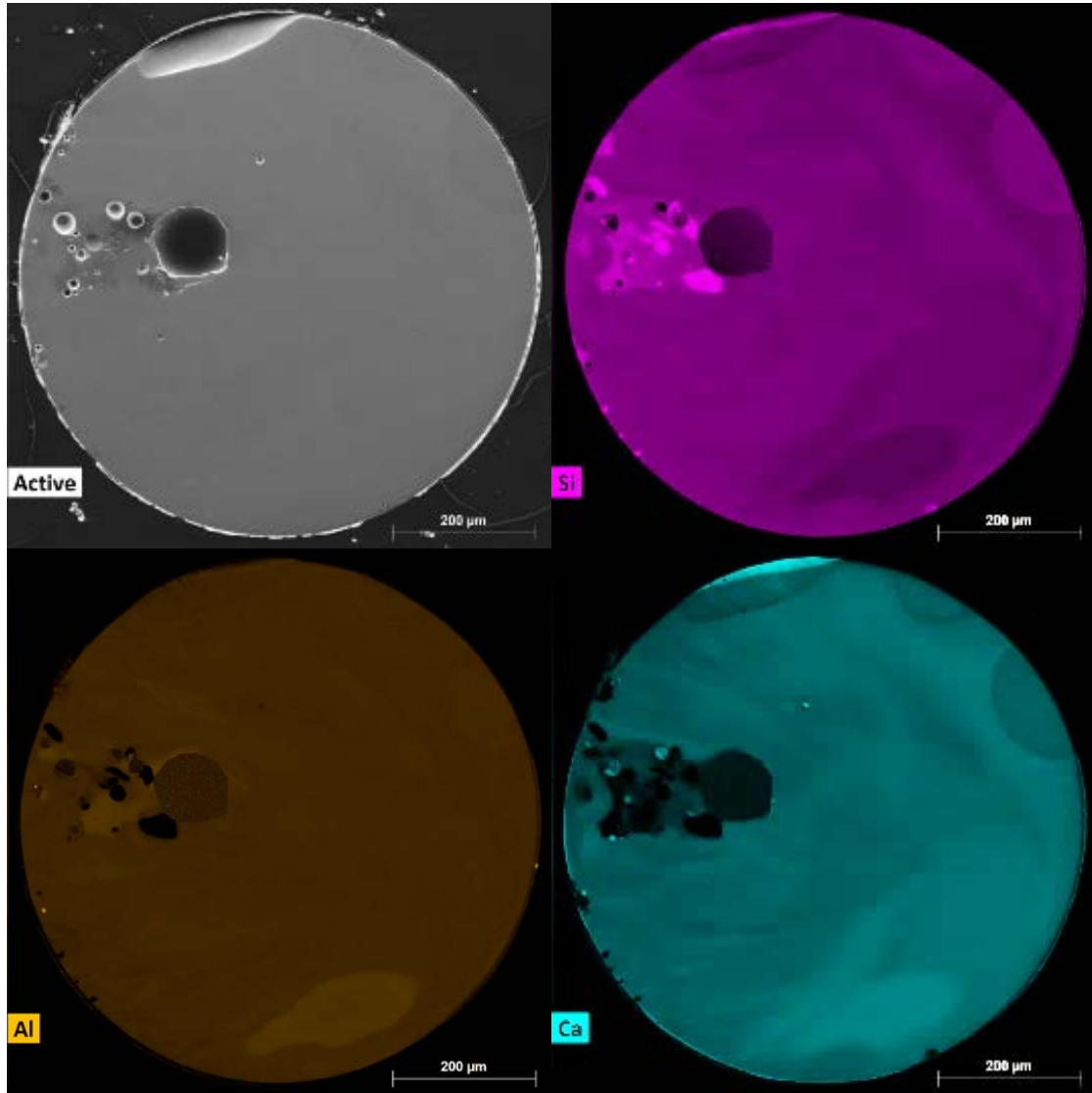
Figure 13. SEM results for sample 47. The top left image shows the secondary electron image for the sample. The remaining three images show the EDS characteristic x-ray mapping for the specific elements of Si, Al, and Ca in sample 47.
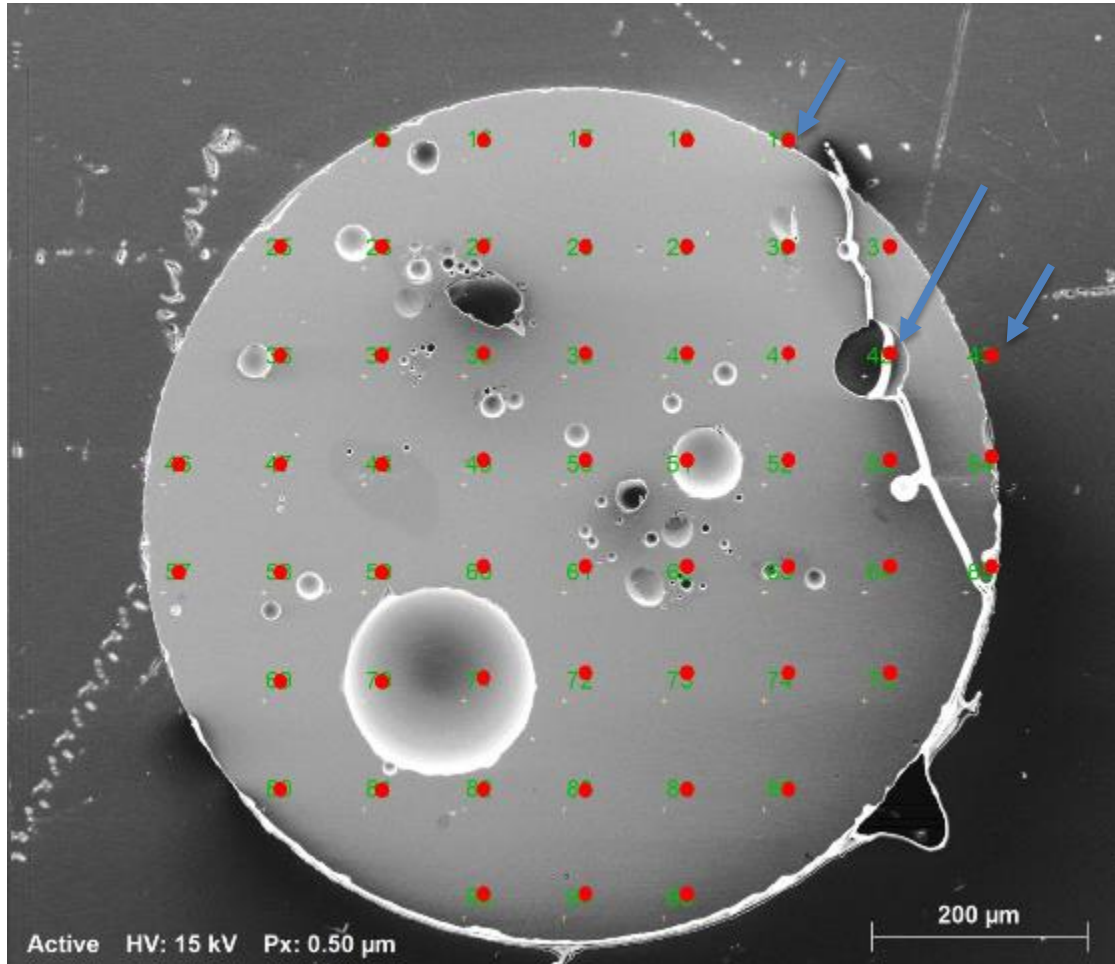
Figure 14. Grid used for EDS spot analysis of sample 47. Sample points that fall off the sample or indicate voids and surface defects are indicated with the blue arrows.

A spot analysis was completed using the energy dispersive spectroscopy (EDS).

Using a spot analysis ensures that the bulk characteristics of the samples are captured.

Additionally, spot sampling provides a rapid method of characterization for each sample.

Each sample was scanned using a uniform grid as shown in Figure 14. This grid provides

a uniform density of points for each sample.

The settings for the Inspect SEM for the EDS measurements stayed the same as

for the BSED with the addition of a 15 second live time per data point. On average, each

sample will have 35-50 data points before any filtering to remove invalid data points.

33

These invalid points can be due to voids or cracks in the surface or sample spots near the sample edge, points of this type are shown with blue arrows in Figure 14.

3.4.   X-ray Florescence

X-ray florescence provides complementary information to the EDS characteristic x-ray spectrums collected with the SEM. While both provide a similar method to determine the elemental composition each has its own advantages and can be more suitable for different elements [20]. The micro-XRF data collection is scheduled to be completed at AFIT using the Horiba XGT 7200 after the completion of the x-ray mapping with the LLNL SEM. Each sample will be raster scanned and spot scanned to provide a similar data set as already discussed in the SEM set up. The recommended settings for the Horiba XGT are recorded in Table 3. These settings will take advantage of the machines calibration settings and maintain consistency with the SEM data.

Table 3. Recommended settings for the Horiba XGT micro-XRF.

Acceleration Voltage (KeV)	Spot Size (microns)	Live time (s)	Raster resolution
15	100	15	512x512

3.5. Principal Component Analysis

Principal components are mathematical constructs that solve the eigenvector problem by assigning weighting factors to the original variables. The summation of the weighting factors and original variables make up the linear combination. To ensure that only valid data points are used the EDS data must be evaluated. As stated earlier any surface irregularities will affect the returning energy of the electrons and thus enter additional errors into the system. Data points that fall within this category are removed from the data set.

The remaining spectroscopy data was further reduced by removing any data point that had a sum peak total less than 90% or greater than 110%. For the SEM, the sum peak total is the resulting fit from the collected EDS spectrum using the Inspect software. There are several reasons that the sum peak may depart outside of this range. Any surface defects, data point off the sample, or surface voids and cracks will affect the resultant energy spectrum and the sum peak totals [18]. To ensure a valid model of the elemental concentrations these data points need to be removed. This constitutes the preconditioning that must be completed for any data set prior to obtaining a mathematical solution.

Before establishing the covariance matrix several steps must be completed to ensure that the true data variance is represented by the PCA model. To remove the dependence on large values the data is first mean centered. Mean centering subtracts the mean off each column in the data set [23]. The second step is to remove any unit change between the variables. This is done by dividing the mean centered variable by the standard deviation. This removes any unit dependence. Using EigenVector's PLS

35

toolbox these two steps are accomplished under the auto scaling function [23]. By using these two steps the data is a true representation of the variance between each data point and not arbitrarily inflated by large numerical values from one sample. Once auto-scaled, the solution to the covariance matrix was determined using PLS Toolbox. This program was developed specifically for chemometrics or the study of chemical systems in biochemistry and chemical engineering [23]. This software is well-suited to meet the goal of identifying the chemical elements that are most closely correlated to the autoradiography data. It should be noted that PCA is not the only possible multivariate statistical method that can be employed by the PLS toolbox but will serve as the basis to identify and refine the model of early incorporation of nuclear fuel in the fallout particles.

The resulting solution must be evaluated to determine the suitable number of principal components needed to develop a valid model of the elemental compositions of the samples. This is accomplished using the Scree test, Kaiser's rule, and the proportion of variance captured theorem. The use of these evaluation methods is discussed in Chapter IV.4.3.

IV. Results

Principal component analysis was completed on the elemental composition data obtained through the X-Ray Energy Dispersive Spectroscopy spot sample data collection. By solving the covariance matrix with the data obtained from the spot sample, a model was developed to describe the chemical variations within the bulk sample set. With the principal components, it is possible to evaluate unknown data with the known data. This provides a predictive capability in characterizing new samples without undergoing the same evaluations as the sample set. By plotting the original data points in principal component space, the model co-locates samples that exhibit similar physical characteristics. Additionally, several samples are compositionally similar but did not share the same physical traits such as color, texture, or homogeneity. This difference in physical characteristics could cause mischaracterization of samples' forensics value. This highlights a strength of using PCA to group samples based upon similar chemical compositions, instead of physical traits that may have no correlation to actinides. The resulting principal component model provides a method to identify and characterize those samples that have compositional similarities identified as positive correlation to actinide incorporation.

Specifically, this research has confirmed the importance of calcium in actinide incorporation. Of note was the strong correlation between the presence of aluminum and the unspent nuclear fuel not identified in previous studies. Additionally, the model identified an anti-correlation between unspent nuclear fuel and iron, sodium, potassium, and silica. As the full characteristic x-ray mapping information is completed, the

37

correlations, anti-correlations, weighting of importance and percent concentration can be identified.

Identifying which elements and concentrations are correlated with unspent nuclear fuel will improve the forensics collection and analysis of post-detonation nuclear fallout materials. Furthermore, this will improve fallout development models through additional constraints and boundary conditions. Understanding the fundamental elements and concentrations helps researchers to develop the compositions formed during the toroidal mixing of the nuclear event. These compositions have definitive physical and chemical characteristics that must be understood if improvement to the fallout models are to be developed. Understanding the physical and chemical properties of these actinide incorporating compositions will help to further the understanding of the mobility of the unspent nuclear fuel improving safety and long term environmental impacts from historical tests and future research.

4.1. Optical Microscopy

Optical microscopy was completed using a Leica M165 optical microscope with a Leica DFC 425 digital camera mount. The main purpose of the optical microscopy was to evaluate the macroscopic variations in the fallout samples. The sample set contained a large variation in color, clarity, and porosity. Additionally, optical microscopy provides a second method of identifying surface defects that would affect the accuracy of the SEM data. Recall, that surface defects affect the accuracy of the EDS data. These defects pose a significant error in elemental spectroscopy identification. Performing optical spectroscopy provided a means of grouping the fallout based on physical characteristics such as color, swirls and inclusions. These physical characteristics provide a quick and inexpensive method to characterize samples. In the early days after an event, the decay from fission fragments will saturate most spectroscopy tools. Detectors that rely on x-rays or electrons to provide characterization data, such as those used in this study, will be saturated by the radiation activity. The high activity will also saturate autoradiography films preventing the use of this characterization method. Using the PCA model provides a valuable tool for rapidly sorting of high forensic value fallout material through correlations to physical traits.

The optical spectroscopy images were taken using a 16.5X1 zoom set at 10x. Each image was captured at 5-megapixel resolution and observations recorded for each sample. The resulting images are listed in sample number order from left to right in Figure 15, Figure 16, and Figure 17.

39
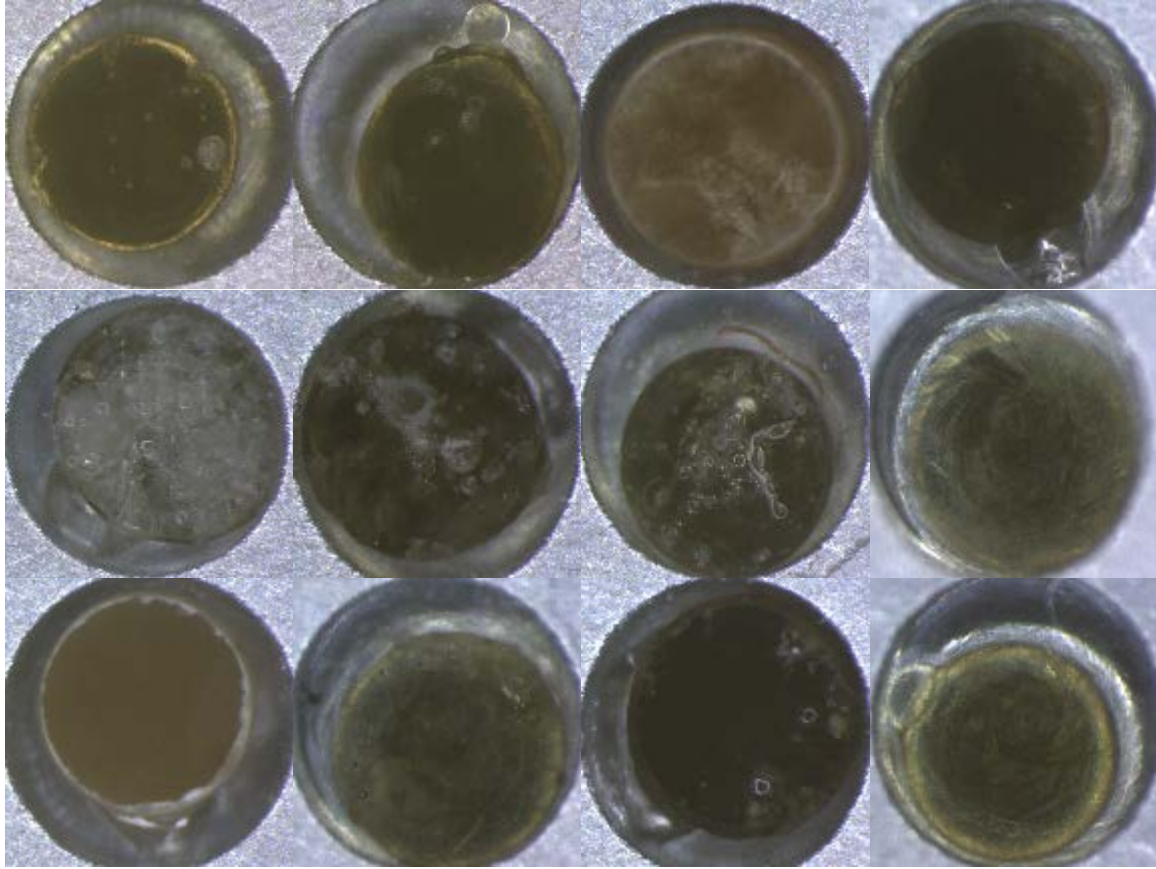
Figure 15. Optical Spectroscopy of samples 1 to 12 numbered from left to right.
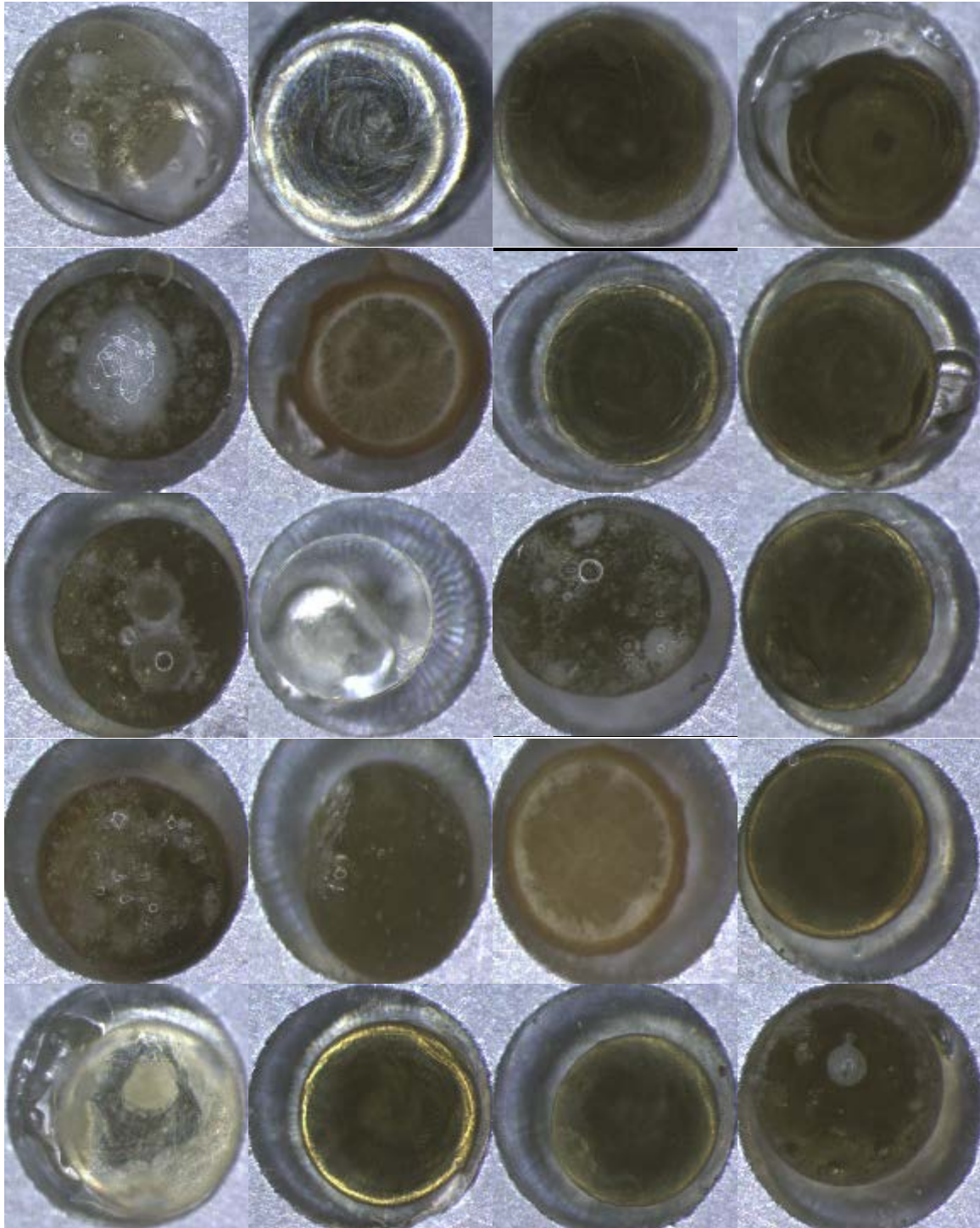
Figure 16. Optical Spectroscopy of samples 13 to 32 numbered from left to right.
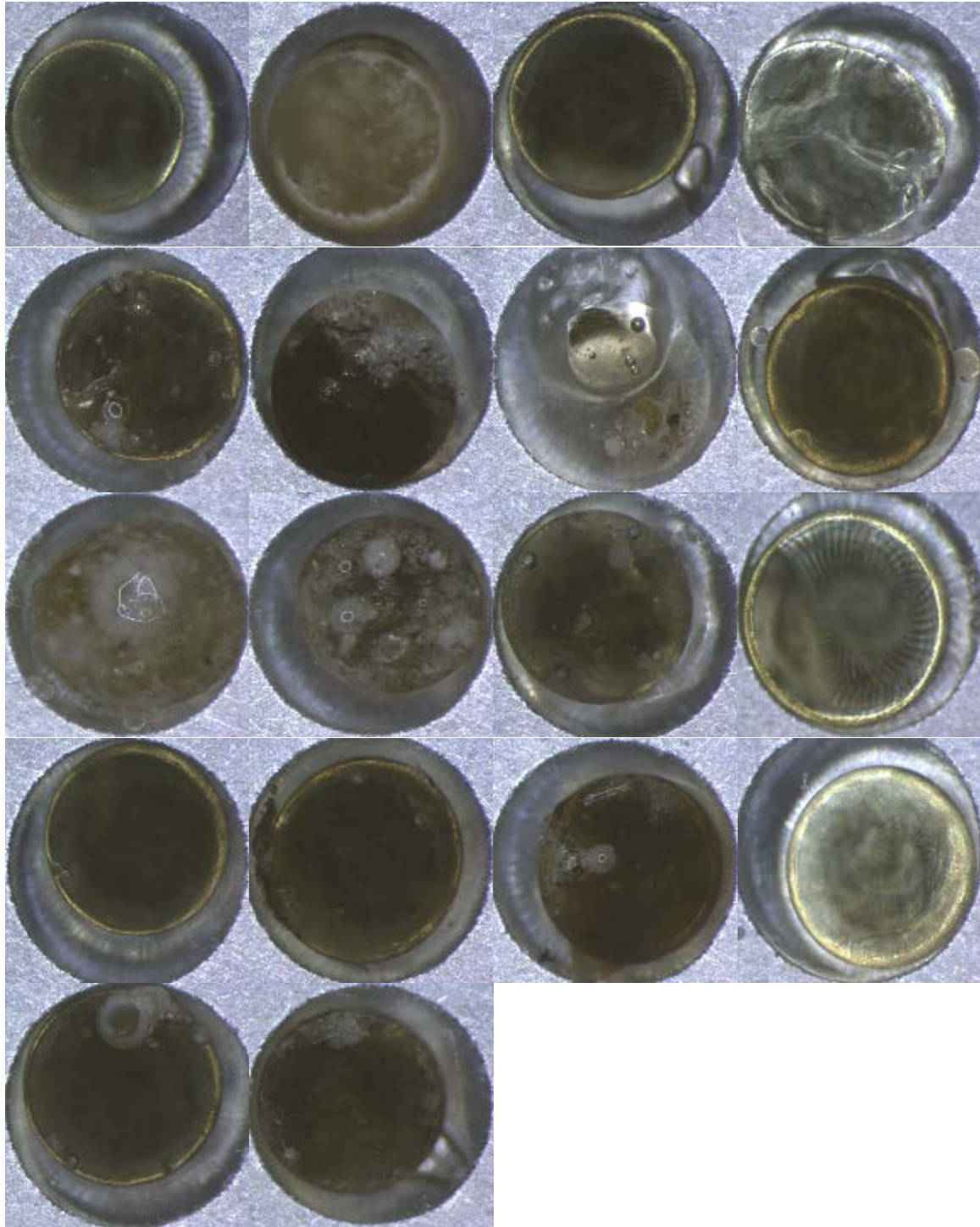
Figure 17. Optical Spectroscopy of samples 33 to 50 numbered from left to right.

The optical spectroscopy revealed a wide range of physical characteristics for the fallout samples including a range of colors from clear to dark brown. Melt characteristics include features such as partial melt inclusions, vortex swirls, bubbles or voids, and optical clarity. Based on previous studies of fallout samples, these features indicate that this sample set includes many of the expected fallout types from a near surface weapon detonation [11] [3] [6] [10] [12]. With this wide fallout sample range, the validity of the resulting model is further supported and provides a useful model for classification of fallout samples from historic weapons tests.

4.2. Autoradiography

Due to the time since the event, it is assumed that only the actinide fuel is left to produce radiation, thus the direct exposure on the image plate is due to the spontaneous decay of the unspent nuclear fuel [3] [12]. As such the autoradiography provides the spatial location of the actinides along with the relative activity within each fallout particle. As alpha particles have a short mean free path and deposit energy locally these energy depositions will record the location of the activity on the image plate within each particle. With direct contact between the film and the particles no magnification of the fallout particles occurs during the exposure. The intensity of exposure is directly related to the amount of unspent nuclear fuel in the sample. An initial exposure time was estimated based on the average activity of the fallout samples prior to the mounting and grinding process. An initial exposure time of 18 hours was used to prevent overexposure. This was adequate to provide enough exposure to image the particles without saturation. A digital processing method provided a secondary control measure to ensure proper

43

exposure without pixel saturation. The resulting raw data was processed using National Institute of Mental Health's program, ImageJ [25].

When viewing the autoradiography image, areas of higher actinide activity and concentration appear as darker pixels as shown in Figure 18. From nuclear physics, we know that alpha particles from a nuclear decay are born monoenergetic and result in sharp local energy deposition [11]. This local deposition will cause a local exposure in the image plate producing clear images. Similarly, beta particles from nuclear decay processes have a spectrum of energies and linear energy deposition as they move through a material. This linear deposition spreads the energy across regions which blurs the image [3]. Based on the total intensity recorded for a particle, it is possible to determine the relative activity within a sample. To a limited degree, the resolution of the image can indicate the type of energy that was deposited in the film plate as indicated by the energy deposition of the types of particles causing the exposure.
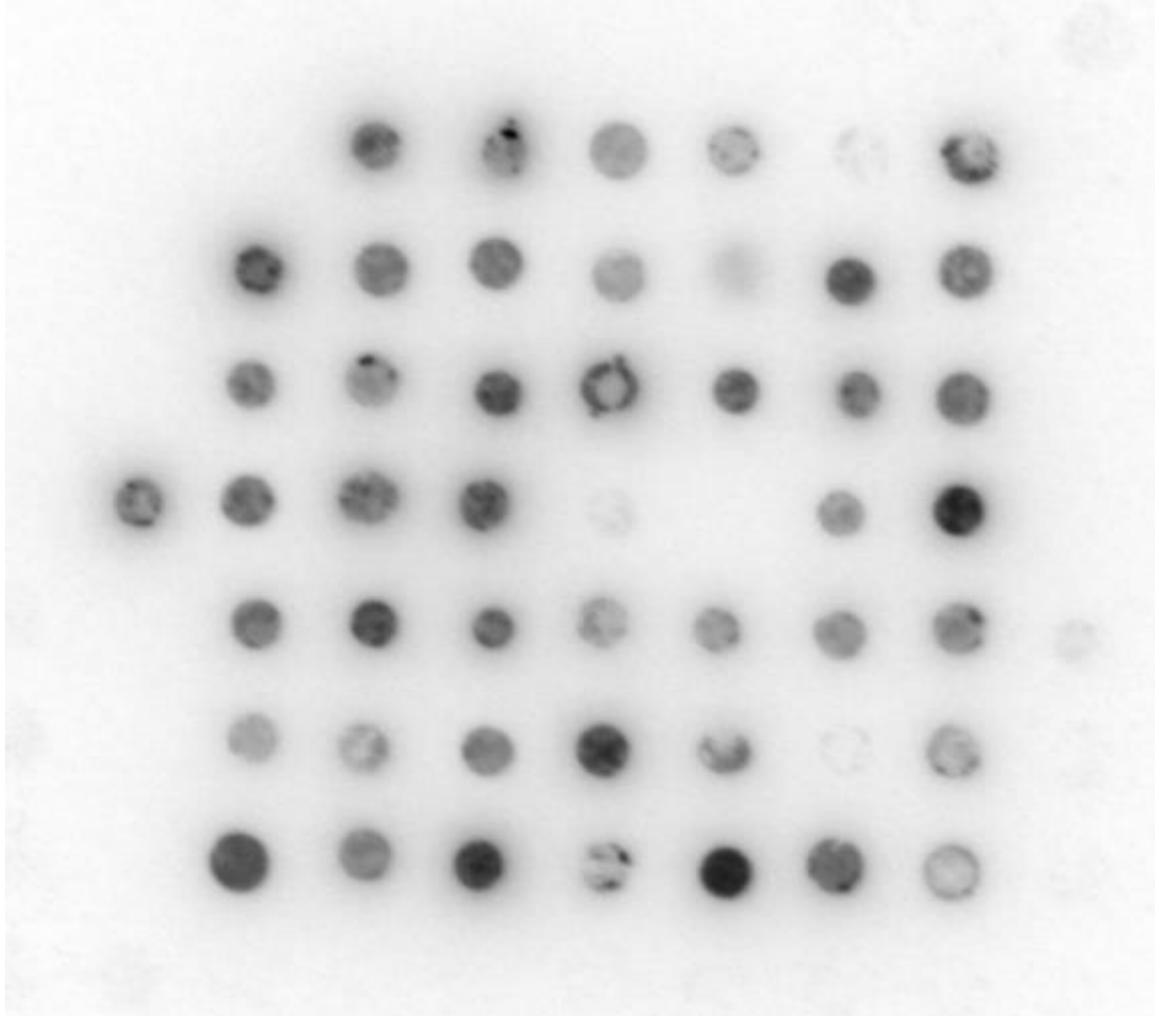
Figure 18. Autoradiography of all 50 samples numbered from left to right. Exposure to radiation results in exposure on the imaging film. Higher radioactivity in a sample results in a darker image.

With ImageJ, it is possible to investigate each sample and produce a multitude of

surface plots, scaling, transformation and other image processing options to build an

anecdotal understanding of each fallout sample. Comparison of physical characteristics

and autoradiography images can provide some information about each sample to help

understand the fallout bulk characteristics. Several of the fallout samples registered

minimal or no discernable activity on the image plate. Since the image plate is recording

alpha and beta energy deposition these samples likely had surface activity that has been

45

removed by the preparation process or is enclosed in the epoxy. With the short mean free path of alpha particles, any surface radiation would be encased within the epoxy and unable to deposit energy on the film [11].

4.3. EDS Spot Sample Model

The fifty samples were analyzed using the EDS function on the Inspect F SEM at LLNL using the settings recorded in Table 2. The highest resolution that would keep all samples in the field of view during the spot sampling was selected. A uniform 10×10 grid and magnification ensured an even density per volume of sample points for each sample, reducing any bias on the model from larger samples. With a uniform grid, it is inevitable that some grid points did not fall on the sample but on epoxy, cracks, or vesicles. These data points provide no elemental spectroscopy of the fallout samples and could potentially affect the resulting model. After removing these grid points a total of 1948 data points were collected to form the basis data set for the elemental model.

The resulting model produces a new mathematical construct that can be used to investigate the covariance between the elements of interest. The most important validation of the model is based on Kaiser's rule, the Scree Test, and portion of variance explained. These methods are used to identify the statistically important number of principal components. To capture 100% of the variance requires a total of eight eigenvalues. Every measurement has some level of uncertainty and noise. Using every principal component ensures that the model represents the data points but also the uncertainty and noise. The statistical noise, variations in machine error and fitting routines are not statistically important, nor do these variations represent the fallout

46

properties and should be removed. Using PCA it is easy to identify these variations due to machine and fitting error. The Scree test identifies inflection points as a method of determining the statistical significant of an eigenvector's importance to the solution of a problem [26]. An inflection point is one that can be described as a knee or bend in the trend line of the eigenvalues when plotted against the principal component number. These inflection points within the eigenvalues are shown in Figure 19. The inflection points occur at PC's 2, 3, 5 and 7. By this test one, three, five, or seven PC's are required to describe the system.
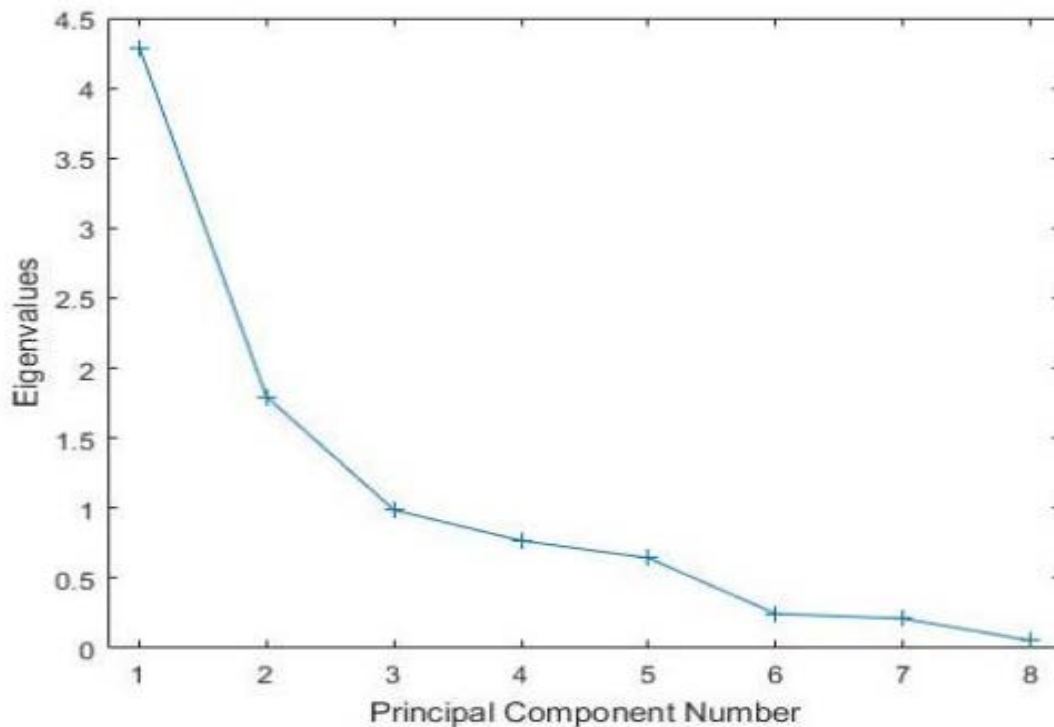
Figure 19. Initial eigenvalues for the resulting model as calculated from the EDS spot data.

To identify the correct number of statistical PC's, Kaiser's rule was also applied. Kaiser's rule states that the statistically important eigenvalues will be greater than one. Eigenvalues that are greater than or equal to one contain at least as much information as a

47

single variable from the system [26]. By looking at the eigenvalues in Figure 19, Kaiser's rule indicates that two principal components may be required to describe the system as the third eigenvalue is 0.987. However, this describes only approximately 60% of the variance in the system leaving nearly 40% unexplained, which by the proportion of variance captured theorem produces an unsatisfying model. This last theorem states that a good analysis will capture at least two-thirds of the variance in the system [26]. Using three principal components 78% of the systems variance was captured by the model as shown in Figure 20.
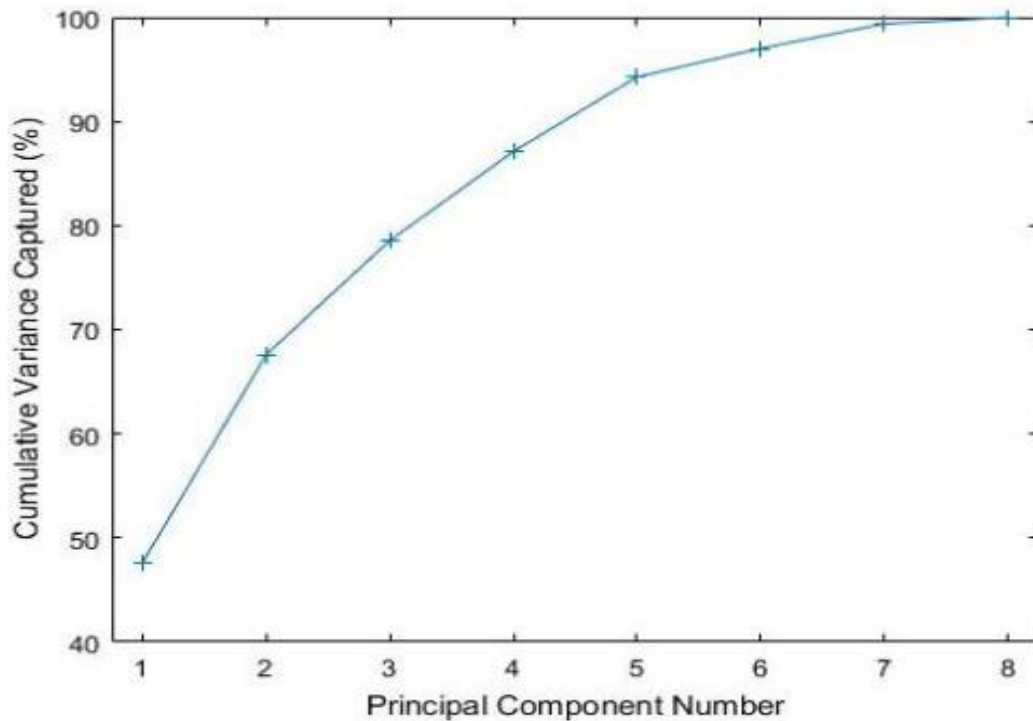
Figure 20. Initial percent variance captured per principal component number as calculated from the EDS spot sample data.

To satisfy all three validations, the fallout model should have three principal components. As expected, each additional eigenvalue added to the model captures less variation. Using PLS Toolbox the final validation of the model is completed

48

automatically. PLS toolbox removes one variable at a time to ensure the eigenvectors represent the most important variations in the system while solving the system of equations returning the best fit from the multiple solutions. This final check ensures that the first eigenvalue is the most statistically important to explaining the model.

With three principal components, the model identified one key feature. This feature is the number of compositions in the system. Since the principal components form an orthonormal basis there must be $n+1$ compositions. With these three principal components, the data set has four main elemental compositions. This conclusion agrees with the research performed by Holliday [12].

After validating the sufficient number of principal components, the powerful tool of PCA is now available. Recalculating each data point's elemental concentration with the principal component weighting factors reframes each data point as a new value. The resulting value is known as a score for that data point in the new reference frame of the principal components. The scores from one principal component can be plotted against the scores from another principal component much like a traditional Cartesian x-y coordinate system. It must be stressed that these principal components are a mathematical construct representing the chemical variations observed in the fallout samples. These scores for the 50 samples and 1948 data points are shown in Figure 21 plotted with PC 1 on the x-axis and PC 2 on the y-axis.
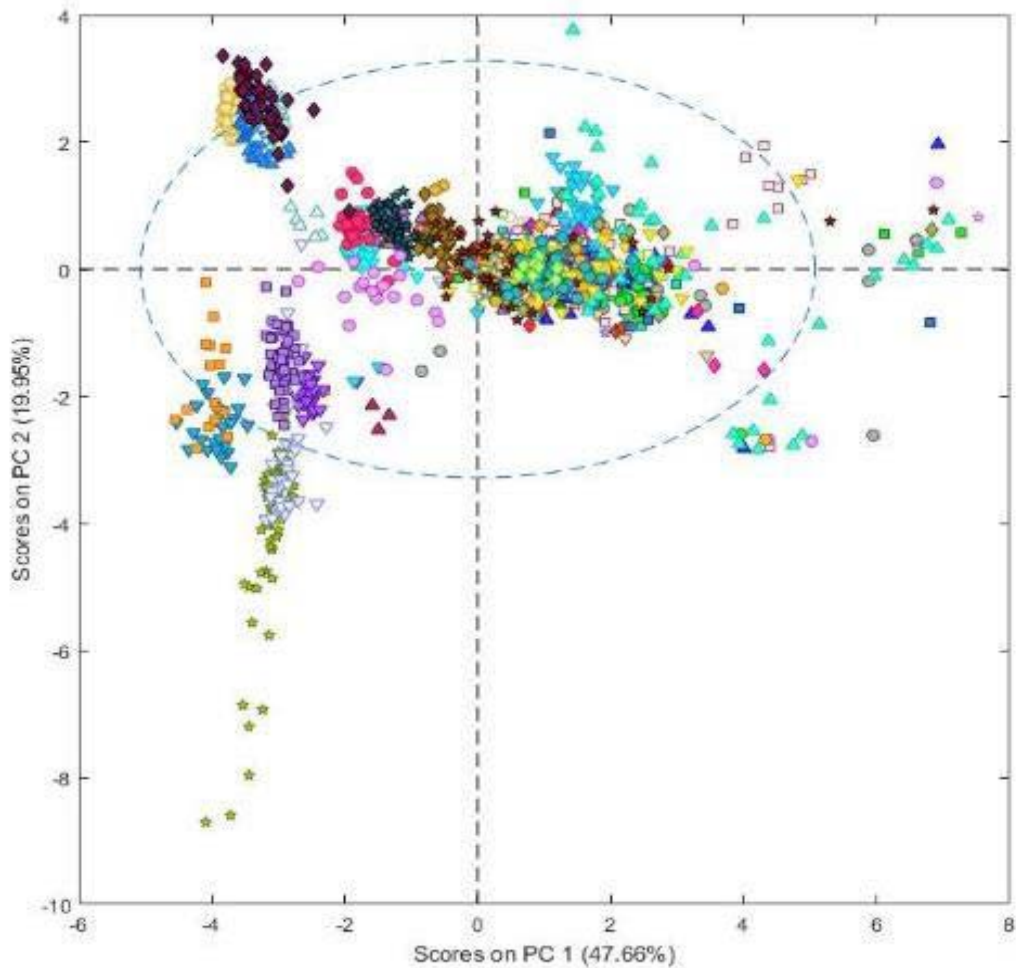
Figure 21. Scores for EDS spot sample data bi-plot for PC 1 vs PC 2. The bi-plot represents the samples data points in PC space. Sample points with similar chemical variations will be plotted in the same region. Sample points with little variation will be closely plotted in PC space. A scattering of data points from a sample indicate regions of wide chemical variation in that sample.

By plotting these scores one sample is identified as a possible concern. The scores for sample three (green stars, bottom left quadrant) indicate a strong negative correlation to PC 2 due to the negative scores along the y-axis. However, this linear skew could also indicate some analytical problem with that sample. Upon investigation, this quadrant and direction on PC 1 vs PC 2 scores is due to magnesium as shown in Figure 22. Investigation of the raw data for this sample shows that the magnesium standard

50

deviation was five times higher than the standard deviation for any other element in the sample. The standard deviation for this sample was twice as high as any other samples in this region of PC space.
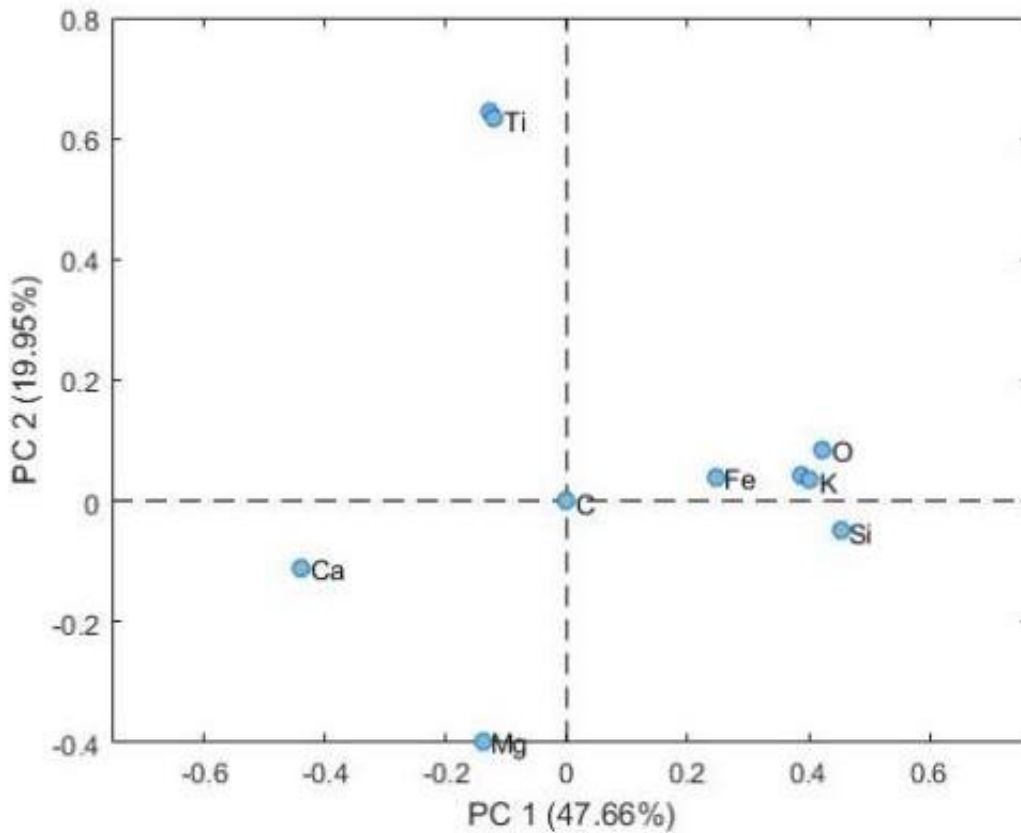
Figure 22. Initial elemental scores for PC 1 vs PC 2.

Using PCA identified a potential problem in the data set otherwise not observed and allowed identification and analysis of this problematic sample. A visual inspection of sample three under high BSED magnification identified a crystalline or porous surface structure. These surface defects could have been responsible for errors in the spectrum or indicate dissolution, or damage during the grinding process leaving a rough surface. This analysis suggests that sample three should be removed from the model.

51

Initially, carbon was expected to be zero and was included in the model to verify that no interference from the carbon coating preparation was being forced into the model. Since carbon was always found at the origin of the scores plots, this assumption was proven to be true allowing that element to be removed from the model. Oxygen often has a high variance when conducting EDS. As every element is assumed to be an oxide, oxygen can be removed from the model for elemental variance without loss of integrity in the model while improving the models ability to identify variance in minor elements that may be overshadowed by the higher variability of oxygen.

Removing the data points from sample three and removing the variables of oxygen and carbon produced a slight change to the overall model. The same number of principal components were identified for the final model using the same criteria as before. As shown in Figure 23, the eigenvalues for this system are 3.7, 1.5 and 1.17 satisfying the Scree test (inflection points) and Kaiser's rule (greater than one eigenvalue) as explained previously.
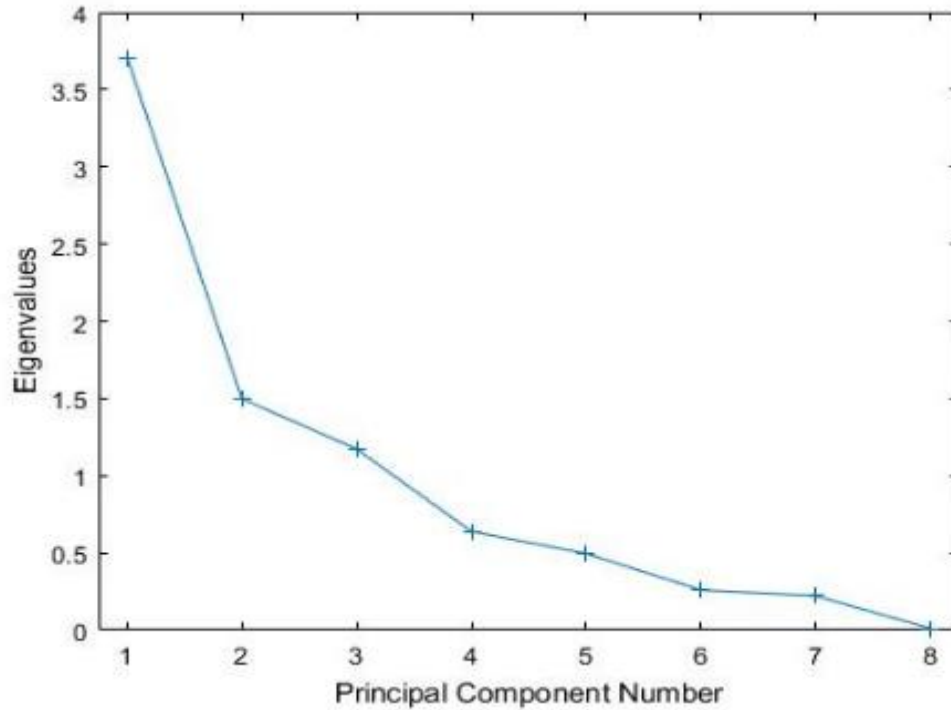
Figure 23. Eigenvalues for each principal component for the final PCA model based on the EDS spot sample.

The increase in principal component three's eigenvalue supports the decision to remove sample three due to the large variance in the magnesium. These three eigenvalues describe 79.66% of the variance in the EDS spectrum data, as shown in Figure 24, supporting the proportion of variance captured theorem. As in Figure 21, the scores for the data points are plotted to identify any trends or possible problematic data points or samples. When looking at the scores plots it is customary to plot PC 1 vs PC 2 (Figure 25) and PC 1 vs PC 3 (Figure 26). In these bi-plots each sample is a different symbol allowing visual representation of the variations within a sample and within the entire data set. Plotting PC 2 vs PC 3 does not provide any additional insights into the system, the variance is already captured by using PC 1 versus the other two.

53
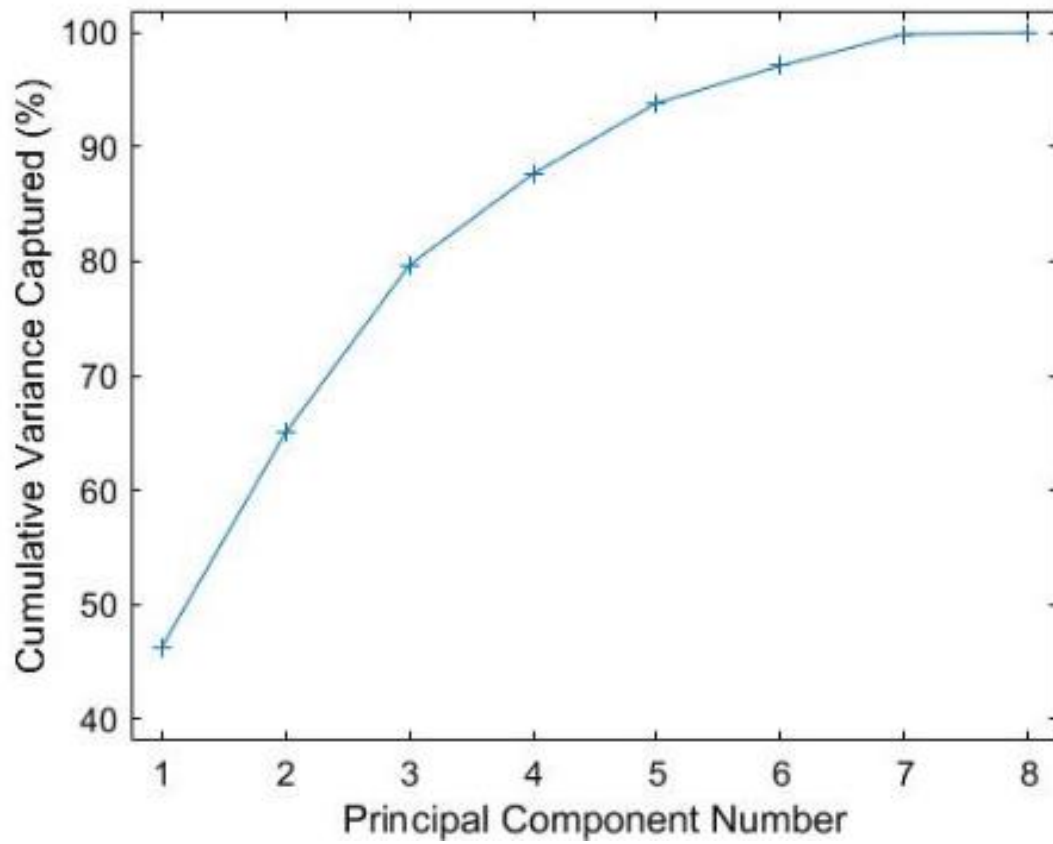
Figure 24. Cumulative percent variance captured by each principal component.

54
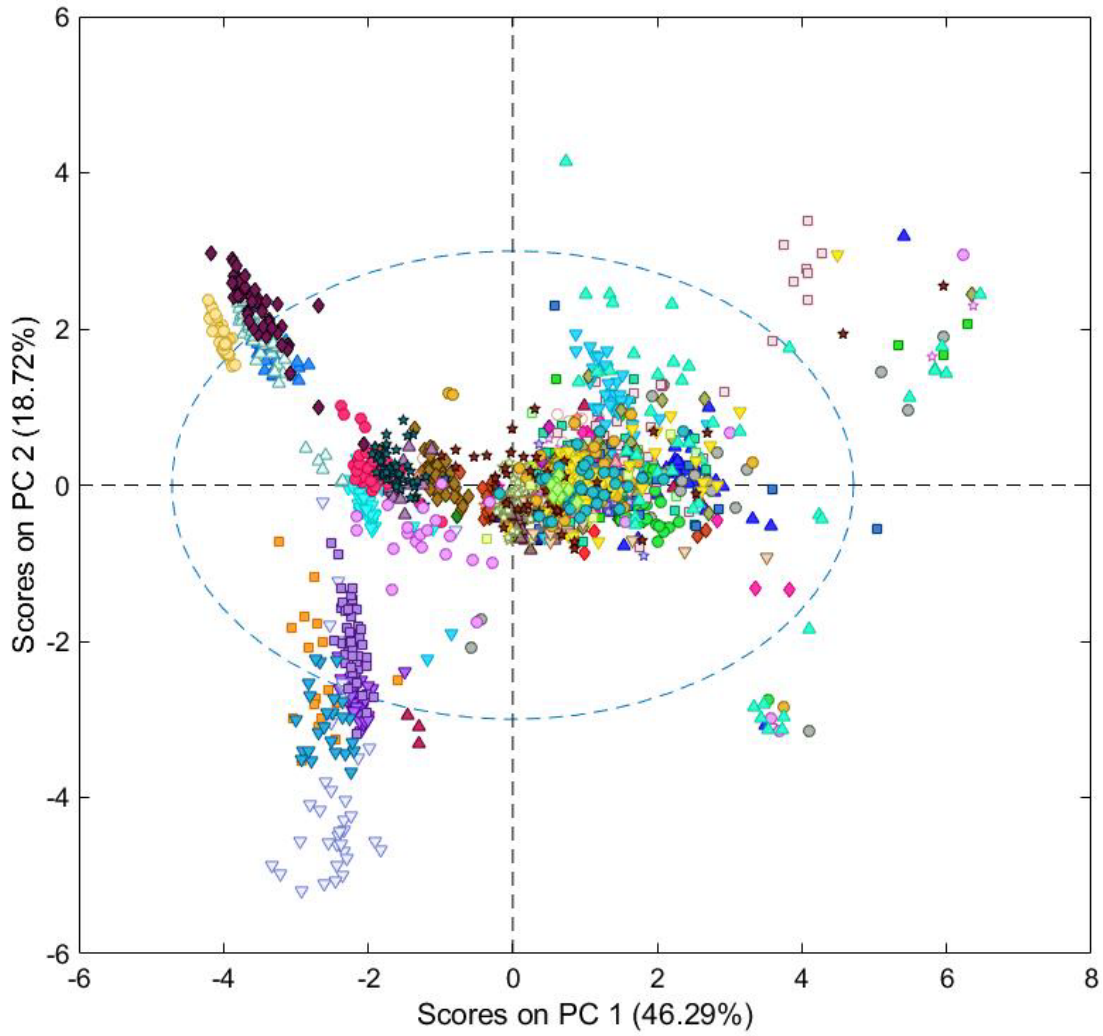
Figure 25. EDS spot sample scores for PC 1 vs PC 2. The dashed ellipse represents the 95% confidence interval for the generated solution and resulting scores.

55
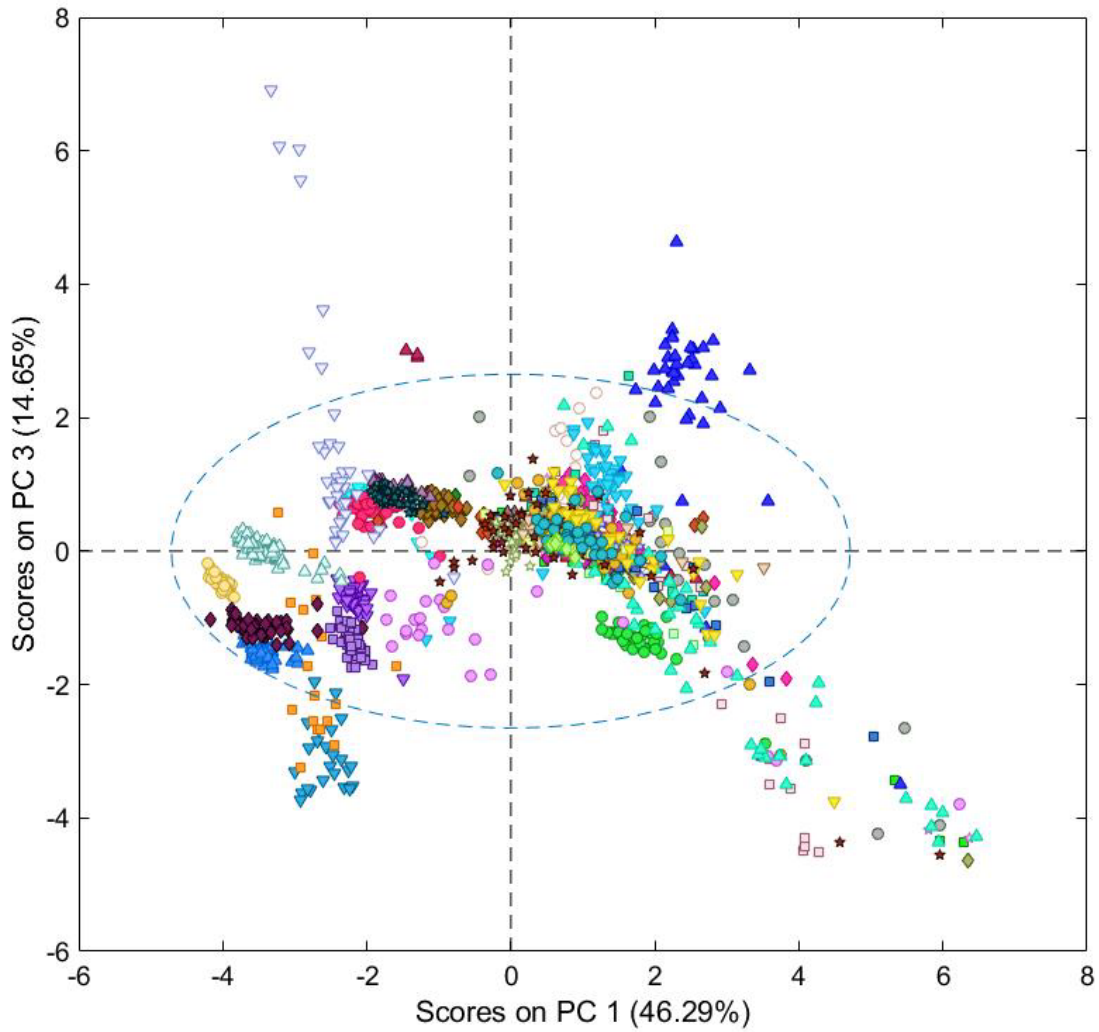
Figure 26. EDS spot sample scores for PC 1 vs PC 3. The dashed ellipse represents the 95% confidence interval for the generated solution and resulting scores.

The scores do not provide a full description of the system. Additional information is provided by the element vectors for each principal component. These vectors describe how the variance in each element causes the scores to shift along each axis. For example, when viewing the element vectors for PC 1 vs PC 2, in Figure 27, a sample that has a

56

higher concentration of aluminum or titanium will be found in the top left quadrant.
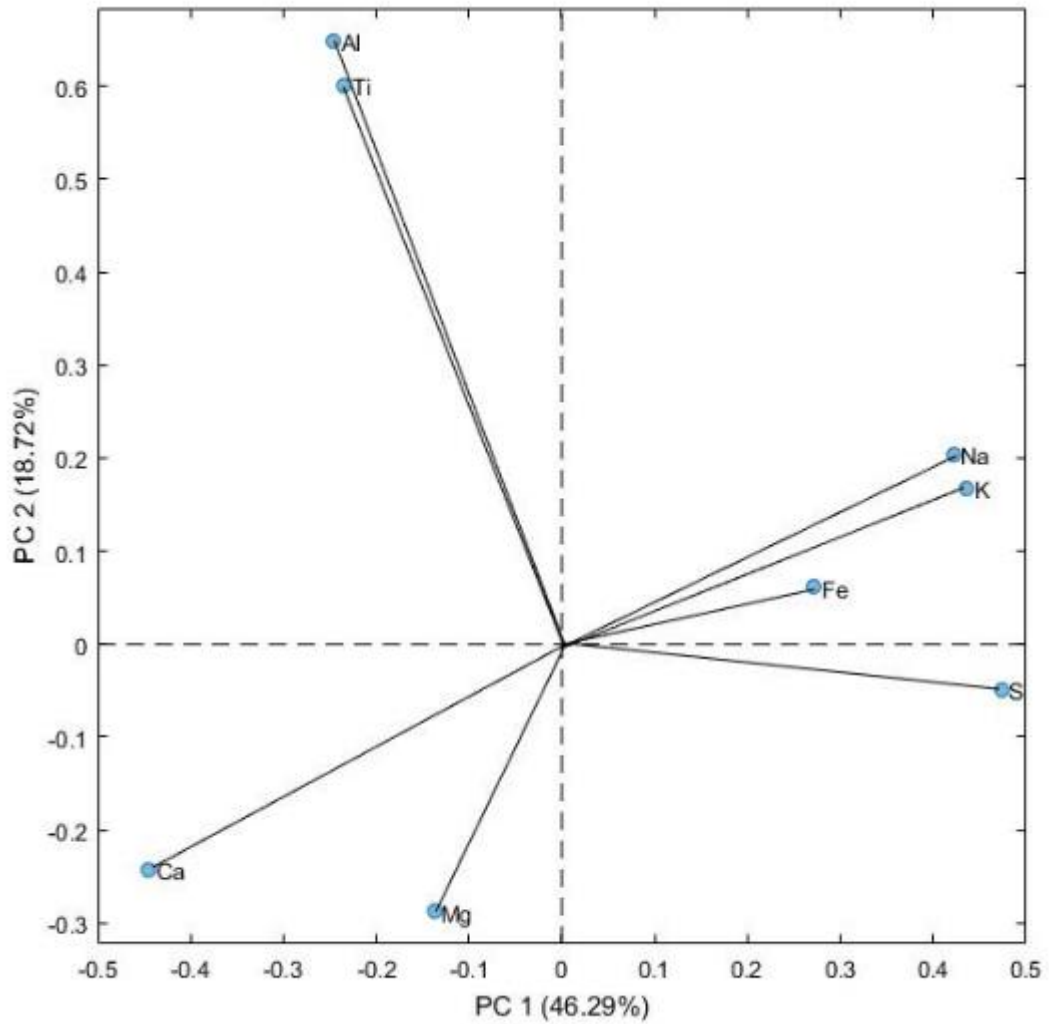
Figure 27. Element vectors for PC 1 vs PC 2 indicating the weighting factors and correlations for the elements in the model.

This also indicates a strong positive correlation in PC 2 for those elements and a negative correlation in PC 1. Both of these facts are developed by looking at the scores for the individual elements as plotted in Figure 27. These correlations developed from the scores will be key to understanding how the actinides are incorporated into the fallout particles and the major elemental compositions. Visible correlations are possible by

57

viewing the average intensity of the autoradiography for a given sample and its location

on the bi-plot in Figure 25 and Figure 26. Once a quadrant and vector is established for

the samples average score correlations can be made about the major elements and the

nuclear fuel. A benefit of the multiple principal components and plotting different

configurations is apparent when viewing PC 1 vs PC 3 in Figure 28 resulting in the vector

separation of aluminum and titanium. This separation can provide the key to

understanding the various element's affinity to the actinides during fallout formation.

From the PCA model the final elemental weighting factors for each of the three

principal components can be recorded. These weighting factors are the values from the

solution assigned to each eigenvector while solving the covariance matrix. Each value is

recorded in Table 4.

Table 4. Principal component elemental weighting factors for the EDS spot sample model.

|	Na	Mg	Al	Si	K	Ca	Ti	Fe
PC 1	0.4221	-0.1378	-0.2462	0.4736	0.4364	-0.4455	-0.2347	0.2718
PC 2	0.2045	-0.2877	0.6490	-0.0488	0.1678	-0.2425	0.6009	0.0616
PC 3	-0.1193	0.6761	-0.0733	-0.0286	-0.0822	-0.1903	0.3246	0.6117
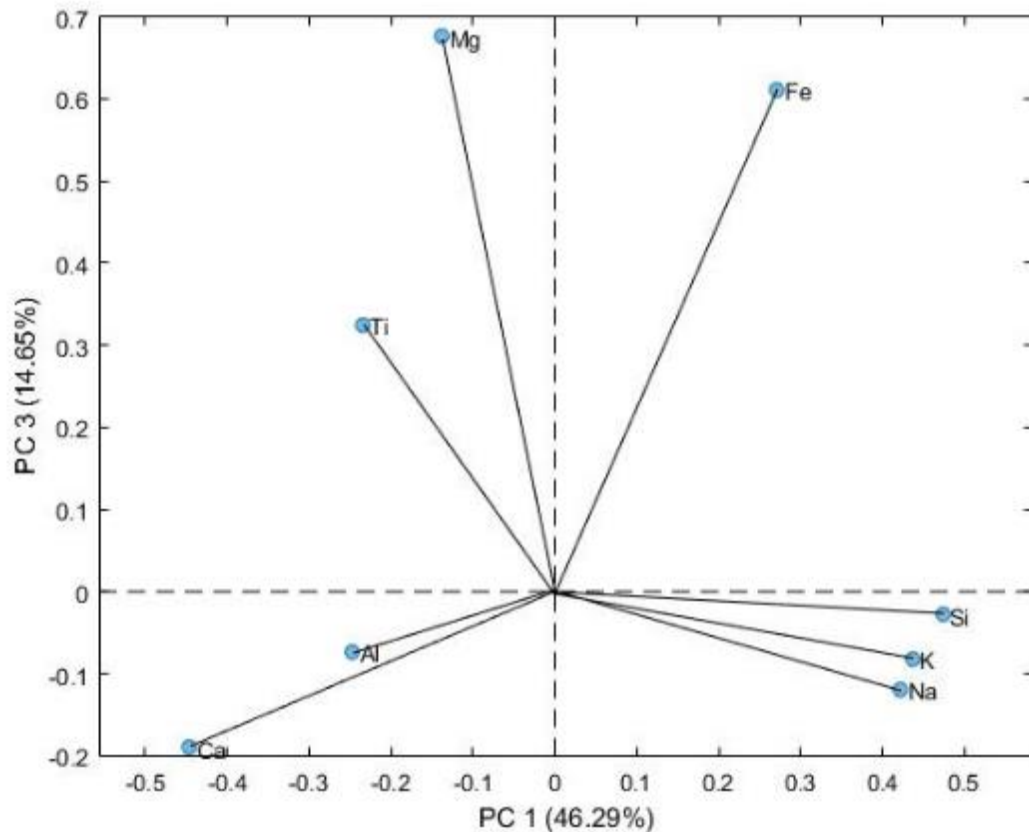
Figure 28. Element vectors for PC 1 vs PC 3 indicating the weighting factors and correlations for the elements in the model.

Each of the samples was further classified as homogenous or heterogeneous using the BSED catalog of the samples. A class of "porous" was added to the traditional homogenous and heterogeneous classification to identify the samples that exhibited the porous surface defects. Pull out is used to describe a surface that has been marred during the polishing process. Given that all of these samples have similar physical characteristics, pull out could be due to the composition's reaction to the preparation to a hemisphere or the natural structure of these samples due to another factor not examined. A high magnification of sample 34 is shown in Figure 29 to highlight the porous structures.

59

| det | mag □ | HV | spot | WD | dwell | HFW | ⊢————— 4 µm ————— |
| ETD | 20 584 x | 15.00 kV | 5.0 | 10.0 mm | 30 µs | 12.4 µm | DW1 25_34_SE_Edge_HighMag |
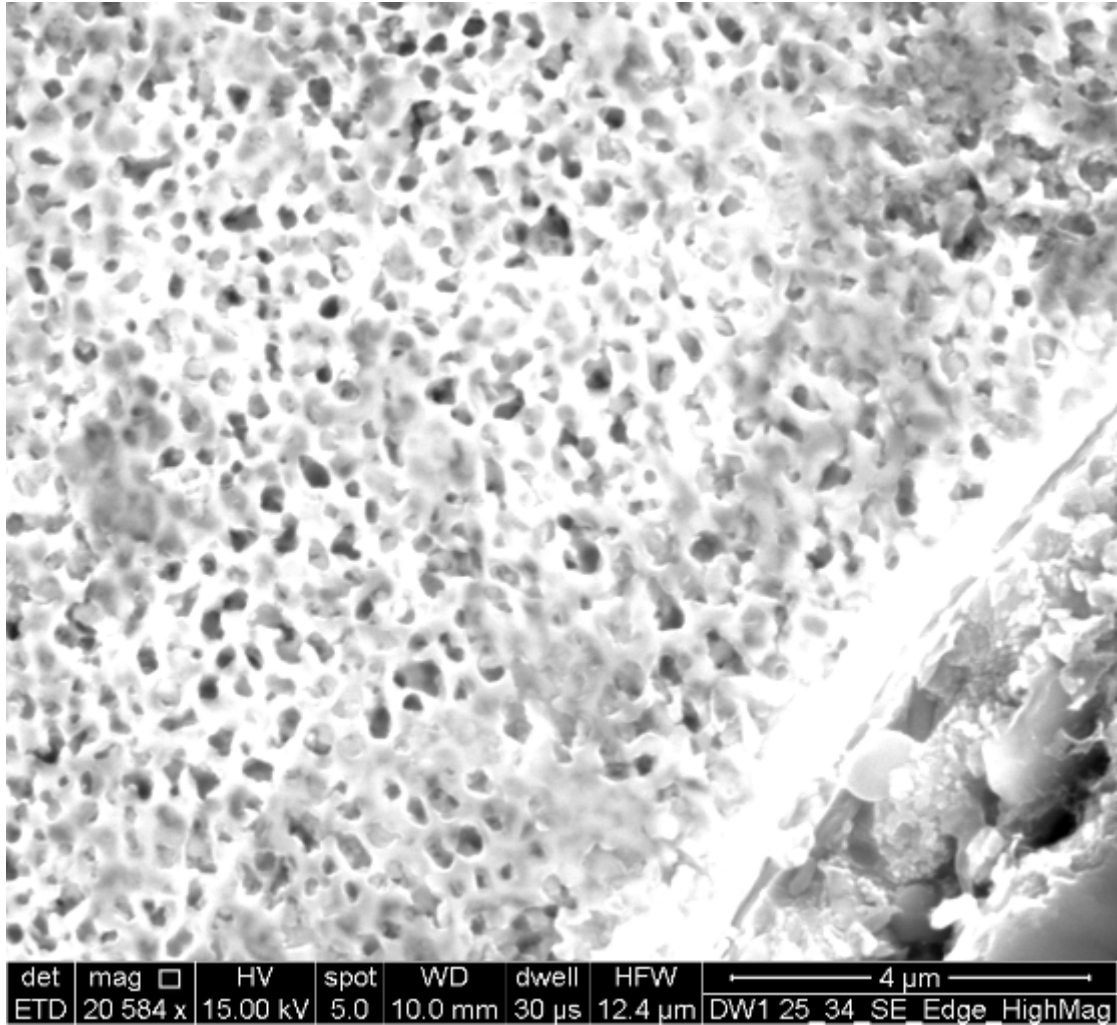
Figure 29. High resolution BSED of sample 34 edge highlighting the porous surface features.

All of the porous class samples appears to have the same characteristics under optical, BSED and EDS imaging. This classification system can be used to provide some insight as to the elements that are predominate in each of the categories. Additionally, it can help to reduce the amount of information that is presented in a bi-plot allowing analysis of bulk properties that would otherwise be hidden among the individual sample characteristics. A representative sample for each of the three classes is shown in Figure 30.
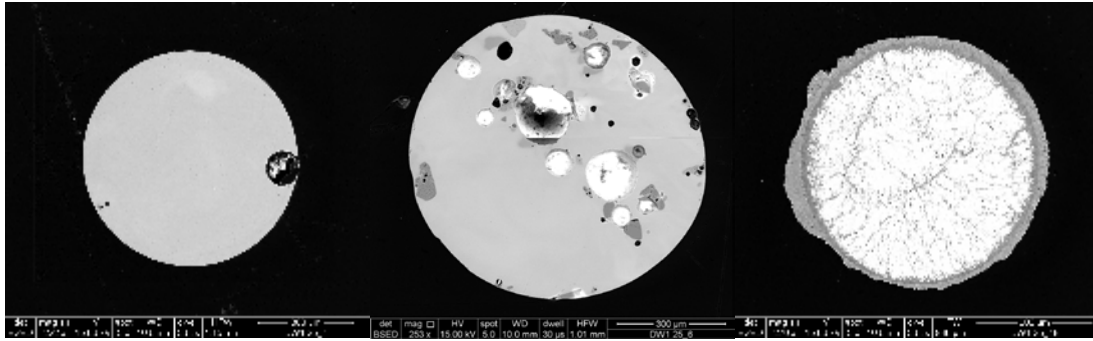
Figure 30. Representative samples of the three classes homogenous, heterogeneous, and porous.
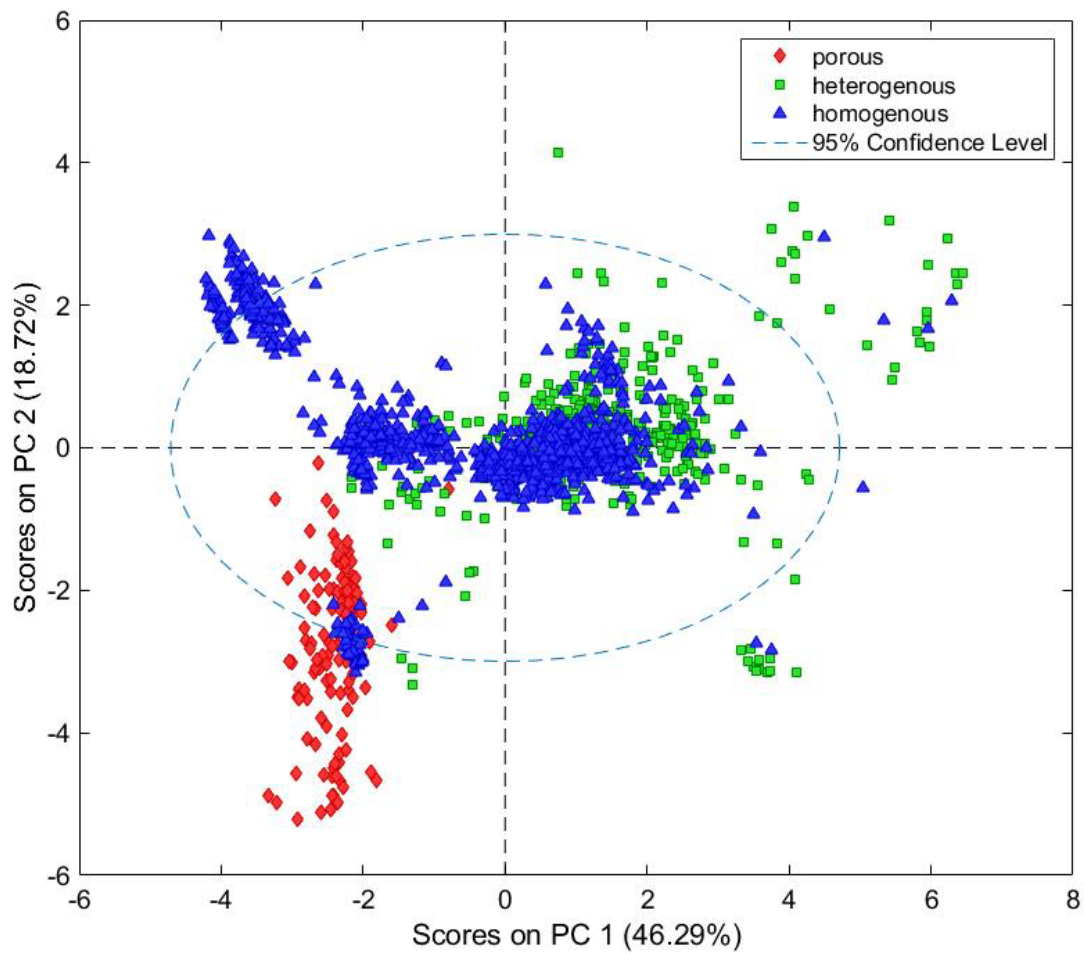
Figure 31. Sub-categorized bi-plot for PC 1 vs PC 2 showing the grouping of homogenous, heterogeneous, and porous samples.

The bi-plot of the sub categorized samples is shown in Figure 31. With this categorization, it is easy to identify the similarity of the porous samples is due to a specific elemental variance. This variance caused the scores for these samples to be plotted in the bottom left quadrant with a definite trend shown as the red triangles in Figure 31. The nearly vertical distribution indicates that this is due to magnesium in the samples verified by Figure 27 and raw EDS spot data. Clearly, the scores are dominated by a variance in magnesium for these samples. A visual inspection in Figure 32 of the autoradiography for this class shows a non-uniform distribution of activity through the sample and of a medium intensity compared to other samples. This grouping included samples 3, 9, 18, 27, and 34, with sample 3 removed from the model and not shown.
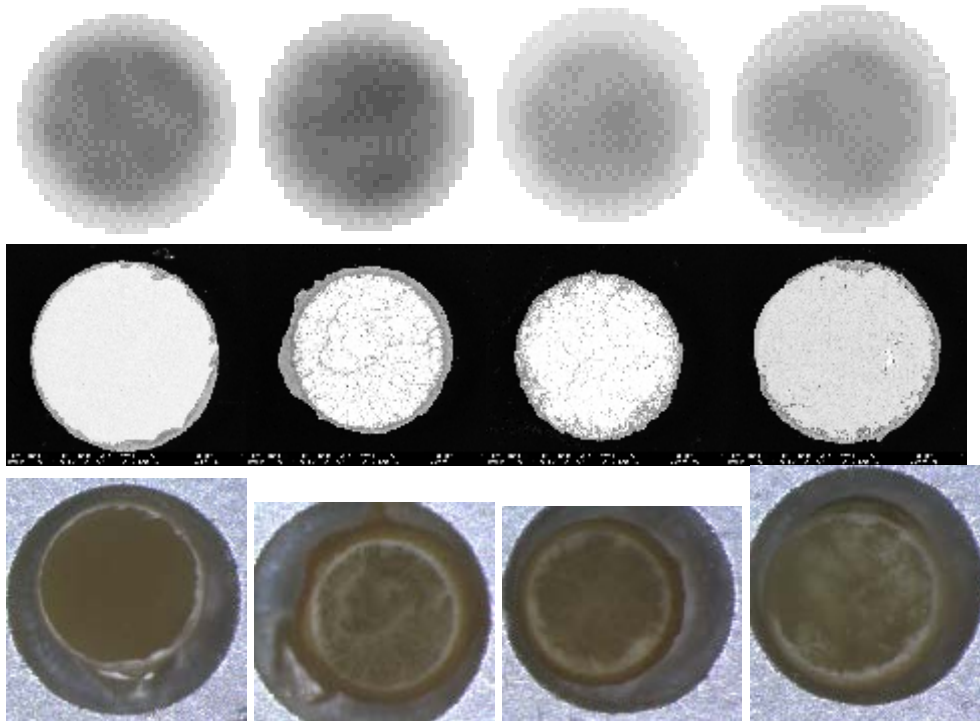
Figure 32. Autoradiography, EDS and optical images of the sub-classification of porous surfaces containing samples 9, 18, 27, and 34.

It is also easy to identify a homogenous group in the top left quadrant of the bi-

plot in Figure 31. This group consists of samples 12, 22, 44, and 48. This grouping is interesting as it contains a homogenous group of samples of similar physical characteristics. This grouping contained all of the clear samples and those of the highest uniform autoradiography intensity. This indicates a high percentage of actinide in the fallout sample that has been uniformly distributed throughout the volume, making this group the highest forensic value group to recover unspent fuel. From Figure 27 this is due to a correlation to aluminum or titanium. From Figure 26 it is apparent that the correlation is due to the aluminum and not the titanium as the scores change quadrants matching the change in aluminums scores from Figure 28 and Table 4.
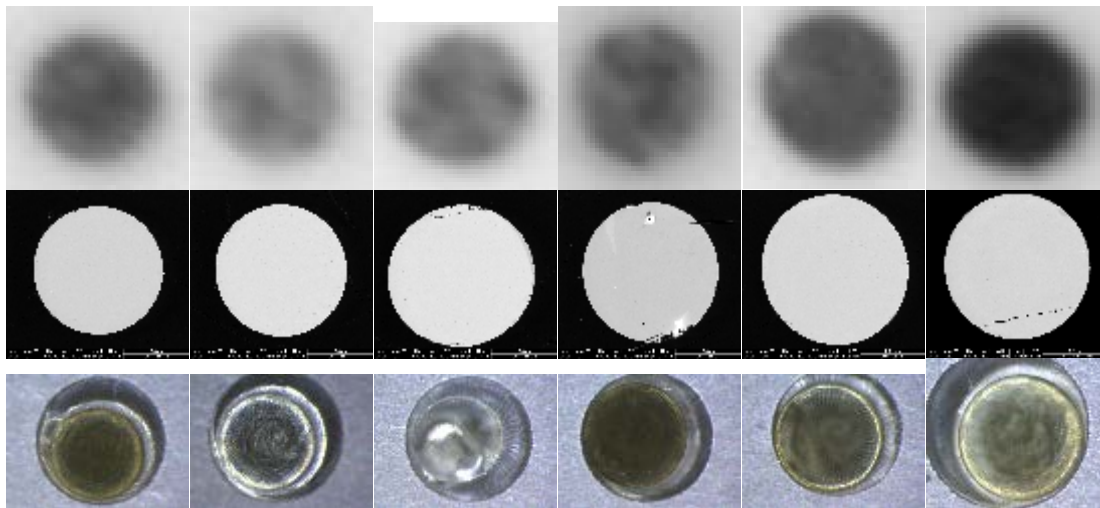
Figure 33. Autoradiography, BSED and Optical images for samples 12, 14, 22, 24, 44, and 48.

The mixed grouping in Figure 31 consists of homogenous samples with surface defects, cracks or visible swirls and heterogeneous samples. The heterogeneous samples contained inclusions, indicators of partial melt, voids, bubbles, and other unique physical features. A common elemental feature of this group was silica, sodium, and potassium with a general non-uniform activity distribution. For high value forensics, this grouping

63

represents a mixed result and should be a secondary choice over the clear homogenous group or the porous group. Based on these findings the anecdotal results suggest that the samples with low silica, potassium, sodium, and iron are more likely to contain unspent fuel. To improve this from an anecdotal to a quantitative finding, the spot sample model will be used to describe individual samples and serve as the basis for the characteristic x-ray mapping model.

4.4.   Characteristic X-ray Mapping

Currently full characteristic x-ray mapping of samples 2, 13, 28, and 47 have been completed using a 1600 x 1600 pixel resolution. These scans were accomplished at LLNL using the SEM over the course of four days each. The length of time is necessary to build up enough counts of the minor elements in each pixel for the selected resolution. As the scan is completed, images are developed for each of the elements with higher concentrations of each element producing a brighter pixel which can be seen in the calcium and silica images from sample 47, shown in Figure 34. For each of the four fallout samples an image was developed for calcium, aluminum, carbon, iron, potassium, magnesium, sodium, oxygen, silica, and titanium. These images are then aligned and saved into a new image matrix that is $1600 \times 1600 \times 10$. The matrix then contains the information for each element at each pixel. This matrix now serves as the complete elemental composition for each sample.
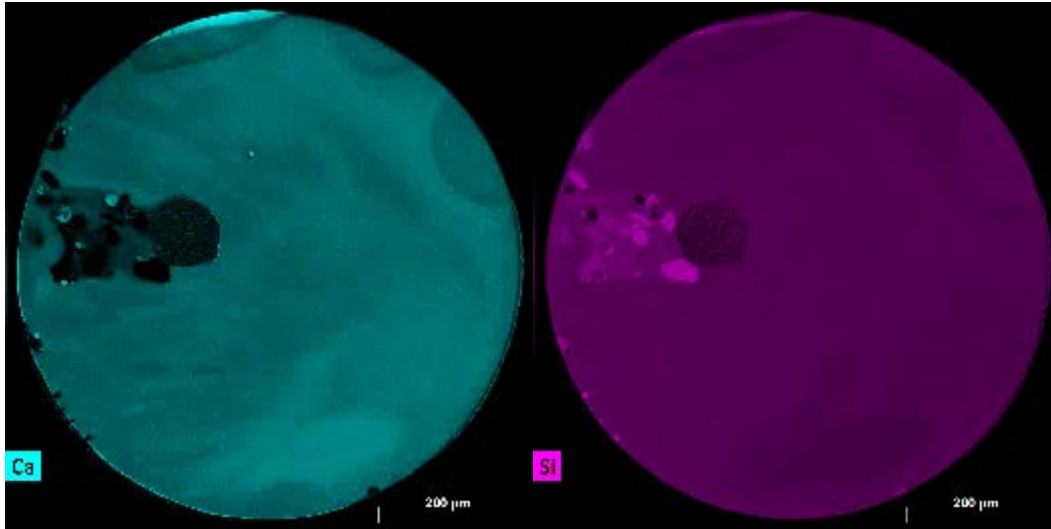
Figure 34. Calcium and silica raster scan image for sample 47.

The autoradiography image for each sample is approximately 40×40 pixels. This low-resolution image must be matched to the high-resolution raster map. This highlights the significant problem with the resolution of the SEM and the autoradiography image. Because of the disparity between the SEM and the autoradiography resolution, it was impossible to incorporate the autoradiography data into the spot data for a quantitative analysis. Using a full raster image with image processing software and scaling it is possible to match up the autoradiography data with the raster elemental data. PLS Toolbox incorporates an image analysis suite that can scale and pixel match between images of different resolutions. To improve computational time each of the raster images were scaled to 640×640 and then loaded into PLS Toolbox to map and align the raster images to the autoradiography. This produces a 640×640×11 matrix where the intensity of each element and the autoradiography intensity are recorded for each entry. Prior to running a PCA model or mapping the principal components from the spot data model, the epoxy and surface defects must be removed. Surface defects are identified using the

65

BSED, EDS, optical and SEM images. Removal requires identification of each pixel and suppressing or removing it in the master matrix. This is accomplished using the image processing suite within PLS Toolbox, shown in Figure 35. As each pixel is removed the data begins to represent the actual sample and not erroneous data points. These removed data points appear as black pixels in the image analysis suite providing a positive method of matching surface defects and data entries in the matrix.

Figure 35. Sample 47 full raster scan with removed surface defects and epoxy (top left image). Individual pixel scores for PC 1 vs PC 3 (top right), PC 3 vs PC 2 (bottom left) an PC 1 vs PC 2 (bottom right).

66

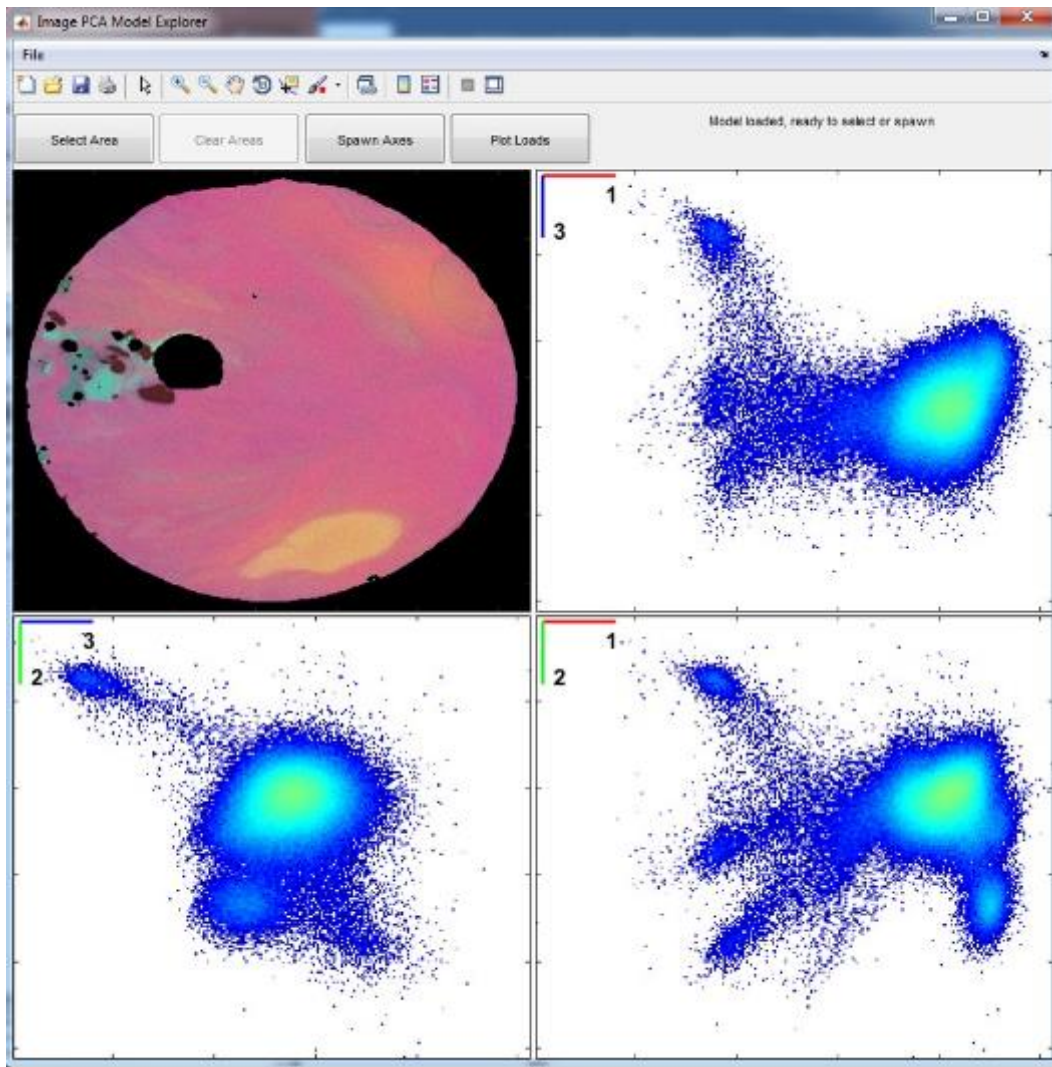The top left image in Figure 35 shows the full data set as an image where each pixel stores the elemental information. The pixels that are included are plotted in the three remaining scores plots. Within the image each included pixel is colored based on the PC scores using RGB theory while those removed from the matrix are black. When pixels are removed from the data set the image is re-processed as an individual PCA model. By processing each sample as an individual model each time data is removed the validity of each pixel in representing the sample is verified along with assisting in the removal of further surface defects. In the image set shown in Figure 35 pixels from surface defects will have scores significantly different from other pixels causing them to be on the extreme edges of the scores bi-plots and oddly colored, compared to neighboring pixels, in the data image. This process was repeated for the other three raster samples. The individual PCA model for the four images were used to verify surface defects were removed. No further information was derived from the image pre-processing analysis. With the raster data pre-processing complete several options exist. The data can be used to form a new model, like the spot data, evaluated using the spot data model, or evaluated as its own data set. Evaluating as its own data set allows identification of areas that are statistically different from the rest of the sample. This is important if we are trying to understand why the actinide is in one region in a particular sample but not distributed throughout the sample. If the fallout particle is not one particle but made up of several fallout particles coalesced together, a conglomerate, it can have a significant effect on the resulting model if viewed as one sample. The variation of this conglomerate sample does not represent a true fallout sample and has different

67

mechanisms that govern its development as a conglomerate particle and not individual particles.

Evaluating the Raster Data with the Spot Model

By using the principal components that describe the entire data set it is possible to describe each sample by its variations compared to the entire sample set. This comparison will be extended to the unspent nuclear fuel to identifying which elements are correlated with the actinides. After data pre-processing, the x-ray map is projected through the spot data model. This projection assumes the eigenvalues from the PCA model are the solutions for the raster data. Application of these eigenvalues to the data set allows direct comparison of each sample against the aggregate 50 sample data set. Each of the three principal components is assigned one of the three primary colors from red, green, and blue (RGB). Then, every possible color combination is possible by adding the various wavelengths together via RGB color theory [27]. Each of the RGB colors has a value from 0 to 255. A sample that can be represented entirely by one of the principal components would have a single color, as shown in Figure 36. For instance, if principal component one was designated as red and represented the fallout sample completely, it would have a value of 255, 0, 0. This basic representation is well suited for the elemental models represented by three principal components.
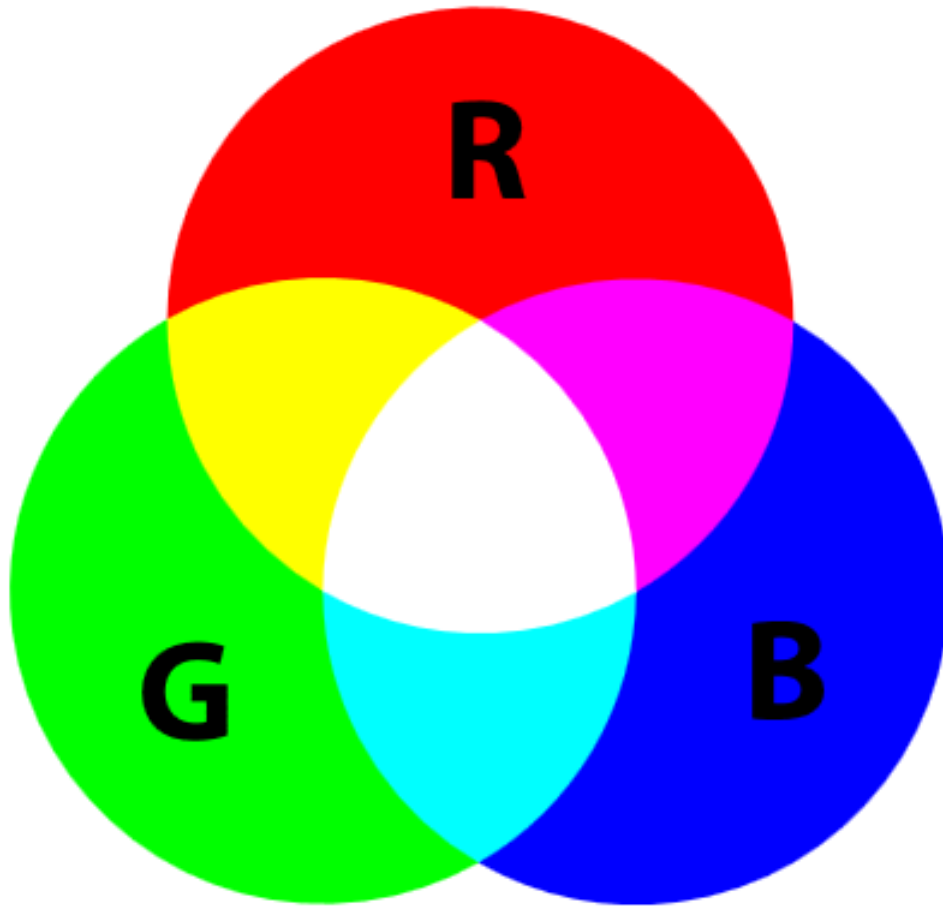
Figure 36. RGB color wheel, used with permission [30].

The four samples come from two distinct regions of the spot data model. Samples 2, 13, and 47 exhibit a positive correlation to PC 1 easily identified by the positive axis location in the bi-plot. The tight clustering in Figure 37 indicates that the elemental vectors are equal in weight, while sample 28 has a negative correlation to PC 1 but maintains the equal influence from the elemental vectors. With all the data points from these four samples clustered around the axis there is positive and negative correlation in PC 2 for these samples indicating that the variations captured by PC 2 are not strongly reflected in these samples. Figure 38 shows the scores for PC 1 vs PC 3.

69
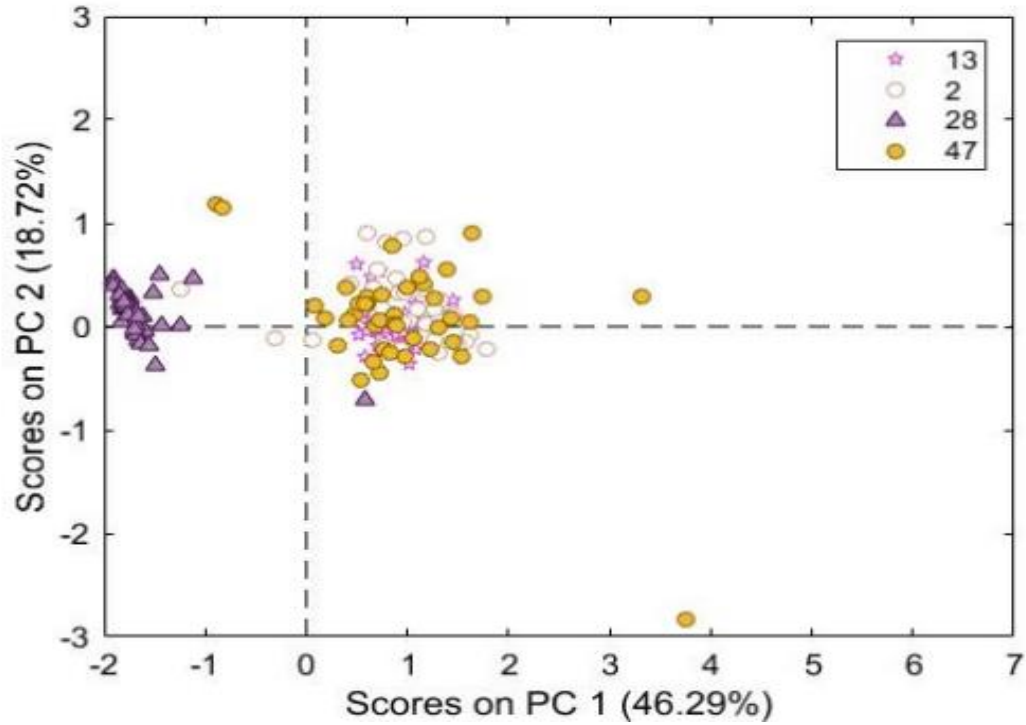
Figure 37. Spot data scores plotted for samples 2, 13, 28, and 47, PC1 vs PC2. The close grouping of the data points indicate that these samples exhibit little variation. Samples 2, 13, and 47 exhibit similar variations as evident in the grouping of the sample points on the bi-plot.

70
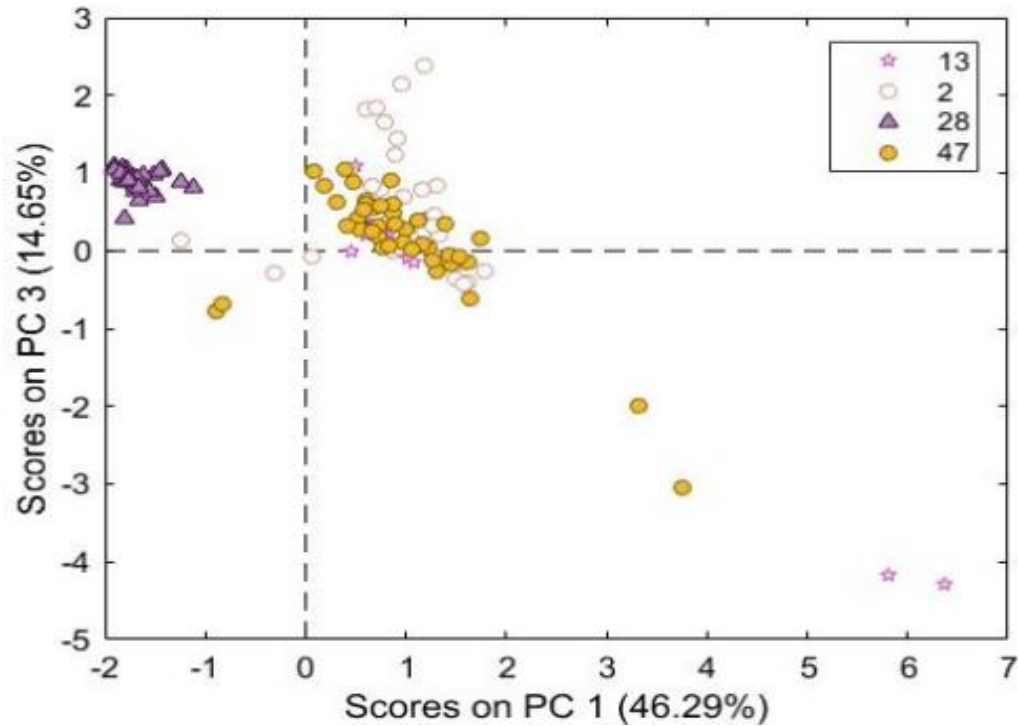
Figure 38. Spot data scores plotted for samples 2, 13, 28, and 47, PC1 vs PC3. Grouping of data points indicate that these samples exhibit little variation across the sample. The negative PC 1 position of sample 28 shows an anti-correlation to variations of the other three samples.

When all three principal components are used to color the four samples the resulting image gives us a three-dimensional representation using RGB color theory. These images combine the full raster data set with the elemental spot data for the entire fallout sample set. When investigating sample 28, in Figure 41, it is apparent that the middle of the sample is an even distribution of all three principal components [27]. Meanwhile, the outer rim is comprised primarily of PC 1 and PC 3. Using the individual coloring images for the PC's in Figure 41 it can be shown that a positive contribution to PC 1 and negative from PC 3 causes this pinkish rim region. Which corresponds to the silica, potassium, and sodium in the samples rim as identified by the elemental vectors shown in Figure 28.

71

Figure 39. Sample 2 raster data projected through EDS spot model using all three principal components colored by RGB color theory (top). Sample 2 raster data when represented by PC 1 (bottom left) to PC 3 (bottom right) where scores range from dark blue (negative) to yellow (positive).
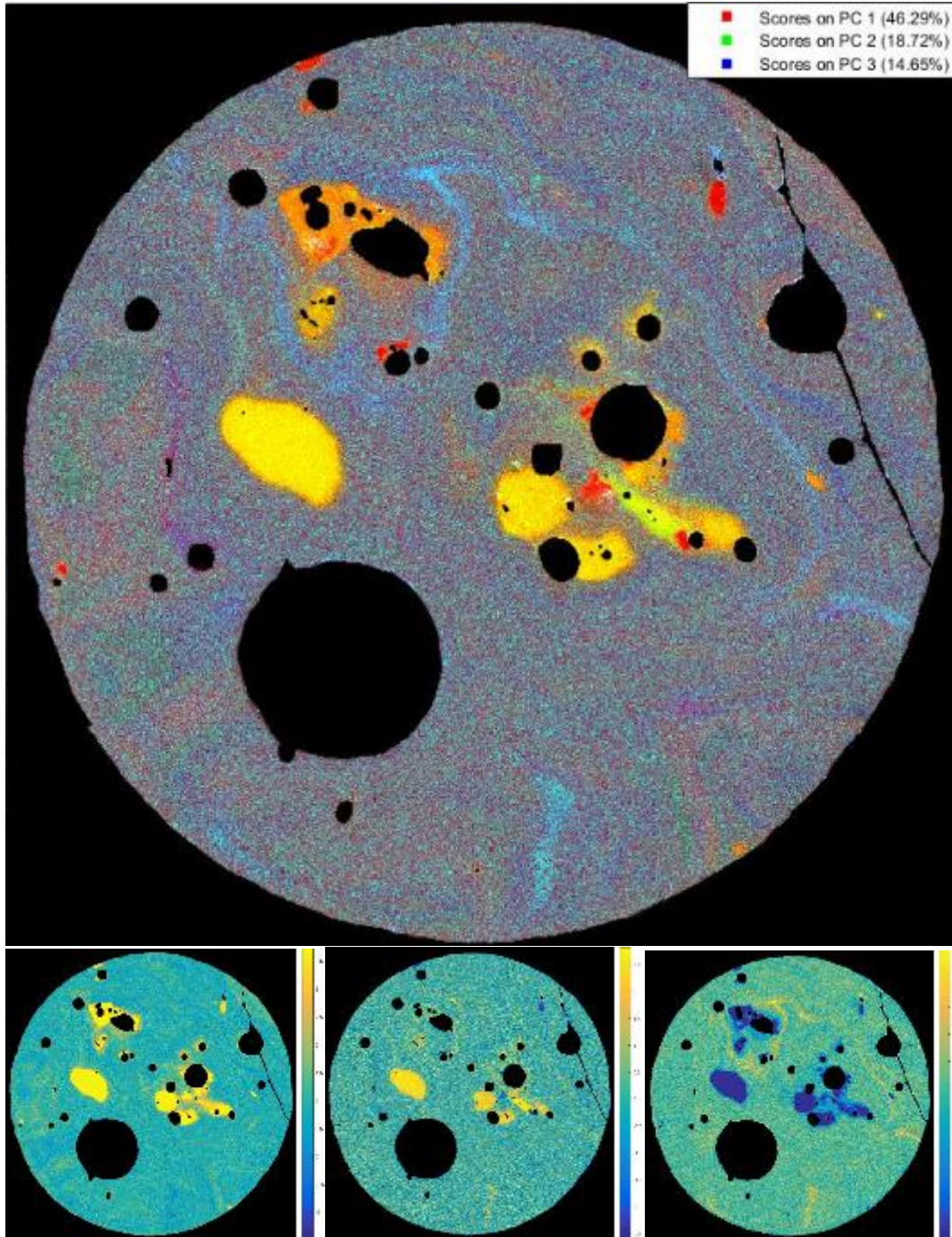
Figure 40. Sample 13 raster data projected through EDS spot model using all three principal components colored by RGB color theory (top). Sample 13 raster data when represented by PC 1 (bottom left) to PC 3 (bottom right) where scores range from dark blue (negative) to yellow (positive).

73

Figure 41. Sample 28 raster data projected through EDS spot model using all three principal components colored by RGB color theory (top). Sample 28 raster data when represented by PC 1 (bottom left) to PC 3 (bottom right) where scores range from dark blue (negative) to yellow (positive).
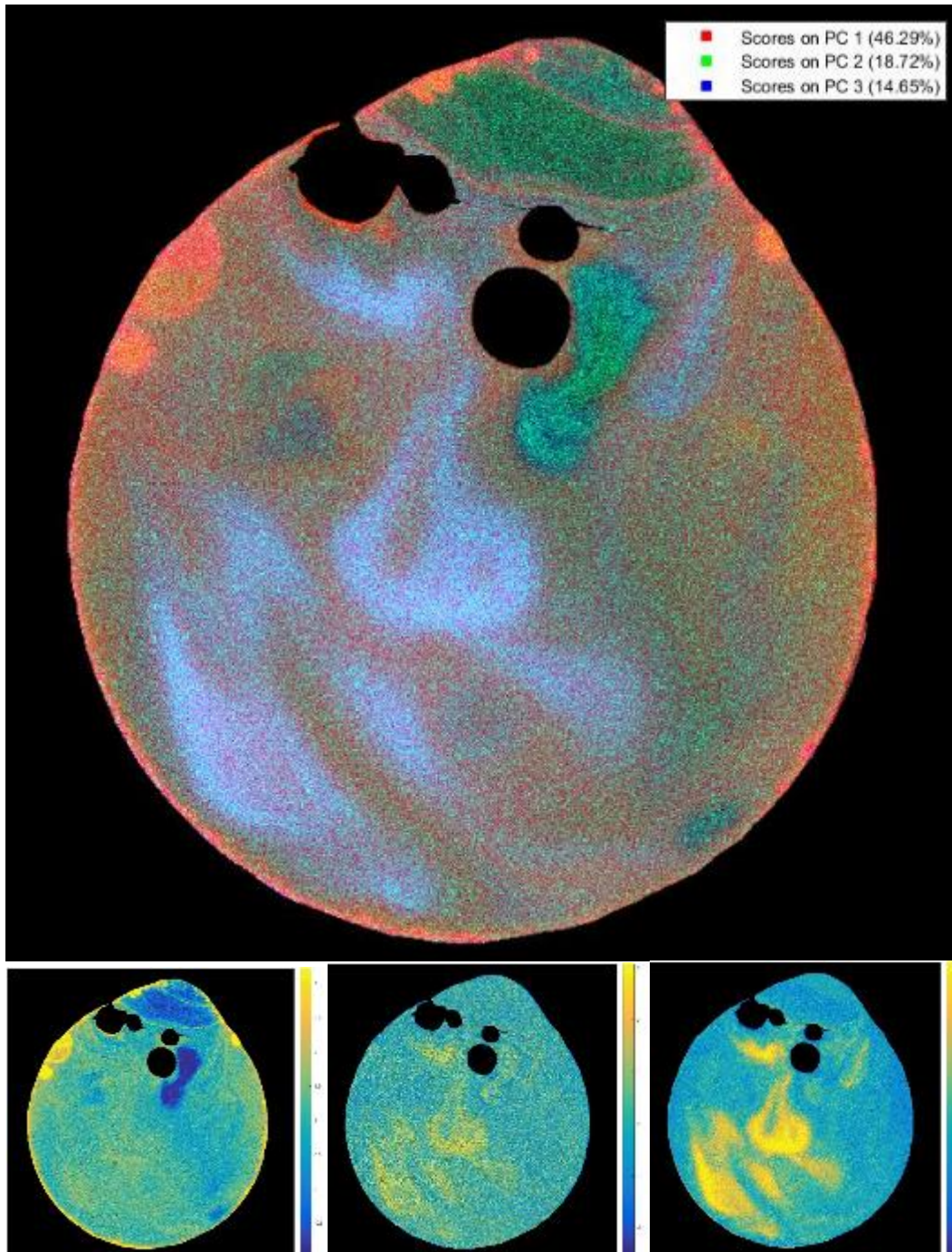
74
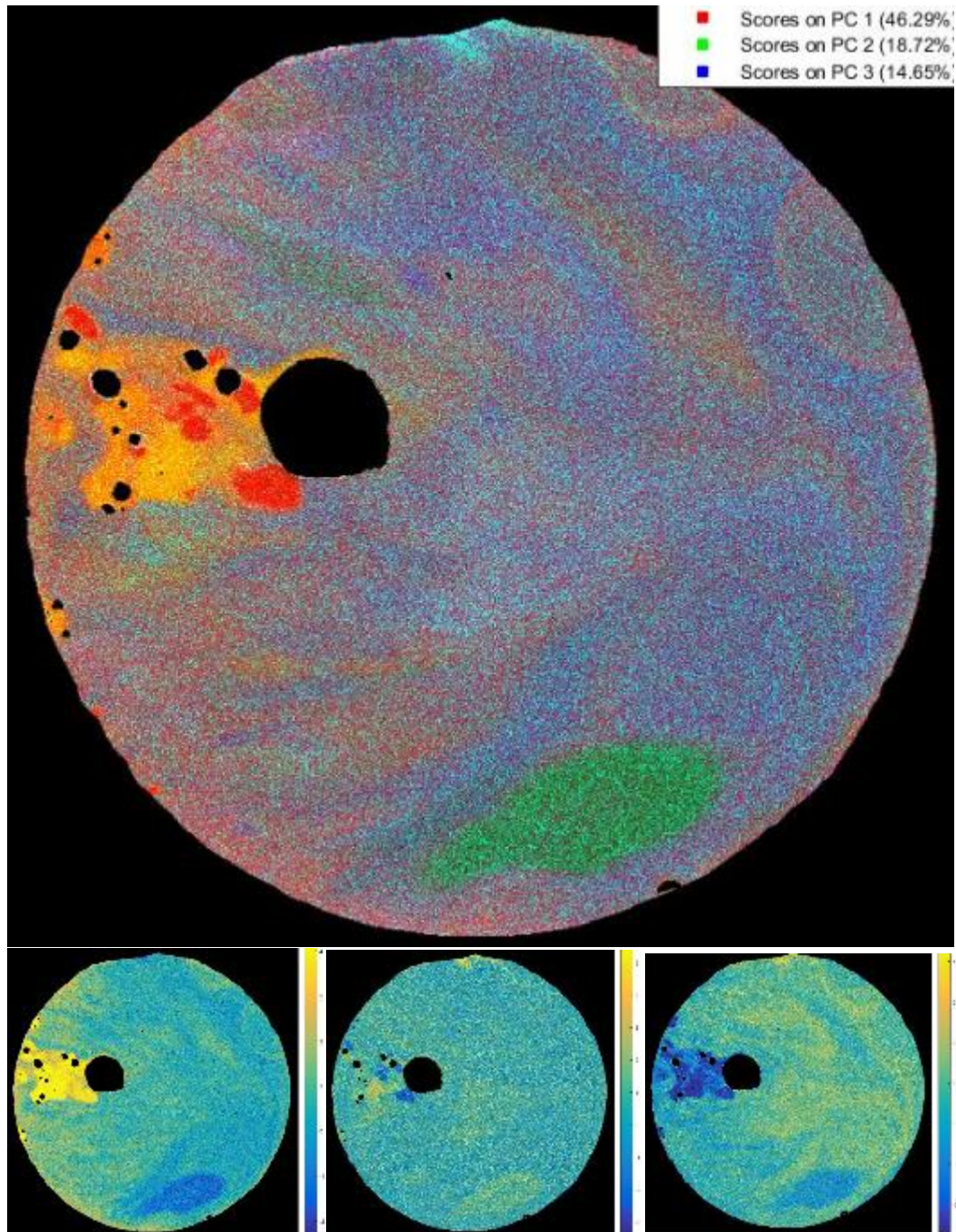
Figure 42. Sample 47 raster data projected through EDS spot model using all three principal components colored by RGB color theory (top). Sample 47 raster data when represented by PC 1 (bottom left) to PC 3 (bottom right) where scores range from dark blue (negative) to yellow (positive).
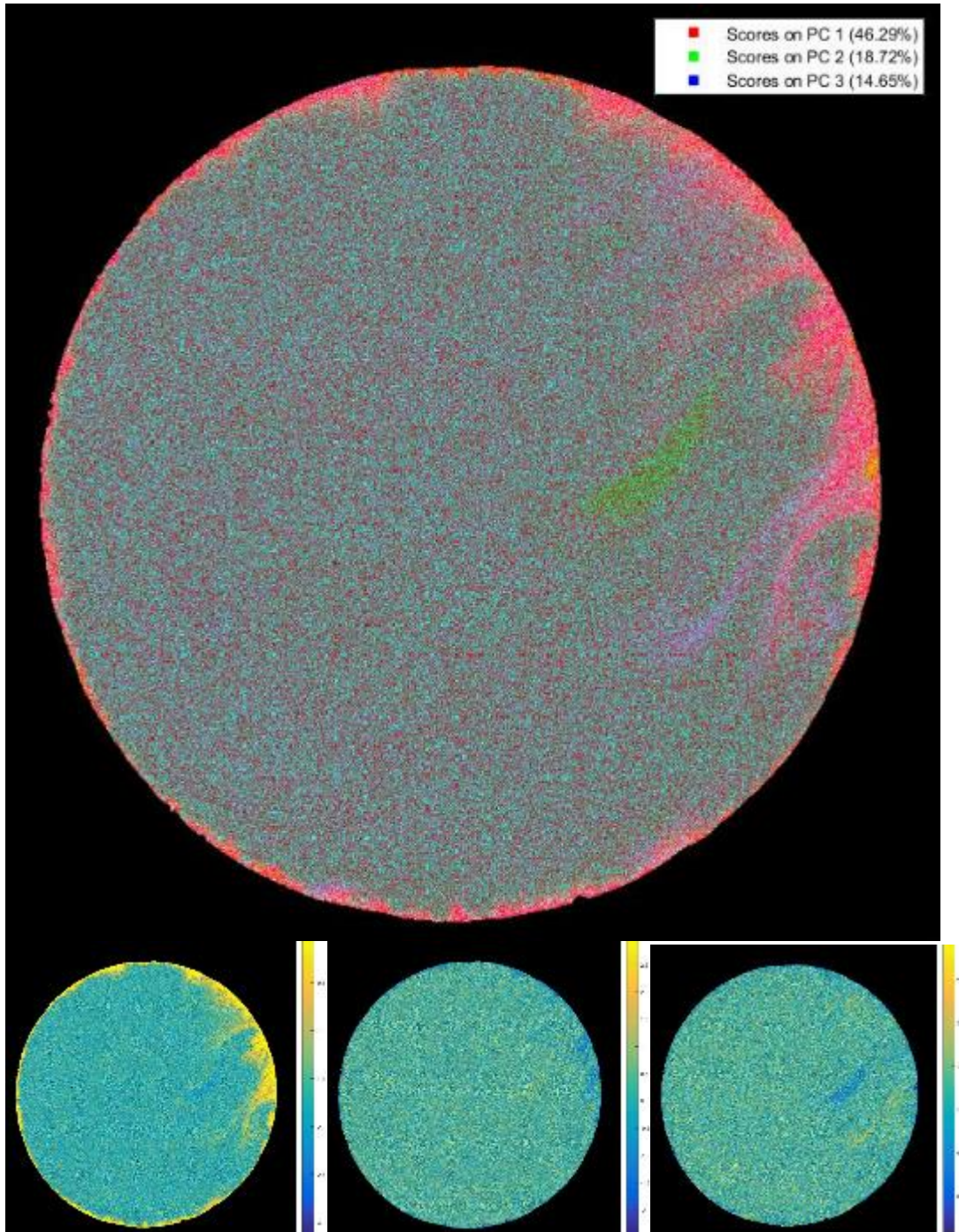
By projecting each of these x-ray maps through the EDS spot sample model, it becomes apparent that several of the particles exhibit mixing behaviors such as those seen in the PC 3 coloring of sample 47 shown in Figure 42. The PC 2 representation in the RGB image corresponds to a peak activity region. However, there is a second peak in this sample that is not represented by PC 2. This highlights a limitation of the spot data in determining the exact element correlation to the unspent nuclear fuel. Using just the EDS spot sample data is limited to anecdotal correlations due to the low concentration of actinides in the sample and the unavailable activity data in this model. This sample also shows inclusion characteristics of silicon dioxide in the PC 1 coloring. These regions are easily identified on the optical image and help to establish the positive correlation to silicon dioxide and PC 1, which further confirms the validity of the EDS spot sample model. The resulting individual element weighting factors for the EDS spot sample model for each of the principal components are shown Appendix A, Figure 51, Figure 52, and Figure 53.

Sample 2 highlights the ease of identifying fallout samples that have been formed of multiple samples or conglomerates. The optical image of this sample suggests that it may have been developed from two samples combined during the cooling phase of formation, but is not definitive. However, the EDS PCA model clearly shows that the upper portion of the sample has a different chemical composition from the rest of the sample. Figure 39 shows how the majority of the sample is composed of a different PC mixture than the top portion of the fallout sample.

Raster Elemental Model with Autoradiography

Using the four sample's x-ray maps a consolidated data set was constructed. This

data set improves upon the EDS spot sample with the inclusion of the autoradiography

activity data. The process for the PCA model follows the same principal and steps as the

EDS model. The resulting model showed the same characteristics indicative of a two

Principal Component model. These first three principal components had values of 4.73,

1.35, and 0.939, as shown in Figure 43.
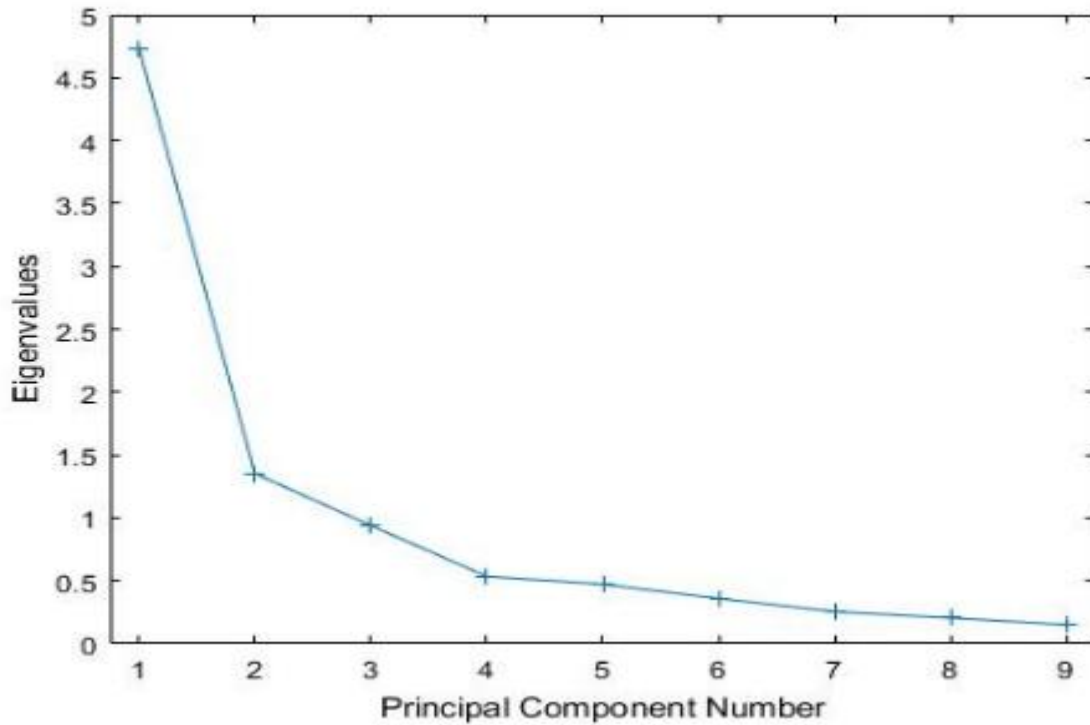
Figure 43. Raster Elemental Model Principal Component values.

By the Scree test, Kaisers Rule, and the proportion of variance captured theorem

it is possible to reduce the number of principal components to just two, compared to the

three used for the EDS spot model. However, with such a limited number of samples in

the model this raises a concern. Additionally, all of these samples came from regions in

77

close proximity in the EDS spot model, meaning that the scores of these samples are similar and have similar elemental compositions. Using the first three principal components captures 78.06% of the variance of the system. For consistency, and to account for the small sample size and similar scores, the model will be developed using the first three principal components. Recall that additional PCs begin to capture statistical noise and measurement error further reducing the value added through additional PCs when developing a mathematical model to explain the variations within the system. The principal components percent variance captured is recorded in Figure 44.
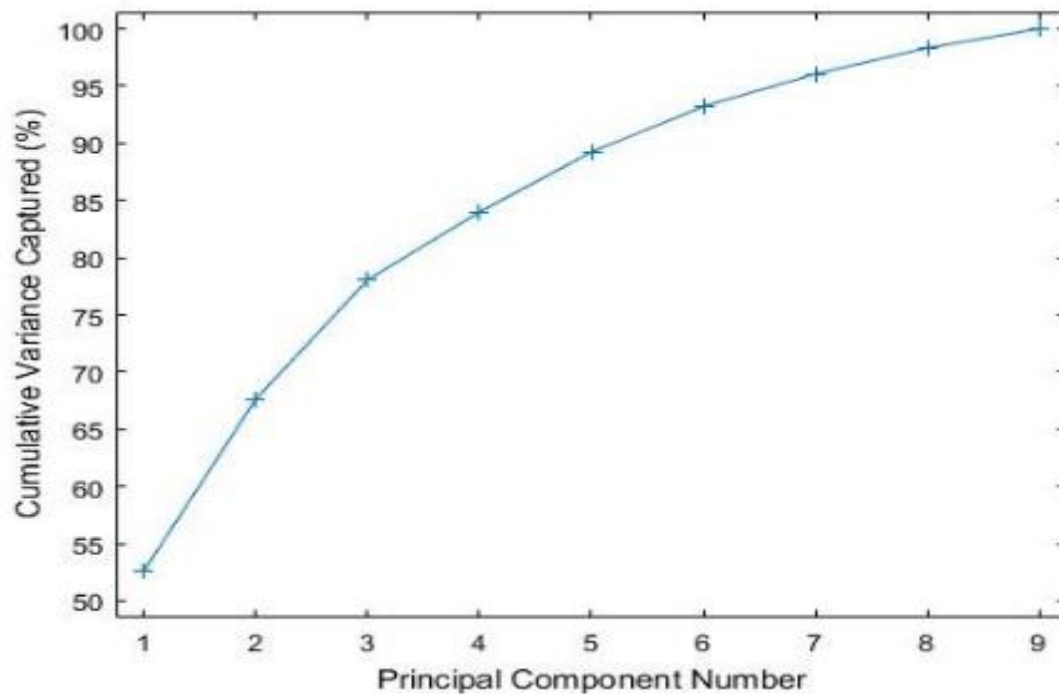
Figure 44. Raster Elemental Model Principal Component percent variance captured.

Based on the limited number of samples in the model, the results from such an analysis must be taken with caution and are not necessarily representative of the 50-sample set. The results do, however, provide valuable insight into the methods proposed

78

in this paper and validate the methods used for future research in this area. The first thing to consider is element vectors for the principal component mapping. When viewing PC 1 vs PC 2 (Figure 45) a few differences are noted compared to the EDS spot data model, Figure 27. The addition of the autoradiography data, denoted as AR, caused aluminum and titanium to become separated in the first two principal components. A division that was not available until the first and third analysis, Figure 28. However, the association between sodium, potassium, and silica is maintained along with the anti-correlation to the calcium and magnesium grouping. This correlation between aluminum and the unspent nuclear fuel is accounted for in 67% of the data set's variance.

Figure 45. Raster elemental model, PC 1 vs PC 2 element vectors. The model indicates a correlation between the activity of the unspent nuclear fuel and aluminum along with an anti-correlation to sodium.

79

When comparing, the element grouping for PC 1 vs PC 3, see Figure 46, the correlations and anti-correlations remain for the two main groups from PC 1 vs PC 2. Titanium and iron become anti-correlated which is a new data point from the analysis of the raster data. The close grouping of calcium and the autoradiography in PC 1 vs PC 3 is due to the small value in PC 3. Looking at Figure 45 it is apparent that the calcium and autoradiography have nearly the same value in PC 1 and that it is PC 2 and PC 3 that cause the vertical separation or lack of it. This correlation identifies the co-location of actinides with calcium, magnesium, and aluminum, at least within these four samples. The values of these three principal components are recorded in Table 5.
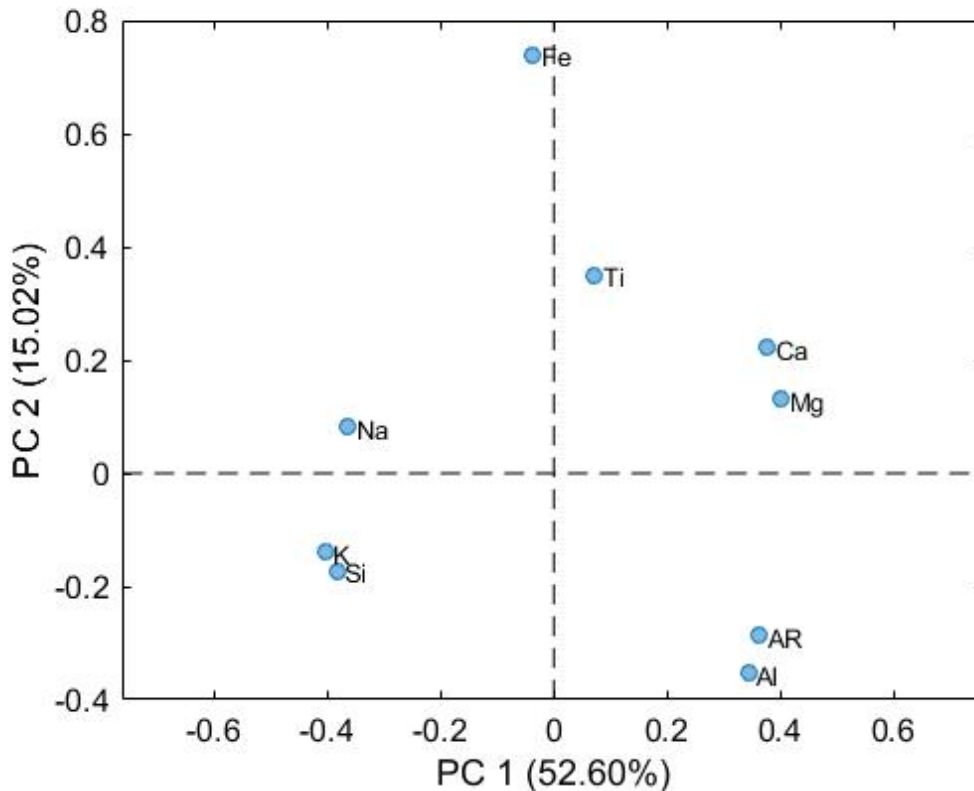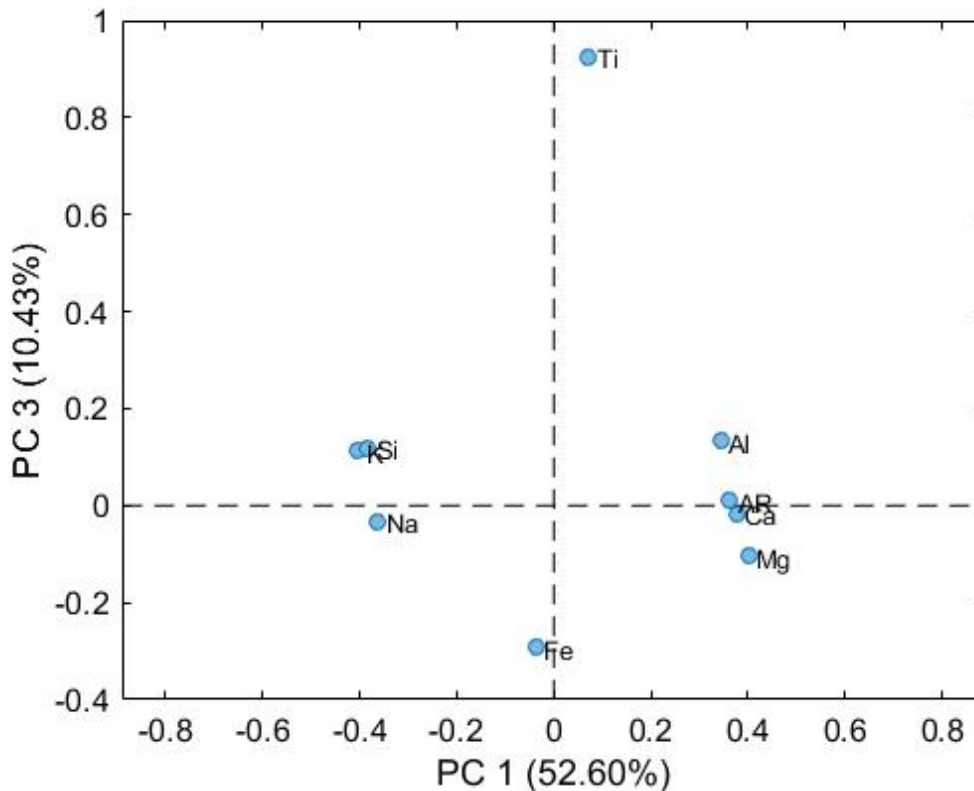

Figure 46. Raster elemental model, PC 1 vs PC 3 element vectors. The model indicates that the unspent nuclear fuel, aluminum, and calcium represent a positive correlation while sodium is anti-correlated to the nuclear fuel.

80

Table 5. Principal component scores for the raster model developed with samples 2, 13, 28, and 47.

	AR	Al	Ca	Fe	K	Mg	Na	Si	Ti
PC 1	0.363	0.344	0.377	-0.037	-0.404	0.402	-0.362	-0.382	0.718
PC 2	-0.288	-0.354	0.222	0.740	-0.139	0.131	0.082	-0.172	0.349
PC 3	0.113	0.132	-0.015	-0.294	0.112	-0.105	-0.033	0.120	0.926

Since the data loaded for this model comes from images, the resulting scores look much like the ones from before with the RGB color scheme, rather than the scatter plot seen in the EDS spot sample. Instead of being predictive of how the model is represented in the samples like earlier, these RGB images show how the sample affected the final PCs. With this understanding it is expected that three samples, 2, 13, and 47, will have similar RGB coloring images. This assumption is based on the EDS spot sample model and the co-location of these samples, as seen in Figure 37. The co-location is due to similar scores resulting in the data points being plotted near one another in PC space. With the higher sampling rate, it is expected to also expose new features in these samples.

81
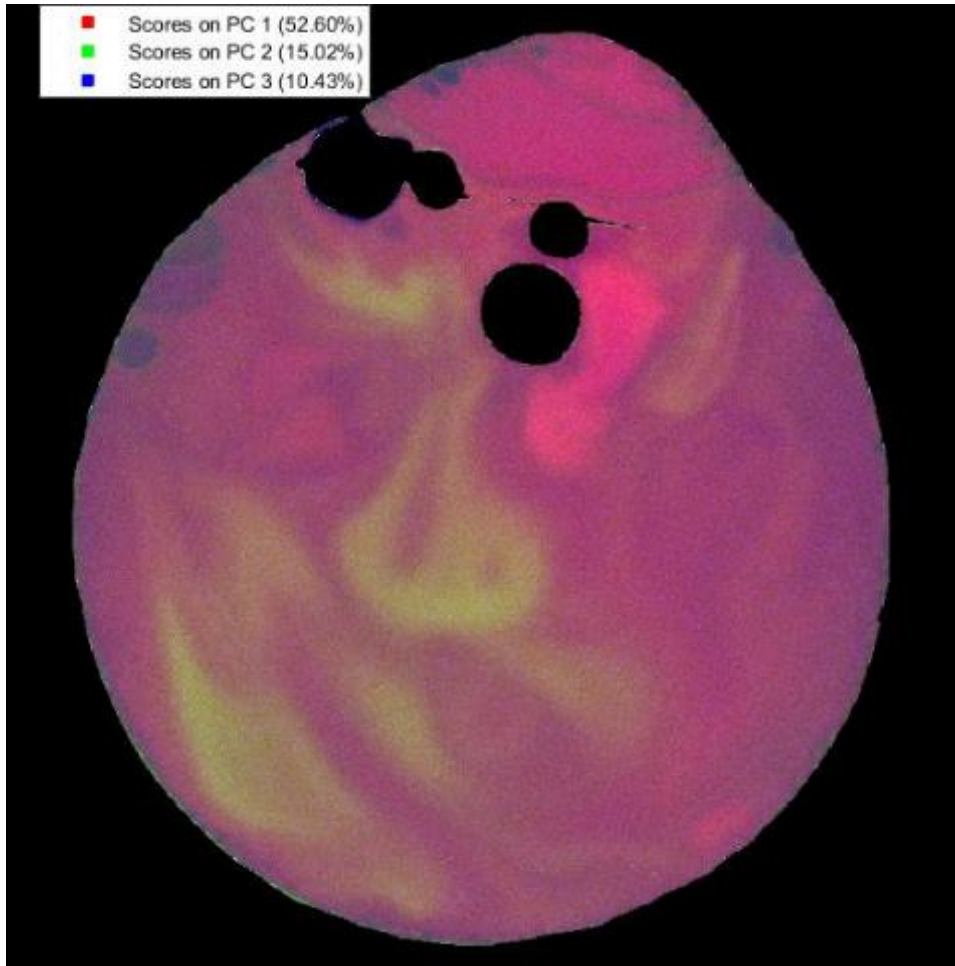
Figure 47. RGB scores image for sample 2 using the three principal components from the raster model.

Sample 2, see Figure 47, shows many of the same properties as before. Obvious vortex mixing along with a definitive two-part coloring are the predominate features of the sample. As expected the sample is heavily colored from PC 1, due largely in part to its similar major elemental composition as the other two samples from this region of the EDS model. Unfortunately for this sample, no new features appear due to the higher resolution images.
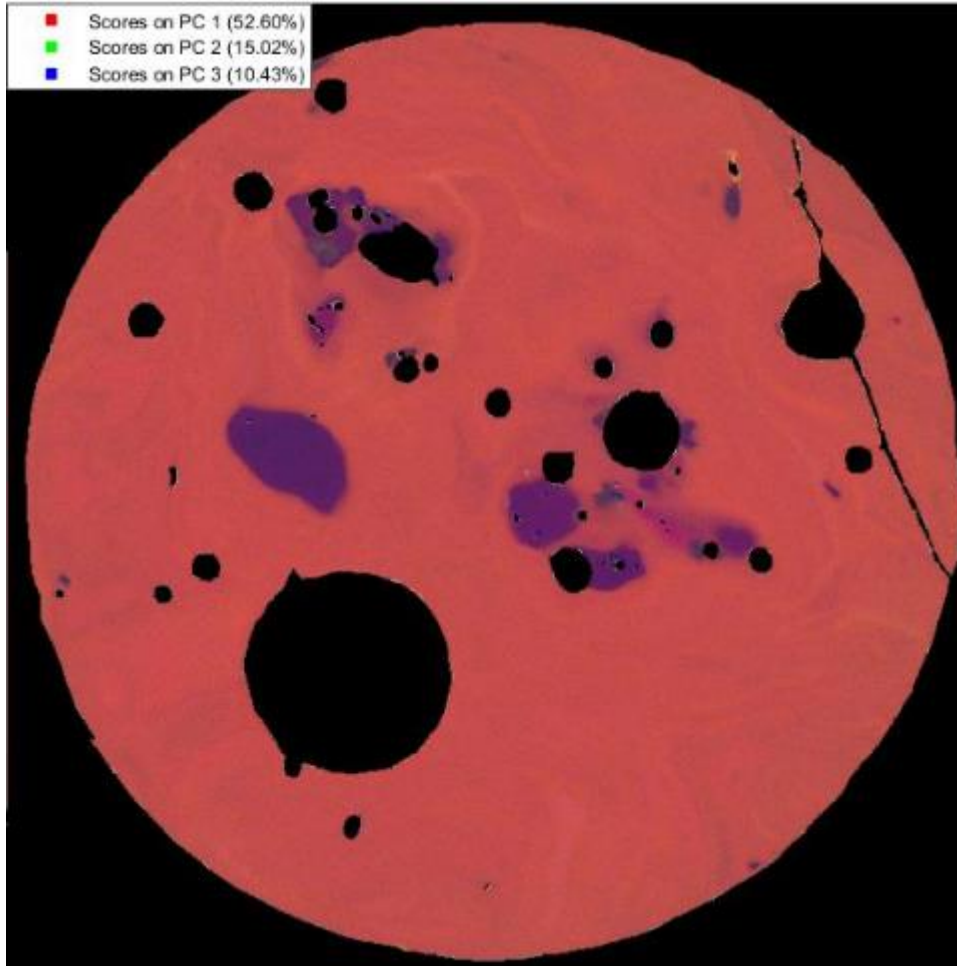
Figure 48. RGB scores image for sample 13 using the three principal components from the raster model.

Like sample 2, sample 13 (Figure 48) shows many of the same features previously identified using the EDS model. The higher resolution does identify more vortex swirling in the sample that was not readily visible in the EDS spot model. The RGB coloring does lean heavily to PC 1 as expected but is closer to sample 28 than the other two samples from the same region in the EDS model.

83
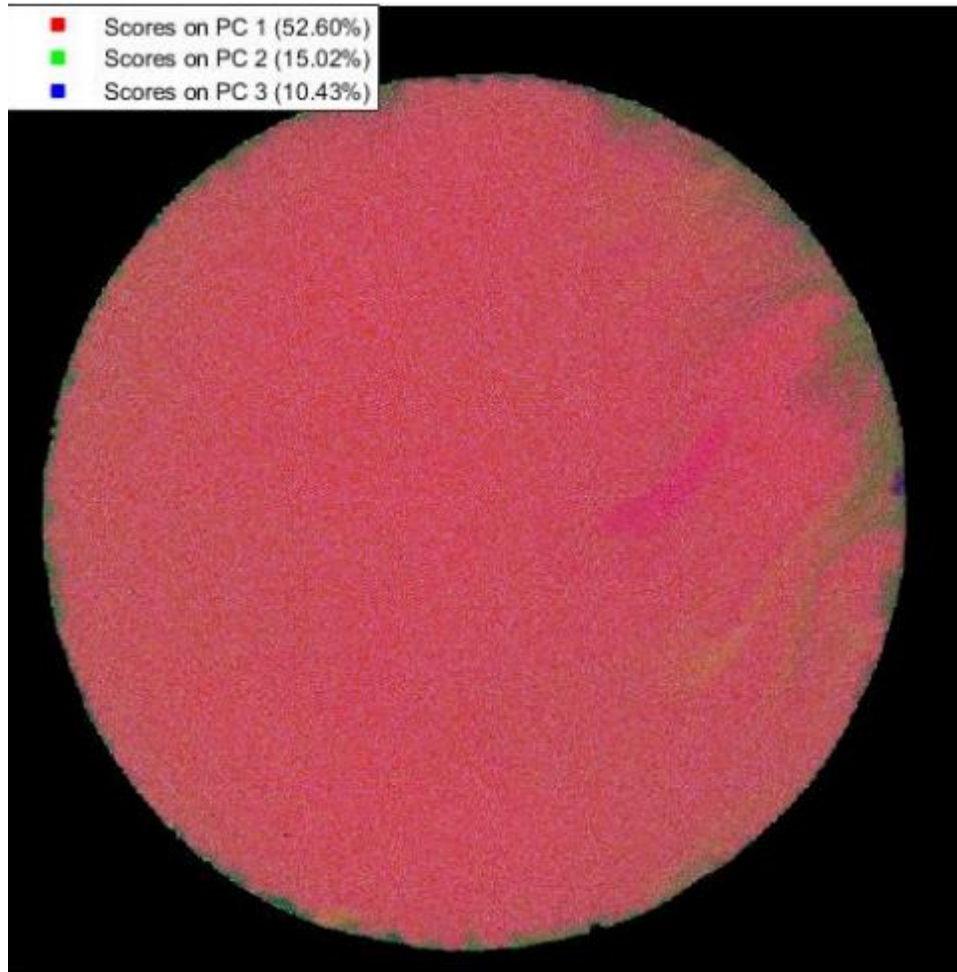
Figure 49. RGB scores image for sample 28 using the three principal components from the raster model.

When reviewing sample 28, shown in Figure 49, it is similar in coloring to sample 13. This is surprising considering its location compared to the grouping of the other three samples. This sample is homogenous and uniform compared to the other samples in this model set.

84

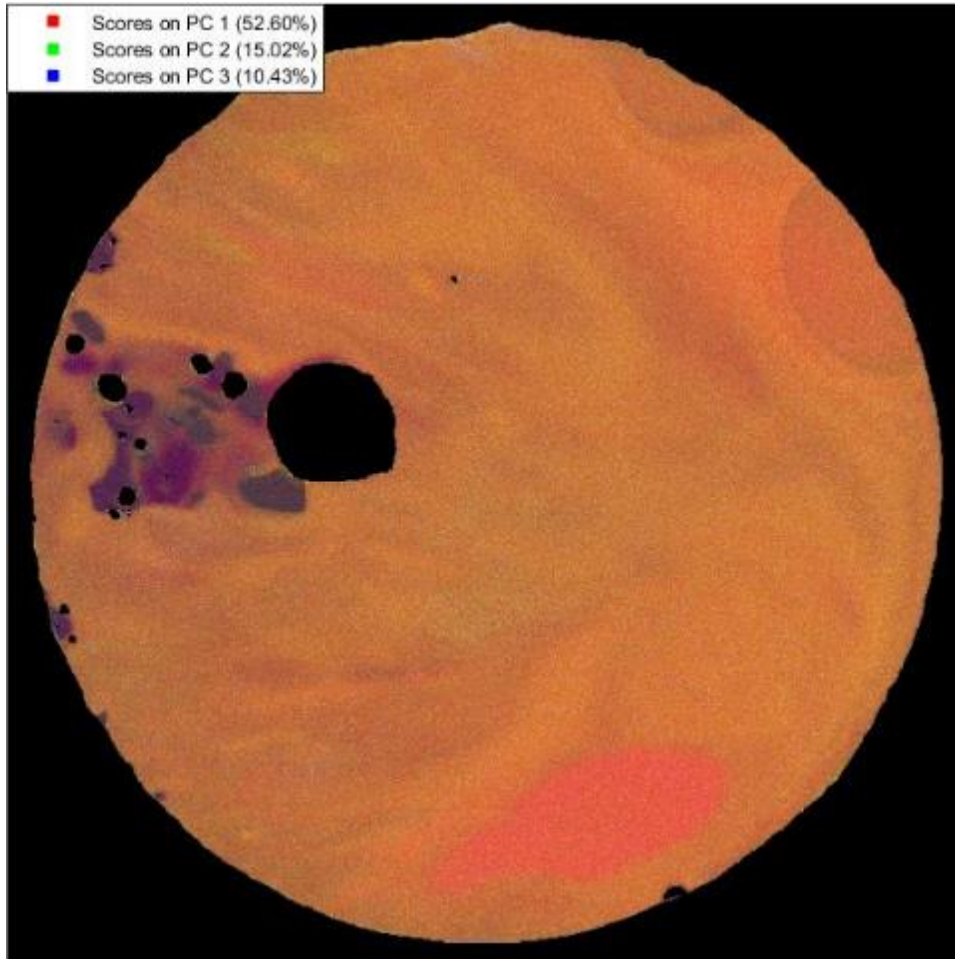**Figure 50. RGB scores image for sample 47 using the three principal components from the raster model.**

Sample 47 exhibits the most variation and deviation from the other three samples which is not expected, as shown in Figure 50. The features of the sample are still consistent with the EDS spot model. There is an improvement to the vortex swirl and a reduction in pixilation when compared to the EDS model.

85

V. Conclusion

This research used application of PCA and multiple imaging techniques to improve the scientific understanding of fallout formation, identified particles that represent the most valuable types for forensics purposes, and established elemental compositions and correlations between major soil elements. The wide range of physical characteristics within the fallout samples ensured a representative sample set of the bulk fallout formation characteristics leading to improvements in the resulting model. The application of principal component analysis to this fallout sample set has proven to be a viable method in understanding the underlying elemental system. This system describes the correlation between major elemental constituents and the incorporation of unspent nuclear fuel. Using multiple spectroscopies and imaging techniques produced a robust and detailed data set that was easily manipulated and evaluated through the use of PCA. With PCA's ability to reduce the difficulty of the problem, additional information can be added to the model without an increase in solution difficulty. By using principal component analysis, the correlation between major elements and the unspent nuclear fuel moves from an anecdotal solution to a quantifiable result.

5.1. Research Conclusions

The EDS model showed that the fifty fallout samples could be grouped into three regions. One region consisted of the apparent porous surface samples high in magnesium and calcium. The second group consisted of the homogenous samples with a uniform high activity high in aluminum and titanium. The final group was the mixed set of homogenous and heterogeneous samples with high and low activity regions. By first

86

developing the spot sample model, it was possible to identify unknown samples for forensic value. The time required to develop the spot sample model was relatively short and could be completed in hours depending on the number of samples used. Using the EDS spot sample model first would drastically reduce the amount of time spent on time-intensive forensic methods for fallout of low forensic value.

The highest forensics group was shown to be the homogenous group with high aluminum and titanium or those that are low in silica, potassium, sodium and/or iron. This homogenous group was transparent with no physical deformations or surface features. Additionally, the samples that had high heterogeneity exhibited regions of low activity making these samples of low forensics value when attempting to recover unspent nuclear fuel.

The development of a representative x-ray mapping model is required to incorporate the autoradiography images and activity data. The autoradiography data couples the major elemental compositions with the trace unspent nuclear fuel. Through the development of this model, with older fallout samples, the quantitative results will improve the understanding of fallout development and the incorporation of unspent nuclear fuel. Older samples are required due to the fission product saturation in newer samples. The full raster quantitative results can be used to draw physical characteristics of high value forensic samples reducing the need for instrumentation time and evaluation during a time critical event.

87

5.2. Future Research

Several key insights were developed during this research that will improve future work in this area of nuclear forensics. First SEM and XRF are equivalent spectroscopy techniques that provide similar information. However, the FWHM resolution of a typical SEM is higher than most XRF machines. This should be approached with caution as an order of magnitude in resolution on the spectroscopy may prove to be significant for major elemental compositions and actinide incorporation.

Secondly, high resolution raster images do not provide enough additional information to justify the time required to develop such images. The orders of magnitude difference between these images and the autoradiography require scaling down the raster image and upscaling the autoradiography images. This approach adds multiple cases where error can be introduced into the model. By selecting lower resolution images a larger data set can be investigated in the same amount of time improving the model with more data points.

Finally, in an effort to reduce any bias or size fraction dependency the same process should be performed on a larger size fraction of fallout. The change in size fraction may improve the minor/major elemental concentrations such as magnesium or titanium improving the model's prediction capability for incorporation of actinides. Additionally, changing the size fraction may yield information about dependencies or correlations between major elements and the actinides that is due to fallout particle size.
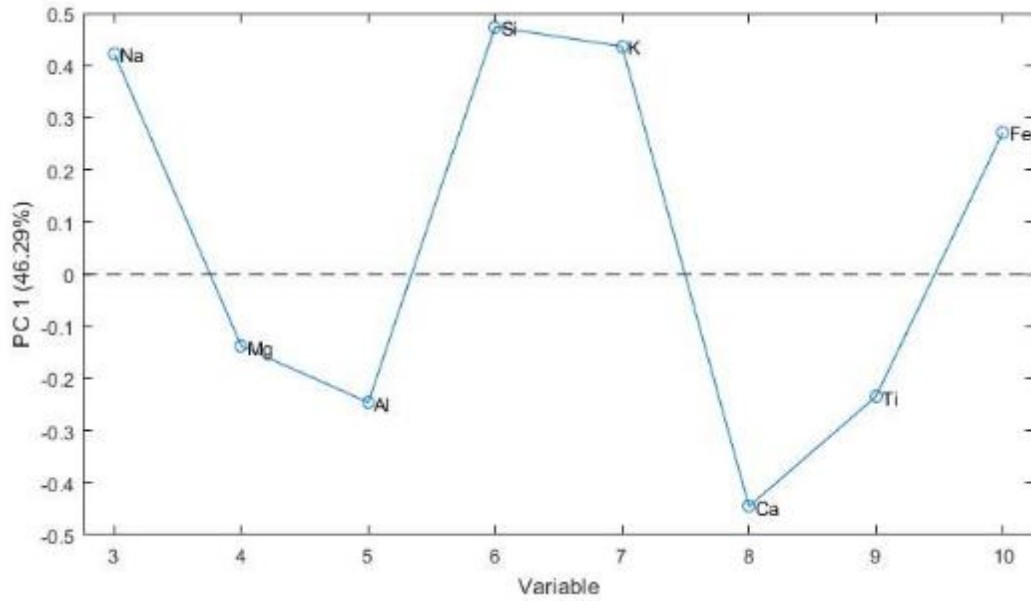
88

VI. Appendix A

Figure 51. EDS spot sample principal component 1 elemental variable weighting.
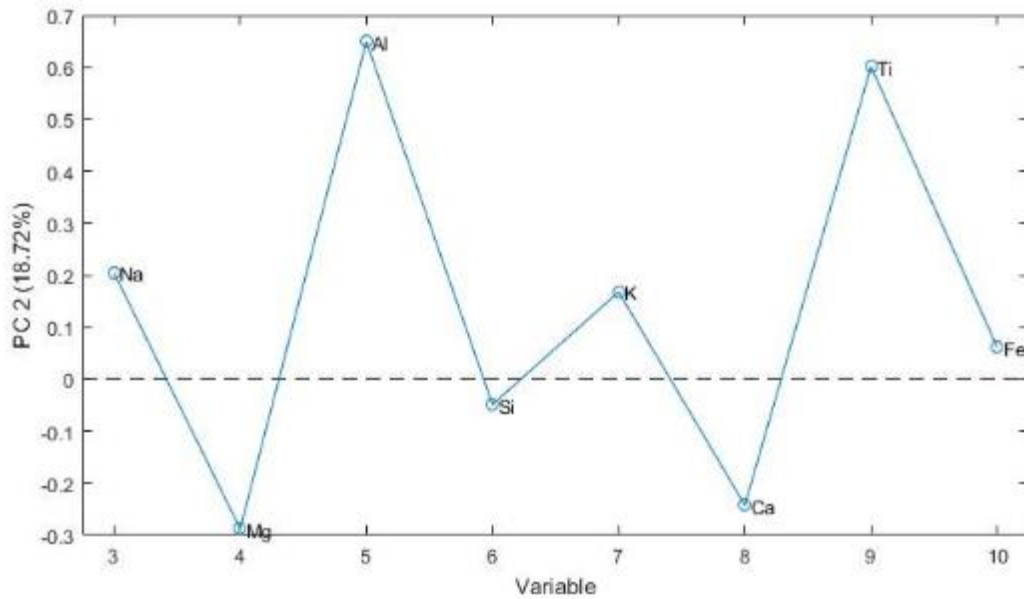

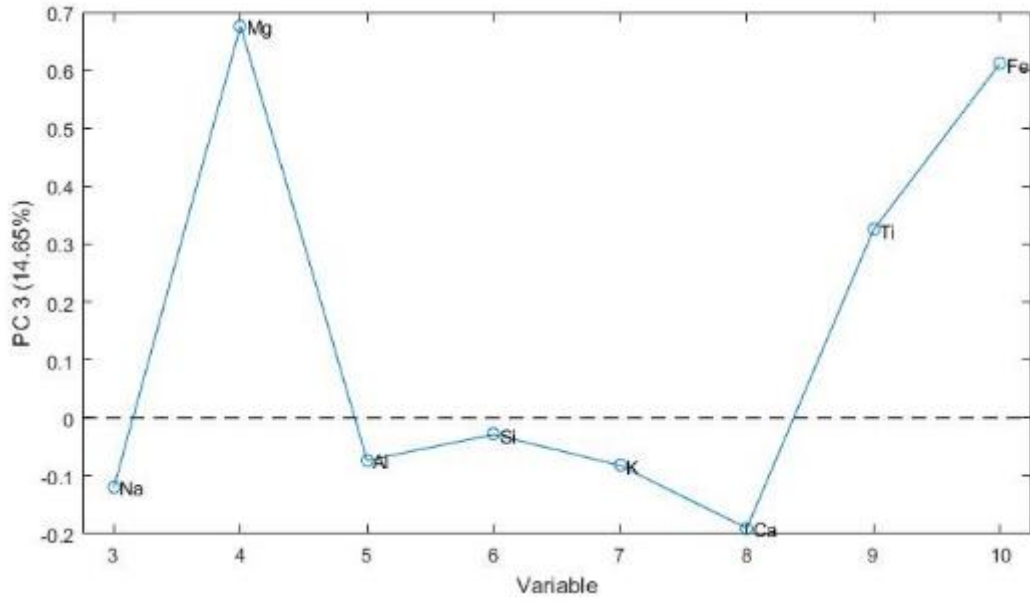**Figure 52. EDS spot sample principal component 2 elemental variable weighting.**

89

Figure 53. EDS spot sample principal component 3 elemental variable weighting.

90

Bibliography

[1]   P. H. Donohue, A. Simonetti, E. C. Koeman, S. Mana and P. C. Burns, "Nuclear Forensic Applications Invloving High Spatial Resolution Analysis of Trinitite Cross-sections," *Journal of Radioanalytical and Nuclear Chemistry,* vol. 306, pp. 457-467, 2015.

[2]   J. W. McClory, "Applying Principle Component Anlysis to Fallout Characterization: The link between Actinides and Composition," Defense Threat Reduction Agency, 2016.

[3]   J. M. Dierken, "Analysis of Fallout Particles Using Image Registration of Autoradiography and Scanning Electron Microsopy," *Master's thesis, Air Force Institute of Technology,* 2014.

[4]   M. L. Monroe, "FORENSICS ANALYSIS FOR ELEMENTAL IDENTIFICATION IN DEBRIS," *Master's thesis, Air Force Institute of Technology,* 2013.

[5]   J. Schlens, "A Tutorial on Principle Component Analysis," Systems Neurobiology Laboratory, 10 12 2005. [Online]. Available: http://www.cs.cmu.edu/~elaw/papers/pca.pdf. [Accessed 29 9 2016].

[6]   S. T. Castro, "Nuclear Forensics Applications of Principle Component Analysis on Micro X-ray Flourescence Images," *Master's thesis,* 2016.

[7]   J. McClory and J. Matzel, "MIDAS QPR," AFIT, WPAFB, 2016.

[8]   K. J. Moody, I. D. Hutcheon and P. M. Grant, Nuclear Forensic Analysis, Boca Raton, FL: CRC Press, 2005.

[9]   P. J. Glasstone and S. Dolan, The Effects of Nuclear Weapons, United States Department of Defense and Department of Energy, 1977.

[10]   G. R. Crocker, J. D. O'Connor and E. C. Freiling, "Physical and Radiochemical Properties of Fallout Particles," US Naval Radiological Defense Laboratory, San Francisco, 1966.

[11] C. J. Bridgman, Introductio to the Physics of Nuclear Weaopons Effects, Defense Threat Reduction Agency, 2001.

[12] K. S. Holliday, "Plutonium Segreagtion in Glassy Aerodynamic Fallout from a Nuclear Weapon Test," Dalton Transactions, 2016.

[13] K. J. Moody, I. D. Hutcheon and P. Grant, Nuclear Forensic Analysis, Boca Raton, FL: CRC Press, 2005.

[14] C. E. Adams, N. H. Farlow and W. R. Schell, "The Compositions, Structures and Origins of Radioactive Fall-out Particles," *Geochimica et Cosmochimica Acta,* vol. 18, pp. 42-56, 1960.

[15] N. A., "History of Radiography," [Online]. Available: https://www.nde-ed.org/EducationResources/CommunityCollege/Radiography/Introduction/history.htm. [Accessed 27 9 2016].

[16] W. Hendee, Medical Imaging Physics (4th Ed), New York: John Wiley and Sons, 2002.

[17] N.A., "Overview of X-ray Fluorescence," 8 2012. [Online]. Available: http://archaeometry.missouri.edu/xrf . [Accessed 28 9 2016].

[18] Y. Leng, Materials Characterization: Introduction to Microscopic and Spectroscopic Methods, Singapore, Thailand: John Wiley and Sons, 2008.

[19] W. Bambynek, "X-ray Flourescence Yields, Auger, and Coster-Krong Transition Probabilities," *Review of Modern Physics,* vol. 44, p. 716, 1972.

[20] C. G. Worley, L. Tandon, P. T. Martinez and D. L. Decker, "Application of mico-XRF for Nuclear Materials Characterization and Problem Solving," Los Alamos National Laboratory, Los Alamos, NM, 2013.

[21] E. Mankin, "Principle Components Analysis: A How-to Manual for R," [Online]. Available: http://people.tamu.edu/~alawing/materials/ESSM689/pca.pdf. [Accessed 1 10 2016].

[22] J. A. Shlens, "Tutorial on Principle Component Analysis," [Online]. Available:

https://www.ics.forth.gr/mobile/pca.pdf. [Accessed 29 9 2016].

[23]   Eigenvector Research Inc., "Chemometrics 1: Principle Components and
       Exploratory Data Analysis," 2012. [Online]. Available:
       http://eigenvector.com/courses/EigenU_Chemo1.html. [Accessed 16 9 2016].

[24]   J. I. Goldstein, Scanning Electron Miscroscopy and X-ray Microanalysis (2nd Ed),
       New York: Pelnum Press, 1981.

[25]   NIH.gov, "ImageJ," NIH.gov, [Online]. Available:
       https://imagej.nih.gov/ij/download.html. [Accessed 16 June 2016].

[26]   D. A. Jackson, "Stopping Rules in Principal Components Analysis: A Comparison
       of Heuristical and Statistical Approaches," *Ecology,* vol. 74, no. 8, pp. 2204-2214,
       1993.

[27]   R. W. G. Hunt, The Reproduction of Colour (6th Ed), Chichester, UK: Wiley,
       2004.

[28]   A. W. Rogers, Techniques of Autoradiography (3rd ed), New York: Elsevier North
       Holland, 19979.

[29]   G. J. DiIorio, Direct Physical Measurement of Mass Yields in Thermal Fission of
       Uranium 235, New York: Garland, 1979.

[30]   M. Horvath, Artist, *RGB colour wheel.* [Art].
       https://commons.wikimedia.org/wiki/File:AdditiveColor.svg, 2006.

[31]   R. Schreiber and H. Glocker, *Annalen der Physik,* vol. 85, p. 1089, 1928.

[32]   M. Zhang, "Image Deconvolution in Digital Autoradiography," 2 2008. [Online].
       Available: http://www.ncbi.nlm.nih.gov/pmc/articles/PMC2668928. [Accessed 10
       9 2016].

REPORT DOCUMENTATION PAGE

Public reporting burden for this collection of information is estimated to average 1 hour per response, including the time for reviewing instructions, searching existing data sources, gathering and maintaining the data needed, and completing and reviewing this collection of information. Send comments regarding this burden estimate or any other aspect of this collection of information, including suggestions for reducing this burden to Department of Defense, Washington Headquarters Services, Directorate for Information Operations and Reports (0704-0188), 1215 Jefferson Davis Highway, Suite 1204, Arlington, VA 22202-4302. Respondents should be aware that notwithstanding any other provision of law, no person shall be subject to any penalty for failing to comply with a collection of information if it does not display a currently valid OMB control number. **PLEASE DO NOT RETURN YOUR FORM TO THE ABOVE ADDRESS.**

1. REPORT DATE *(DD-MM-YYYY)* 23-03-2017	2. REPORT TYPE Master's Thesis	3. DATES COVERED *(From - To)* June 2015-March 2017

4. TITLE AND SUBTITLE Using Principal Component Analysis to Improve Fallout Characterization	5a. CONTRACT NUMBER
	5b. GRANT NUMBER
	5c. PROGRAM ELEMENT NUMBER

6. AUTHOR(S) Haws, Derek W., Capt, USAF	5d. PROJECT NUMBER
	5e. TASK NUMBER
	5f. WORK UNIT NUMBER

7. PERFORMING ORGANIZATION NAME(S) AND ADDRESS(ES) Air Force Institute of Technology Graduate School of Engineering and Management (AFIT/EN) 2950 Hobson Way Wright-Patterson AFB OH 45433	8. PERFORMING ORGANIZATION REPORT NUMBER AFIT-ENP-MS-17-M-096

9. SPONSORING / MONITORING AGENCY NAME(S) AND ADDRESS(ES) Defense Threat Reduction Agency DTRA-J9-NTF POC: LT Col Matthew Zickafoose (matthew.s.zickafoose.mil@mail.mil) 8725 John J. Kingman Road Ft Belvoir, VA 22060	10. SPONSOR/MONITOR'S ACRONYM(S) DTRA
	11. SPONSOR/MONITOR'S REPORT NUMBER(S)

12. DISTRIBUTION / AVAILABILITY STATEMENT
Distribution Statement A. Approved for public release; Distribution Unlimited

13. SUPPLEMENTARY NOTES
This material is declared work of the U.S. Government and is not subject to copyright protection in the United States.

14. ABSTRACT
Previous research conducted at Lawrence Livermore National Laboratory (LLNL) and the Air Force Institute of Technology (AFIT) has shown a correlation between actinide location and elemental composition in fallout from historic weapons testing. Fifty spherical fallout samples were collected from near ground zero of a surface burst weapons test. The samples were mounted in an aluminum puck then ground and polished to a hemisphere exposing the central plane. Physical morphologies of the samples ranged from clear to opaque with inclusions, voids, and/or uniform characteristics. Spectroscopy data were collected using optical microscopes and scanning electron microscopy (SEM), with radioactivity recorded through autoradiography. Principal component analysis (PCA) was used to quantify the variations within the samples and to determine the correlations between major elemental compositions and the incorporation of unspent nuclear fuel. Principal component analysis identified four statistically significant principal components accounting for 78% of the variations within the spectroscopy data. Principal component analysis was demonstrated as a suitable mathematical approach to solving the complex system of elemental variables while establishing correlations to actinide incorporation within the fallout samples. A model was developed using spot sampling to categorize the samples, identifying three classes of samples. The model correctly identified samples with above average uniform activity, thereby identifying samples with high forensic value for recovery of unspent nuclear fuel. Final analysis of the full elemental composition and the correlation with regions of increased activity for all fifty samples is currently being completed.

15. SUBJECT TERMS
SEM, Principal Component Analysis, Fallout

16. SECURITY CLASSIFICATION OF:			17. LIMITATION OF ABSTRACT	18. NUMBER OF PAGES	19a. NAME OF RESPONSIBLE PERSON Dr. John W. McClory, AFIT/ENP
a. REPORT U	b. ABSTRACT U	c. THIS PAGE U	UU	108	19b. TELEPHONE NUMBER (937)255-3636x.7308; john.mcclory@afit.edu